SYNTHESIS, PHOTOPHYSICS AND ELECTROCHEMICAL STUDY OF TIN MACROCYCLES

A thesis submitted in fulfillment of the requirement for
the degree of

MASTER OF SCIENCE

of

RHODES UNIVERSITY

by

MIELIE SAMSON KHENE

January 2008

DEDICATION

TO MY MOTHER (Constance Khene),

GRANDMOTHER (Julia Radebe),

MY LATE GRANDFATHER (Baningi Mashinini),

AND FATHER (Brendan Tshabalala)

“Mshengu donga laka Mavoso – Baningi into ezimandla”

ACKNOWLEDGEMENTS

“The secret things belong to the Lord our God, but the things revealed belong to us and our children forever, that we may follow all the words of this law” (Deuteronomy 29:29).

First, I would like to thank God for his mercy that endures forever, for his provision and his unfailing love towards me.

I wish to thank my supervisor Prof. T. Nyokong for allowing me to be part of her research group which is more than just a research group (it’s a family away from home). Thank you for your constant encouragement and drawing out the best of me. I appreciate you sending me to the United Kingdom (Norwich) for 3 months; it has made a deep impact in my life.

I would like to acknowledge Caroline Pade, Ashly Sarimana, Prudence Tau, Vongani Chauke, Nthapo Sehlotho, Mopelola Idowu and Danaiela Geraldo for their constant support and encouragements. I appreciate the support of all my friends in S22 and Rhodes University Chemistry Department. My special thanks are dedicated to my mother and grandmother for their unconditional love and for their constant prayers. I love you both very much.

I would also like to extend my gratitude to NRF for financial assistance**.**

ABSTRACT

Three non-peripherally substituted tin(IV) macrocylic compounds, octahexylphthalocyaninato dichlorotin(IV) **(35a)**, octahexyltetrabenzo-5,10,15-triazaporphyrinato dichlorotin(IV) **(35b)** and octadecylphthalocyaninato dichlorotin(IV) **(35c)** were synthesized and their photophysical and electrochemical behaviour studied. Complex **(35b)**, containing a CH group in place of one of the aza nitrogen atom of the phthalocyanine core, shows a split Q band due to its lower symmetry. The triplet state quantum yields were found to be lower than would be expected on the basis of the heavy atom effect of tin as the central metal for phthalocyanine derivatives (**35a** and **35c**). In contrast, **(35b)** shows a triplet quantum yield $\Phi_T = 0.78$. The triplet state lifetimes were solvent dependent, and were higher in THF than in toluene. Cyclic voltammetry and spectroelectrochemistry of the complexes revealed only ring based redox processes.

This thesis also reports on the microwave syntheses of tetrasulphonated tin phthalocyanine and tetrasulphonated tin α,β,γ-tetrabenzcorrole. The latter was only formed at low ratios (< 1:8) of 4-sulfophthalic acid to urea. Both complexes are aggregated in aqueous media, but can be partly or fully disaggregated by the addition of Triton X-100. The SnTSTBC complex has lower triplet life times and yields, while binding constant and quenching (of bovine serum albumin) constant are lower for SnTSTBC, compared to SnTSPc.

Finally Non-peripherally (α) tetra- **(40)** and octa-**(38a)** substituted dodecyl-mercapto tin(IV) phthalocyanines where synthesized and the electrochemical behavior studied.

Cyclic voltammetry and spectroelectrochemistry show ring-based reductions for **(38a)** and (**40)**; the former shows two ring oxidations, while the latter shows only one ring based oxidation. The adsorption kinetics of **(38a)** and **(40)** on a gold electrode have been investigated by electrochemical impedance spectroscopy (EIS). The equilibrium constant (*K*) for the adsorption and the Gibbs free energy (ΔG_{ads}) of the self-assembled monolayer (SAMs) were evaluated based on the Frumkin isotherm. The interaction factor between adsorbate –adsorbate molecules is also discussed.

TABLE OF CONTENTS

LIST OF ABBREVIATIONS

Abs	**-**	**absorbance**
Ac_2O	**-**	**acetic anhydride**
Ar	**-**	**aromatic**
Au	**-**	**gold working electrode**
BAS	**-**	**bioanalytical system**
BSA	**-**	**bovine serum albumin**
C E	**-**	**counter electrode**
$CHCl_3$	**-**	**chloroform**
CDCl3	**-**	**deuterated chloroform**
CPE	**-**	**constant phase element**
CV	**-**	**cyclic voltammogram**
DBU	**-**	**1, 8-diazabicyclo[5.4.0]undec-7-ene**
DCM	**-**	**dichloromethane**
DMF	**-**	**N, N-dimethylformamide**
DMSO	**-**	**dimethylsulphoxide**
EIS	**-**	**electrochemical impedance spectroscopy**
F	**-**	**fluorescence**
FFT	**-**	**fast fourier transform**
GCE	**-**	**glassy carbon electrode**
GPES	**-**	**general purpose electrochemical systems**
H_2O_2	**-**	**hydrogen peroxide**

H_2Pc	**-**	**metal-free phthalocyanine**
^1H-NMR	**-**	**proton nuclear magnetic resonance**
HOMO	**-**	**highest occupied molecular orbital**
HPLC	**-**	**high performance liquid chromatography**
hv	**-**	**absorption energy**
IC	**-**	**internal conversion**
ICP	**-**	**inductively coupled plasma**
IR	**-**	**infrared**
ISC	**-**	**intersystem crossing**
IUPAC	**-**	**International Union of Pure and Applied Chemistry**
LUMO	**-**	**lowest unoccupied molecular orbital**
M	**-**	**metal**
m	**-**	**multiplet**
MCPBA	**-**	**m-chloroperoxylbenzoic acid**
MPc	**-**	**metallophthalocyanine**
$MPcS_{mix}$	**-**	**differently sulphonated metallophthalocyanine**
MS	**-**	**mass spectroscopy**
MTBMPc	**-**	**tetrabenzyl mercapto phthalocyanine**
MTDMPc	**-**	**tetradodecyl mercapto phthalocyanine**
MTSPc	**-**	**tetra-sulfonated metallophthalocyanine**
NLO	**-**	**non-linear optics**
NMR	**-**	**nuclear magnetic resonance**
OCPc	**-**	**octachlorophthalocyanine**

OEPc	**-**	**octa(esterone)phthalocyanine**
OMPPc	**-**	**octa(o-methyl-phenoxy)phthalocyanine**
OPh	**-**	**phenyloxy**
OPPc	**-**	**octa(phenoxy)phthalocyanine**
OSWV	**-**	**Osteryoung square wave voltammetry**
OTos	**-**	**tosyl**
OTf	**-**	**triflate**
OTiPc	**-**	**oxotitanium(IV) phthalocyanine**
OTTLE	**-**	**optically transparent thin-layer electrode**
P	**-**	**phosphorescence**
PBS	**-**	**phosphate buffer solution**
Pc	**-**	**phthalocyanine**
PDT	**-**	**photodynamic therapy**
PP	**-**	**photoporphyrin**
PPh_3	**-**	**triphenylphosphine**
R E		**reference electrode**
s	**-**	**singlet**
S_0	**-**	**ground singlet state**
S_1	**-**	**excited singlet state**
RSH	**-**	**thiol derivatives**
SAM	**-**	**self-assembled monolayer**
SPh	**-**	**thiophenyl**
SWV	**-**	**square wave voltametry**

t	**-**	**triplet**
T_1	**-**	**excited triplet state**
$TBABF_4$	**-**	**tetrabutylammonium tetrafluoroborate**
TBC	**-**	**triazatertrabenzcorrole**
TBTAP	**-**	**tetrabenzotriazaporphyrin**
t-Bu	**-**	**tertiary-butyl**
TCPc	**-**	**tetracarboxyphthalocyanine**
THF	**-**	**tetrahydrofuran**
TLC	**-**	**thin column chromatography**
TNPc	**-**	**tetranitrophthalocyanine**
TPPz	**-**	**tetrapyridylporphyrazine**
TSPc	**-**	**tetra sulfonated phthalocyanine**
UV/Vis	**-**	**ultraviolet/visible**
W E	**-**	**working electrode**
VR	**-**	**vibrational relaxation**

LIST OF SYMBOLS

A	**-**	**geometric or real surface area**
Anal	**-**	**analyte**
C	**-**	**concentration**
C_d	**-**	**double-layer capacitance**
D	**-**	**diffusion coefficient**
E	**-**	**potential**
$E_{1/2}$	**-**	**half-wave potential**
E_{pa}	**-**	**anodic peak potential**
E_{pc}	**-**	**cathodic peak potential**
F	**-**	**Faradays constant**
f	**-**	**frequency**
Hz	**-**	**hertz**
I	**-**	**current**
I	**-**	**intensity**
I(t)	**-**	**sinusoidal current**
I_o	**-**	**incident intensity**
I_o	**-**	**maximum current amplitude**
I_p	**-**	**peak current**
I_{pa}	**-**	**anodic peak current**
I_{pc}	**-**	**cathodic peak current**
j	**-**	**complex number**

K	**-**	**Kelvin**
K	**-**	**adsorption equilibrium constant**
K_b	**-**	**binding constant**
K_{SV}	**-**	**Sternvolmer constant**
$\mathbf{K_D}$	**-**	**dimerization constant**
k_Q	**-**	**bimolecular rate constant**
n	**-**	**Number of binding site**
Q	**-**	**charge**
R	**-**	**universal gas constant**
$\mathbf{R_{ct}}$	**-**	**charge transfer resistance**
$\mathbf{R_E}$	**-**	**electrolyte or solution resistance**
$\mathbf{r_a}$	**-**	**pinhole size**
$\mathbf{r_b}$	**-**	**Distance between pinholes**
T	**-**	**double layer capacitance quantity**
$\nu_{\max}$	**-**	**wavenumber of maximum absorption**
v	**-**	**scan rate**
V	**-**	**volts**
V	**-**	**volume**
V(t)	**-**	**sinusoidal potential**
$\mathbf{V_o}$	**-**	**maximum potential amplitude**
Z	**-**	**impedance (or complex resistance)**
Z'	**-**	**real component**

Z''	**-**	**imaginary component**
Z_w	**-**	**Warburg impedance**
α	**-**	**transfer coefficient**
ΔE_p	**-**	**anodic to cathodic peak potential separation**
ε	**-**	**extinction coefficient**
ε_D	**-**	**dimer extinction coefficient**
ε_M	**-**	**monomer extinction coefficient**
ε_S	**-**	**singlet extinction coefficient**
ε_T	**-**	**triplet extinction coefficient**
λ_{max}	**-**	**maximum wavelength**
ω	**-**	**radial frequency**
Γ_{SAM}	**-**	**surface coverage**
θ	**-**	**phase angle**
θ	**-**	**surface coverage**
π (π*)	**-**	**pi bonding (anti-pi bonding)**
ΔG_{ads}	**-**	**Gibbs free energy of adsorption**
σ	**-**	**Warburg coefficient**
Ω	**-**	**ohm**
δ	**-**	**interaction parameter between adsorbed molecules**
η	**-**	**refractive index**
τ_0	**-**	**absorption band area**
τ_F	**-**	**fluorescence life time**

τ_T	-	**triplet life time**
Φ_d	-	**photodegradation quantum yield**
Φ_F	-	**fluorescence quantum yield**
Φ_T	-	**triplet quantum yield**
Φ_{IC}	-	**Quantum yield of intersystem crossing**

LIST OF FIGURES

LIST OF SCHEMES

LIST OF TABLES

CHAPTER ONE: INTRODUCTION

Introduction

1.1. Discovery and History of Phthalocyanines

Phthalocyanines (Pcs) are remarkable macrocyclic compounds that possess interesting physical and chemical properties. Their bright colours, conductivity, chemical and thermal stability have made them very desirable for many applications. Phthalocyanines continually find their usefulness in contemporary and emerging technologies such as, catalysis [1], photodynamic therapy (PDT) [2], nonlinear optics [3], gas sensors [4], thermal writing displays [5] and solar cells [6]. There are differing views on when the first phthalocyanine was discovered. According Linstead the first phthalocyanine was discovered by chance (in 1928 by a company known as Messrs. Scottish Dyes, Ltd.) during an industrial production of phthalimide [7, 8]. Other views hold that the first phthalocyanine was discovered (in 1907) accidentally by von Braun and Tscherniac [9, 10], as a by-product, during the preparation of ortho-cyanobenzamide **(2)** from phthalamide **(1)** (**Scheme 1.1**).

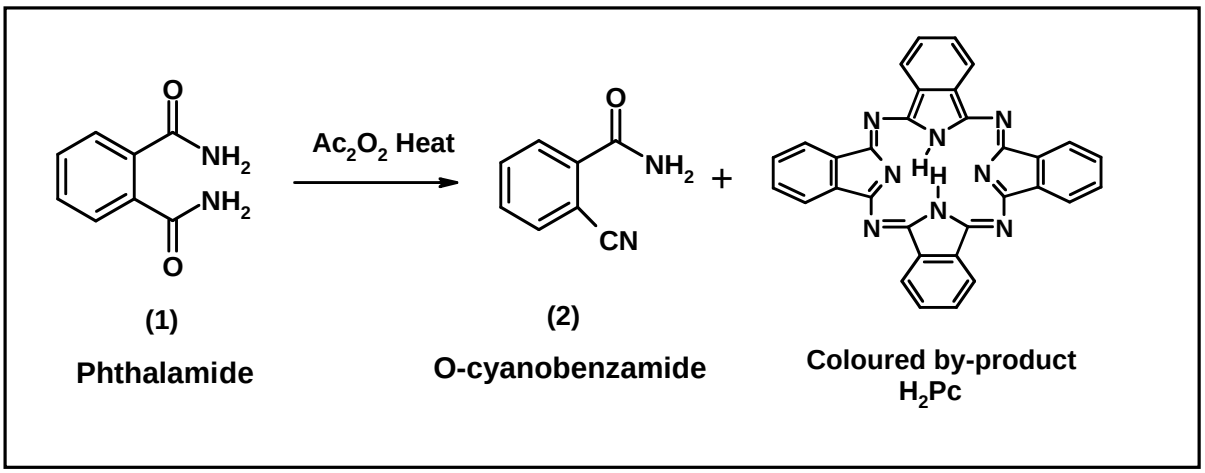

Scheme 1.1: First synthesis of phthalocyanine.

The latter date (1907) makes sense since in 1927 de Diesbach and von der Weid of Freibourg University reported an insoluble copper derivative during the cyanation of ortho-dibromobenzene with copper cyanide in refluxing pyridine [11]. In this period, however, the structure of the phthalocyanine had not been elucidated. The structure of the unmetallated phthalocyanine was elucidated by Linstead *et al*. [12] by performing various chemical analysis techniques. The unmetallated phthalocynine structure was confirmed by X-ray diffraction techniques performed by J. M. Robertson [13].

1.2. Origins of Spectra of Phthalocyanines

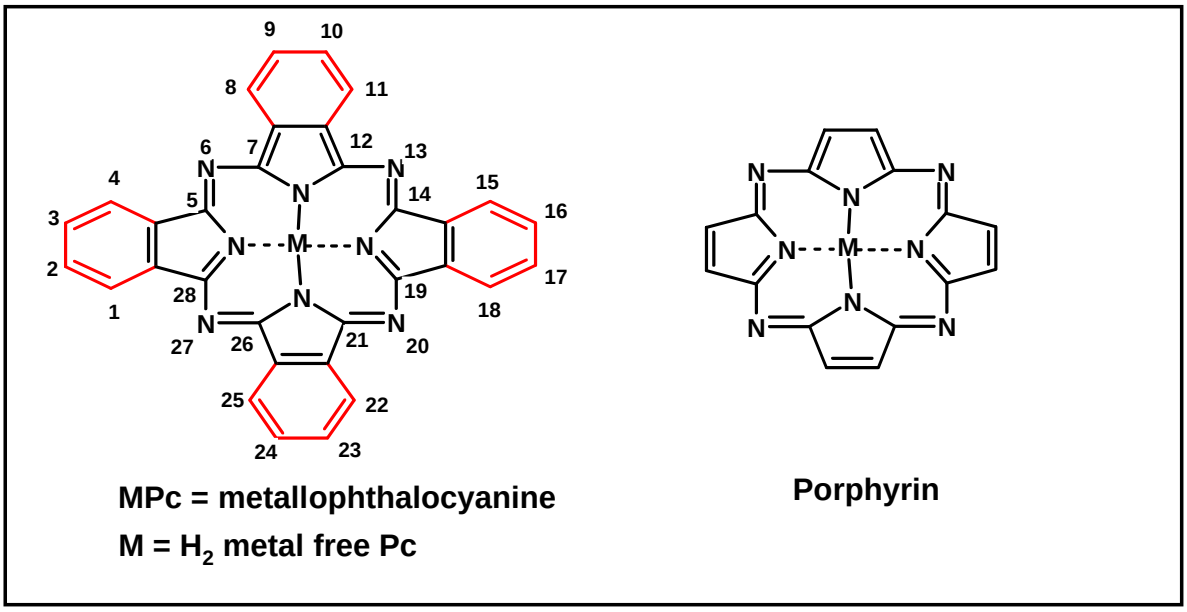

Figure 1.1: Phthalocyanine and tetrazaporphyrin systems.

The inner aromatic ring is responsible for the intense blue-green colour of these macrocycles ($\pi - \pi^*$ transition occurring in the visible region). The phthalocyanine ring is numbered following the International Union of Pure and Applied Chemistry (IUPAC) nomenclature of tetrapyrroles **(Figure 1.1)** [14]. The presence of four benzyl groups

causes solubility and aggregation problems. By substituting functional groups on the periphery of the molecule, solubility can be improved considerably. When a phthalocyanine is coordinated to a central metal it is referred to as metallophthalocyanine (MPc). Most MPc complexes used in photodynamic therapy (PDT) contain non-transition metals in the center. However, mainly Zn, Al, Si Pcs have been explored for PDT. Sn macrocyclic complexes have received less attention as PDT photosensitizers, hence the aim of this thesis is to explore SnPc and related Sn macrocycles as possible photosensitizers, because Sn macrocycles of the porphyrin type (e.g. tin etiopurpurin (SnEt2) [15]) has been used in PDT.

Phthalocyanines generally have two major absorption bands at **660 – 730** nm named the Q band and another at **340 – 450** nm, called the Soret band or B band. The Q band and the B bands occur due to $\boldsymbol{\pi - \pi^*}$ transitions **(see Figure 1.2)**. The Q band arises from $\mathbf{a_{1u}} \longrightarrow \mathbf{e_g}$ transition and the B band arises from $\mathbf{a_{2u}} \longrightarrow \mathbf{e_g}$ and $\mathbf{b_{2u}} \longrightarrow \mathbf{e_g}$ transitions **(see Figure 1.2)**. It is known that the introduction of a metal ion inside the cavity will generate a slight blue shift of the Q band. This occurs because the introduction of a metal ion reduces the electronic density. It has been demonstrated that the more electronegative the metal ion is, the more the blue shift. Some compounds have their metal ions outside the cavity, for example, lead Pcs, often show a red shifted Q band.

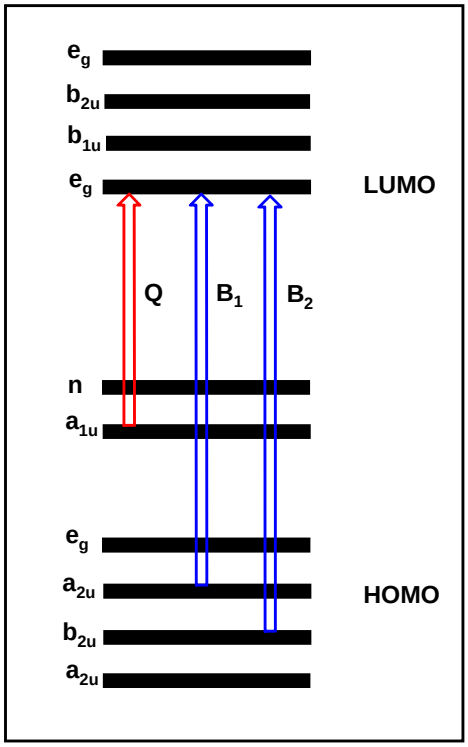

Figure 1.2: Schematic representation of energy levels and origins of Q and B band.

An unmetallated Pc is not symmetrical because it possess D_{2h} symmetry while a metallated Pc is symmetrical and it possess D_{4h} symmetry. The symmetry of the phthalocyanine plays an important role in explaining the number of Q bands observed for metallated and unmetallated Pcs. Due to the lack of symmetry of unmetallated phthalocyanine, the energy levels are not degenerate, therefore giving rise to two Q bands. The symmetry of the metallated phthalocyanine causes the energy level to be degenerate, therefore the two Q bands collapse into one Q band **(Figure 1.3)**. Substitution on the benzene ring gives rise to a shift (bathochromic or hypsochromic shift depending on the type of functional group substituted) of the Q-band relative to unsubstituted Pc. Non-peripheral substitutions show greater shift than peripheral substitutions [16].

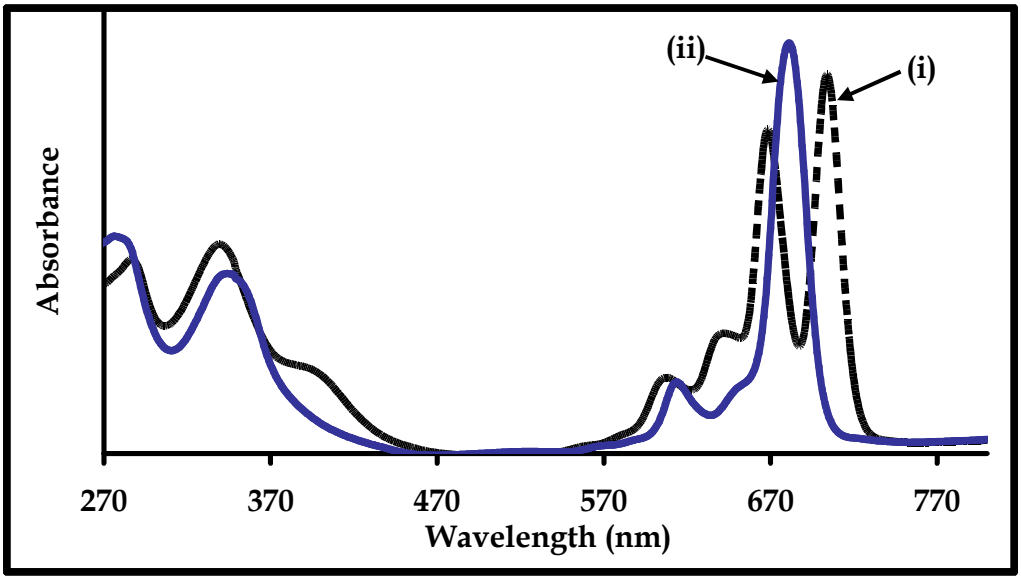

Figure 1.3: Absorption spectra of unmetallated phthalocyanine (i) and metallated (ii).

At high concentrations Pcs tends to self-associate (aggregate), this is indicated by a blue shift of the Q band because the Pc macrocycles align co-facially. This can be explained by the use of a vector model, to depict a weak electron overlap between two Pc rings (molecular exciton coupling theory) [17, 18]. To form the simplest aggregate, the dimer, the dye-dye interaction must be strong enough to overcome other forces which would favor solvation of the monomer [19]. Solvation is generally known to interfere with dimerization – in water the dye-dye interaction is probably not the major force driving the molecules towards aggregation, instead the strong solvent-solvent interaction tends to exclude the dye molecules from the solution and causes them to aggregate.

When the distance between two molecules is sufficiently small, their excited states will interact such that two new exciton splitting energy levels (E" and E') are generated as

shown in **Figure. 1.4**. This splitting is dependent on the intensity of the Pc transition moments, the separation of the two molecules and their relative orientation to each other.

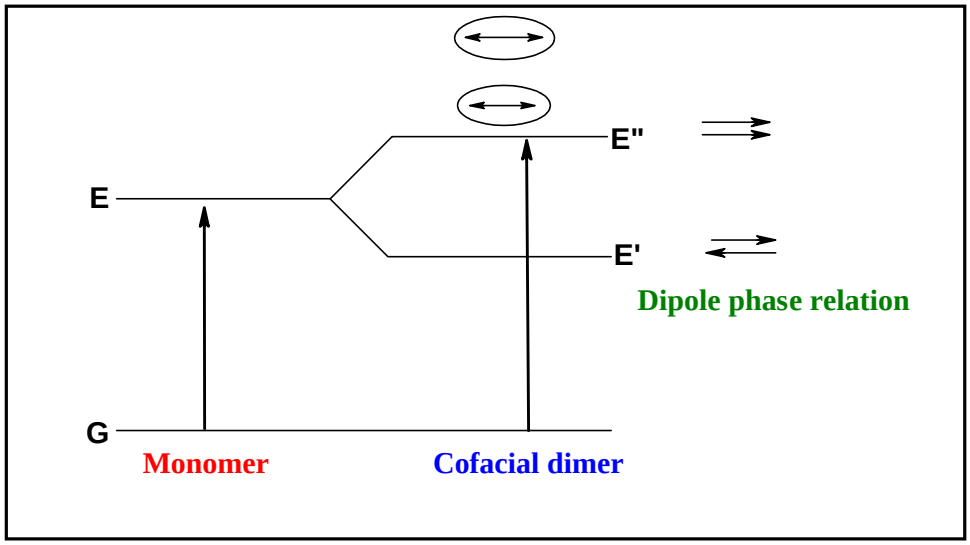

Figure 1.4: Excitation coupling of co-facial Pcs.

The dipoles might be out of phase or in phase. When they are out of phase this will cause a lowering of energy (E') and when they are in phase this will result in raising of energy (E"). The transition moment to E' becomes zero and the transition to it becomes forbidden. This will result in an absorption spectrum that is blue shifted (higher energy). When the molecules are arranged in a co-planar arrangement (**Figure.1.5**) the opposite is observed. The transition to the energy (E") is forbidden because the transition dipole equals zero. Only the transition to E' is allowed resulting in the red shift of the absorption spectrum.

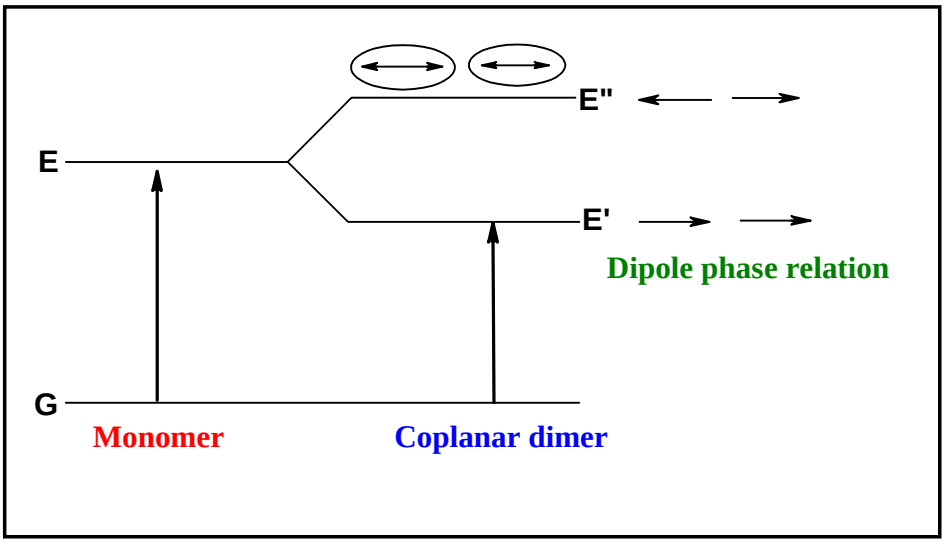

Figure 1.5: Exciton coupling of coplanar Pcs

In the solid state there is a reduction in the degree of freedom compared to liquid state, therefore the transition moments may not equal zero. This implies that the transition E" and E' are allowed. This is the reason for the observation of blue and red shifts as a split Q band, this is called Davydov splitting [17, 18] **(Figure. 1.6**).

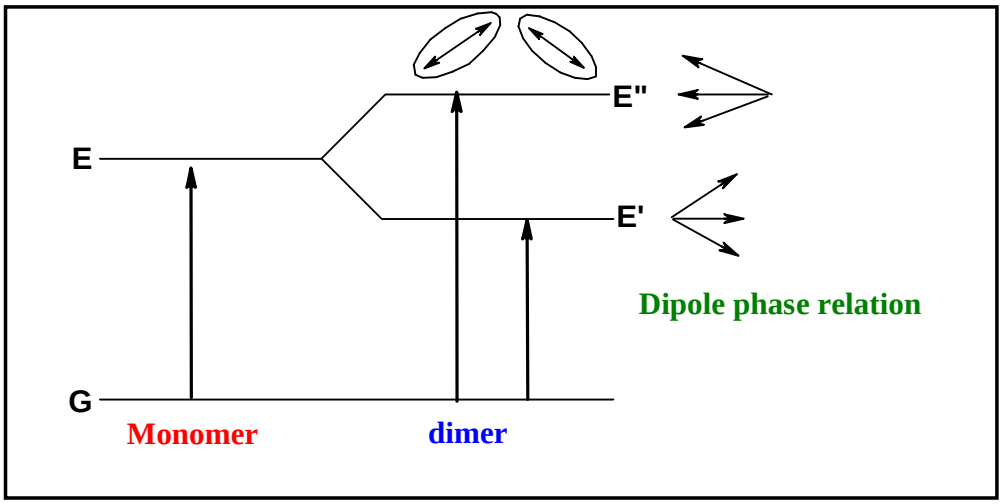

Figure 1.6: Exciton coupling of obliquely arranged Pcs.

The Davydov splitting is the splitting of bands in the electronic or vibrational spectra of crystals due to the presence of more than one equivalent molecular entity in the unit cell.

1.3 Structure and Spectra of Macrocycles Derived from Changes in the Structure of Pcs.

Pcs, benzocorroles (TBC) and triazaporphyrins (TBTAP) complexes of Sn are discussed in this thesis. Pcs are known for over 70 metals and metalloids, while TBC and TBTAP of the form shown in **Figure 1.7** are rare (**Table 1.1)**.

Table1.1. Table of known TBTAP and TBC complexes.

(a) TBTAP complexes

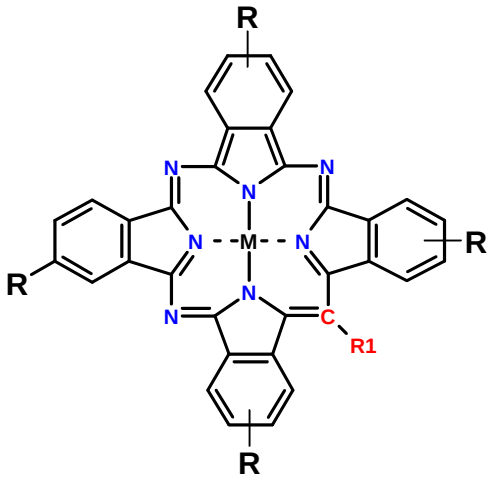

R	R1	Metal	Reference
R = H	R1 = H	M = H_2	[20]
R = $OCH_2C(CH_3)_3$	R1 = $CH_2CH_2CH_3$	M = Mg	[21]
R = $OCH_2C(CH_3)_3$	R1 = $(CH_2)_{14}CH_3$	M = H_2	[21]
R = ^{t}Bu	R1 = $(CH_2)_{14}CH_3$	M = H_2	[21]
R = H	R1 = $(CH_2)_{14}CH_3$	M = Mg	[21]
R = ^{t}Bu	R1 = Ph	M = H_2	[21]
R = H	R1 = Ph	M = Mg	[21]

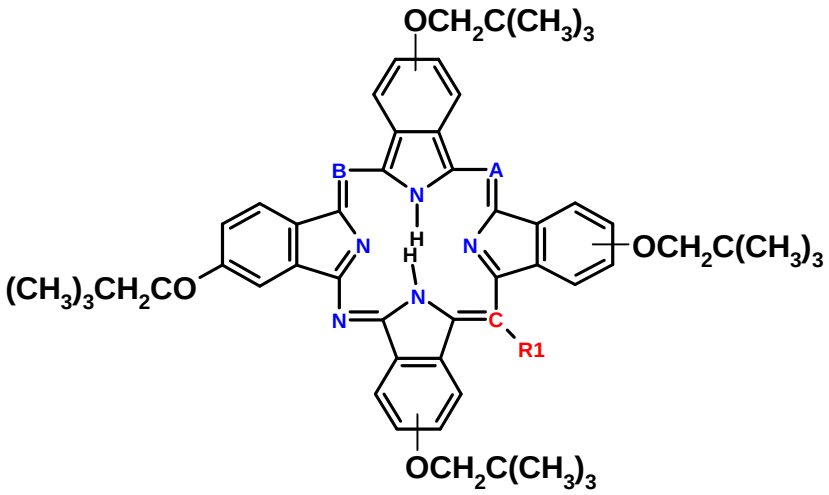

R1	A	B	Reference
R1 = $(CH_2)_{14}CH_3$	A = C-R1	B = N	[21]
R1 = $(CH_2)_{14}CH_3$	A = N	B = C-R1	[21]

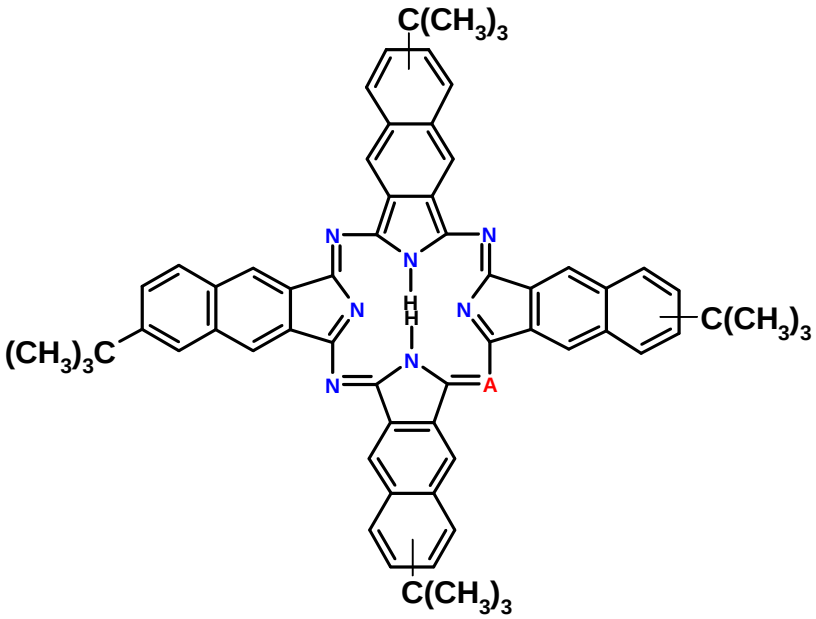

A	Reference
A = N	[21]
A = C-$(CH_2)_{14}CH_3$	[21]

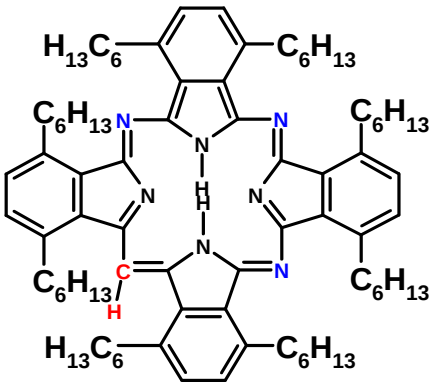

[22]

(b) TBC complexes

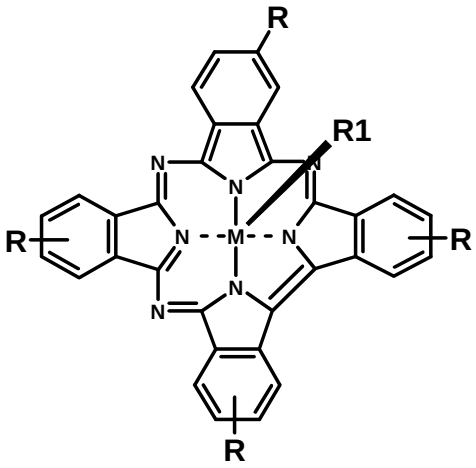

Complexes	Metal	Reference
Ge(OH)TBC	M = Ge, R1 = OH	[23]
Ge(F)TBC	M = Ge, R1= F	[23]
Si(OH)TBC	M = Si, R1 = OH	[23]

Complexes	Metal	Reference
TBCAl	M = Al, R =H	[23]
POTBC	M = P=O, R = H	[24]
$POTBCS_4$	M = P=O, R = SO_3H	[25]

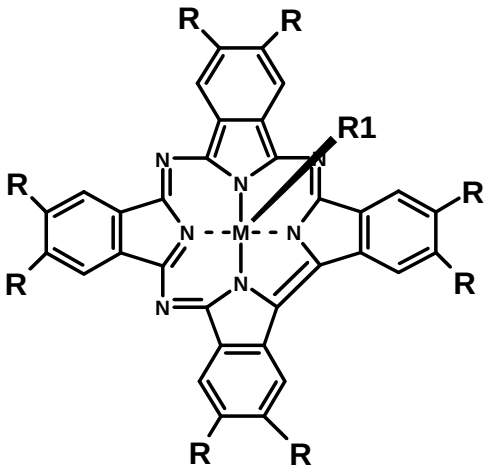

Complex	Metal	Reference
$Si(OH)TCB(C_5H_{11})_8$	M = Si, R = pentyl, R1 = OH	[26]

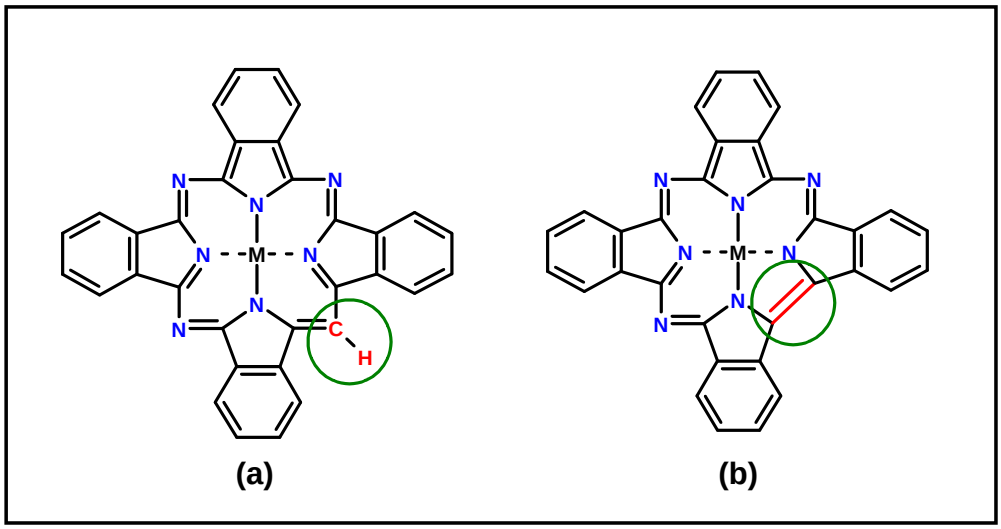

Figure 1.7: Tetrabenzo[5,10,15]triazaporphyrin (MTBTAP) (a) and α, β, γ – Triazatetrabenzcorrole (MTBC) (b) systems.

A replacement of nitrogen atom, at the meso position, with a methine group leads to a formation of tetrabenzo[5,10, 20]triazaporphyrin (TBTAP)**(Figure 1.7a)** [21]. This single meso-carbon may provide an additional site for the attachment of substituent groups, however, there is no substantial evidence in literature that proves that this type of substitution can occur once the TBTAP has formed. Leznoff and Mackeown [21] showed that the introduction of alkyl and aryl substituents attached to the meso-carbon is possible. This is achieved by treating a variety of phthalonitriles with different Grignard reagents to form tetrabenzotriazaporphyrin ring, as metal free or magnesium derivatives. Substituting sterically bulky groups at the peripheral benzo position of a TBTAP may produce derivatives which are readily soluble in organic solvents.

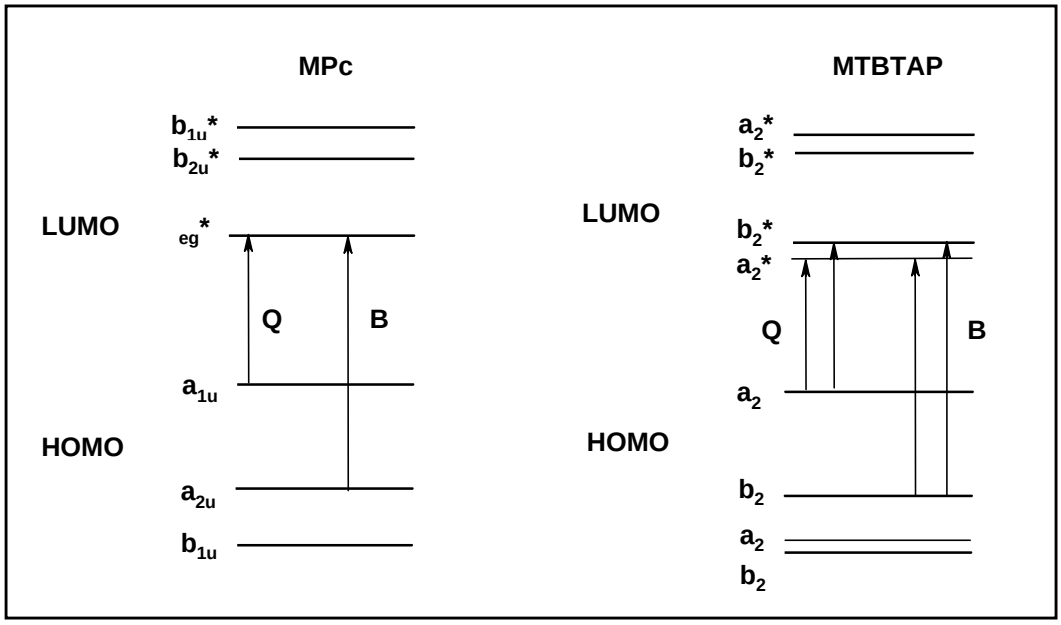

Figure 1.8: Ground state electronic energy levels of MPc and MTBTAP.

The electronic energy levels of MTBTAP have been studied extensively by Mark *et al*. [27]. **Figure 1.8** shows the difference between the energy levels of MPc and MTBTAP. The model predicts that for MTBTAP we should observe two transitions for the Q and B bands. This means that we should observe a split Q and B band from the ground state absorption spectra of MTBTAP.

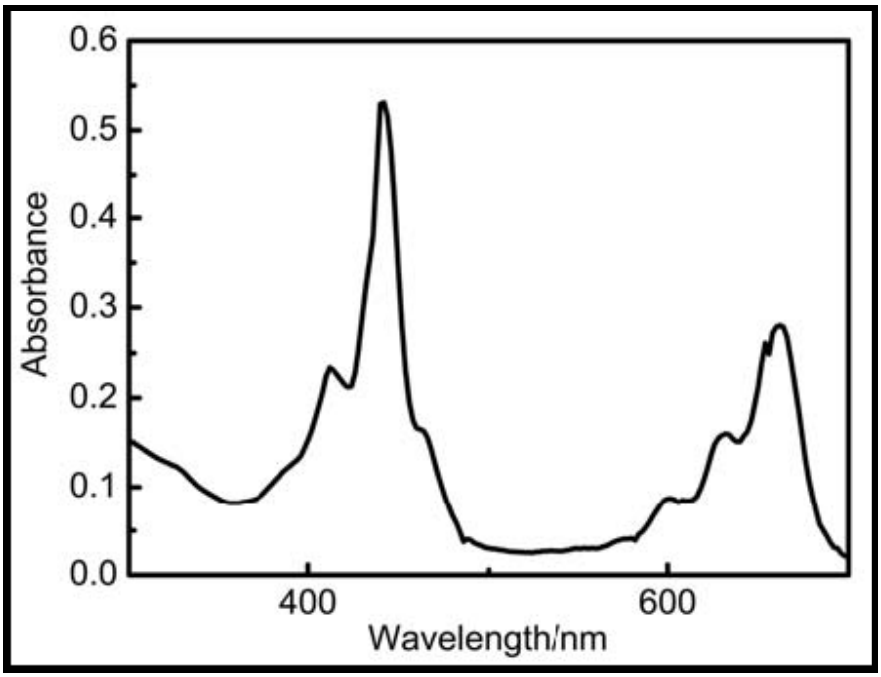

Figure 1.9: UV/vis spectra of oxophosphorus(V) tetrasulfotriazatetraben corrole ($POTBCS_4$) [25].

The splitting of the Q and B band of MTBTAP is due to a loss of symmetry since one of the azamethine nitrogen is replaced by a carbon atom. Changes in the phthalocyanine inner aromatic ring (**Figure 1.1**) can lead to interesting spectral changes. By losing one of the phthalocyanine nitrogens we form a macrocycle known as α, β, γ – triazatetrabenzcorrole (TBC) (**Figure 1.7b**) which has a unique absorption UV/vis spectra, displaying a very sharp absorption band around 448 nm (Soret band : **Figure 1.9**) with an intensity nearly twice that of the Q band [28, 29]. Synthesis of Ge, Si, Ga, and Al TBC complexes have been reported by Fujiki *et al*. [23] and Li *et al*. [30]. Attempts to prepare SnTBC were unsuccessful, hence, in this work the complex is prepared by microwave synthesis.

The energy levels giving rise to Q and B band of MTBC have not been reported extensively in literature. Fujiki *et al*. [30] briefly discuss the energy level but do not make use of molecular orbital calculations for determining energy levels. MTBC chemistry can be used to understand biological systems, such as vitamin B_{12} coenzyme models [31].

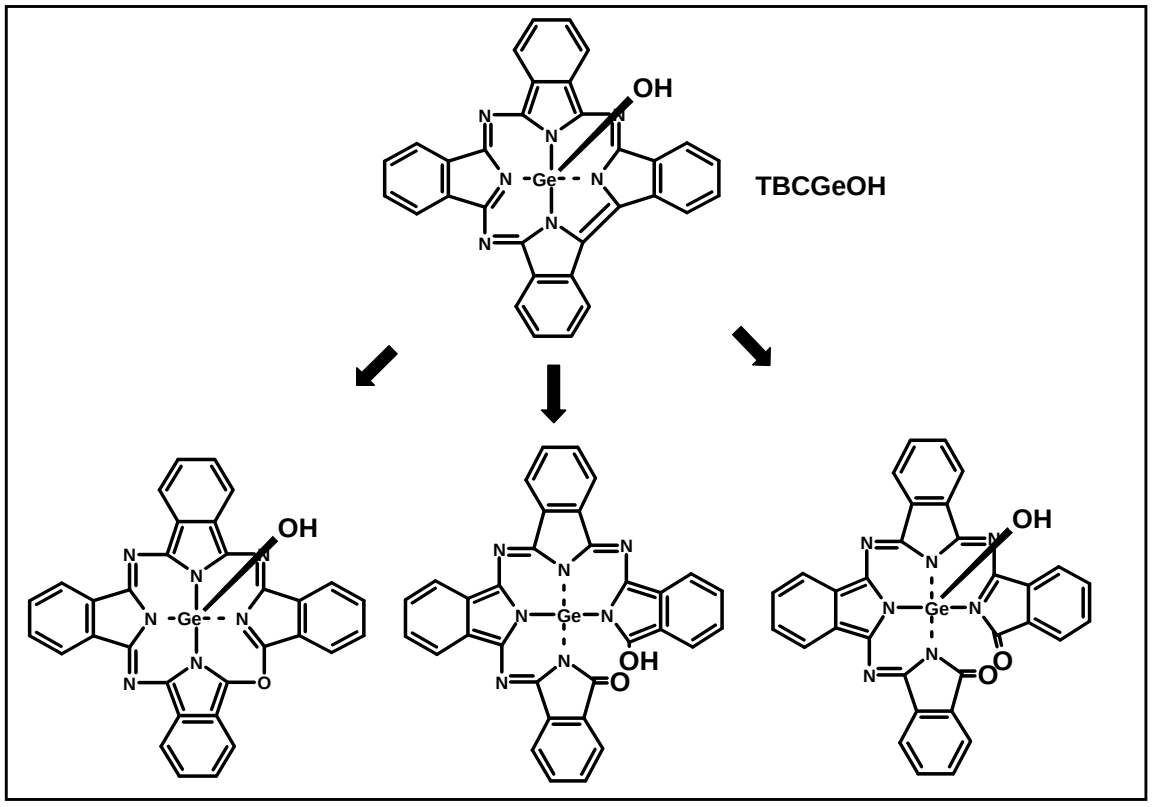

Figure 1.10: Proposed structures of ring cleaved and ring expanded compounds [30].

Complexes with the inner *meso*-nitrogen replaced by O have also been reported [30], **Figure 1.10**.

Fujiki *et al*. [30] proposed that TBCGeOH is not stable in the presence of light and easily decomposes to form a ring cleaved or ring expanded TBCGeOH complex, which is red in colour. The predicted structures of ring cleaved or ring expanded TBCGeOH are shown in **Figure 1.10**. However, the ring cleaved compounds in **Figure 1.10** could not be

isolated due to their strong adhesion in the silica gel column. **Table1.1** shows a list of ring contracted compounds that are substituted with different alkyl subtituents at the meso carbon and known TBC complexes.

1.4 Phthalocyanine Synthesis

Pc complexes may be synthesised from a wide variety of starting materials. The synthetic route that is generally used involves the use of unsubstituted or substituted phthalonitrile (or dicyanobenzene) derivatives as starting materials to produce unsubstituted Pc or peripherally and non-peripherally substituted molecules. Phthalonitrile forms phthalocyanines under various conditions, **Scheme 1.2**.

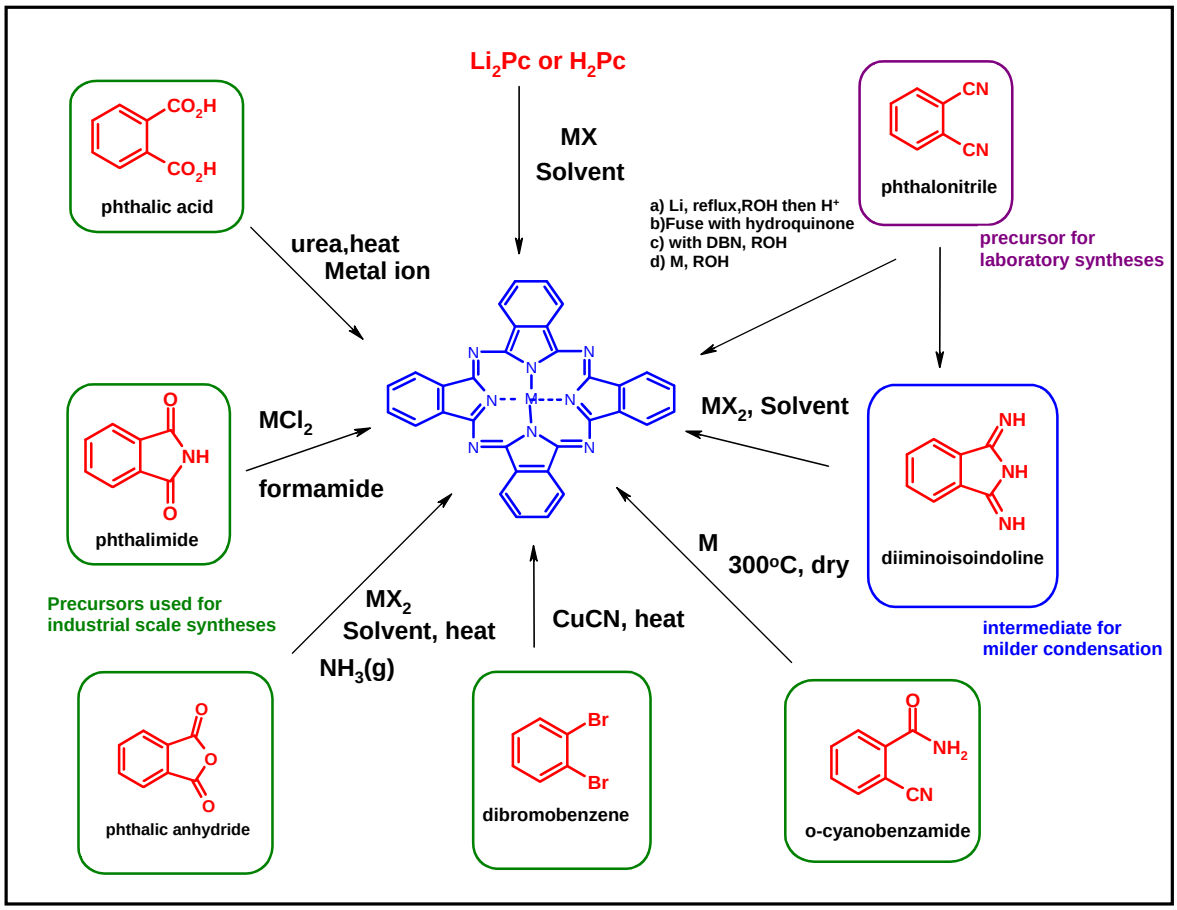

Scheme 1.2: General phthalocyanine synthesis.

1.4.1 Synthesis of Tetrasubtituted Phthalocyanine

Substituted phthalocyanines can be prepared by direct substitution of a preformed phthalocyanine or by using appropriately substituted precursors eg. phthalonitrile.

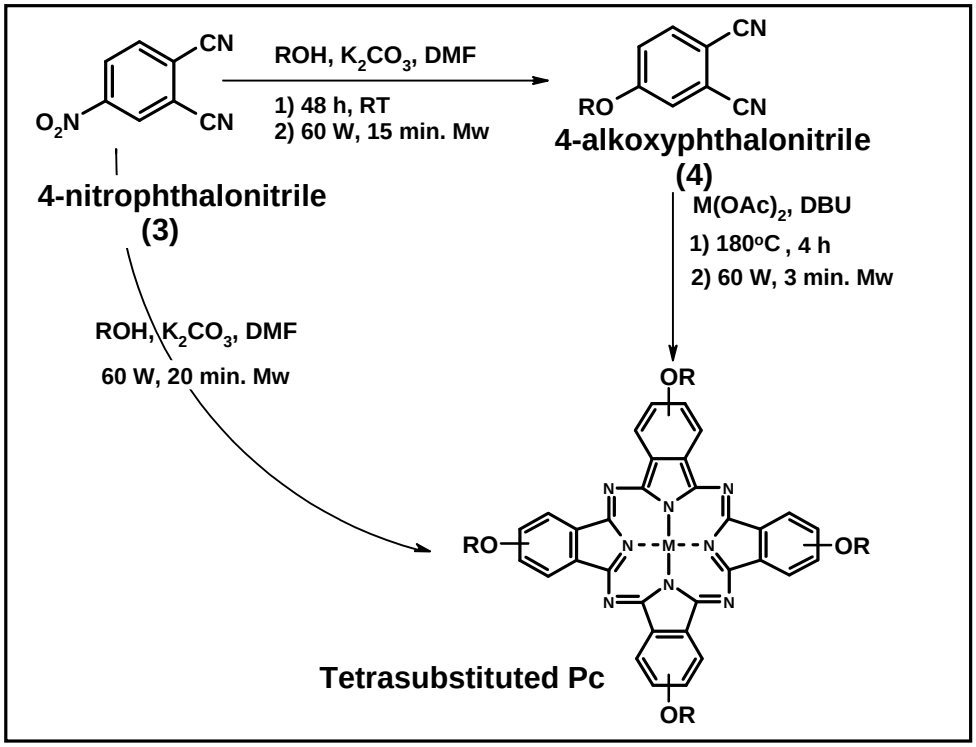

Scheme 1.3: Microwave assisted synthesis of tetrasubstituted phthalocyanine.

Preparation of tetrasubstituted phthalocyanines (isomers) uses nucleophilic aromatic substitution of 4-nitrophthalonitrile **(3)** with an alcohol to produce the 4-alkoxyphthalonitrile precursor **(4)** (**Scheme 1.3**) [32]. Monosubstitution at the 3-position will lead to four single isomers of (C_{4h}) 1, 8, 15, 22-, (D_{2h}) 1, 11, 15, 25-, (C_{2v}) 1, 11, 18, 22- and (C_s) 1, 8, 18, 22- tetrasubstituted complexes. Substitution at the 4-position, single isomers of tetrasubstituted complexes are obtained ((C_{4h}) 2, 9, 16, 23-, (D_{2h}) 2, 10, 16, 24-, (C_{2v}) 2, 9, 17, 24- and (C_s) 2, 9, 16, 24-).

Preparation of phthalonitriles **(4)** or phthalocyanines can also be performed by using microwave irradiation (Mw) [33]. **Table 1.2** shows a list of examples of known MPcs synthesised by using microwave radiation. The table includes octa and tetrasubstituted derivatives.

Table 1.2: A list of examples of known Pcs synthesizes by the use of microwave radiation.

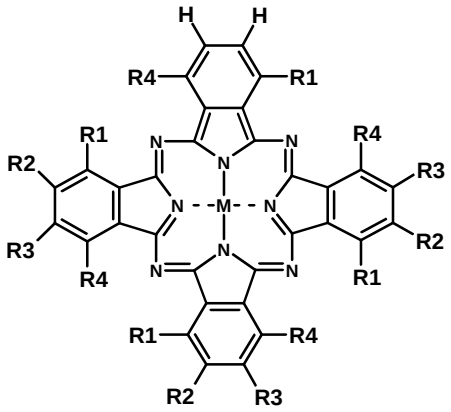

R1 and R2	Complexes	Metal	Reference
R1 = R4 = H, R2 = R3 = Cl	$MPcCl_8$	M^{+2}: Fe, Co, Ni, Cu, Zn	[34]
R1 = R2 = R3 = R4 = Cl	$MPcCl_{16}$	M^{+2}: Fe, Co, Ni, Cu	[34]
R2 = R3 = R4 = H, R1= NO_2	M(TNPc)	M^{+2}: Fe, Co, Ni, Cu, Pd	[34]

MTNPc = tetranitrometallophthalocyanine

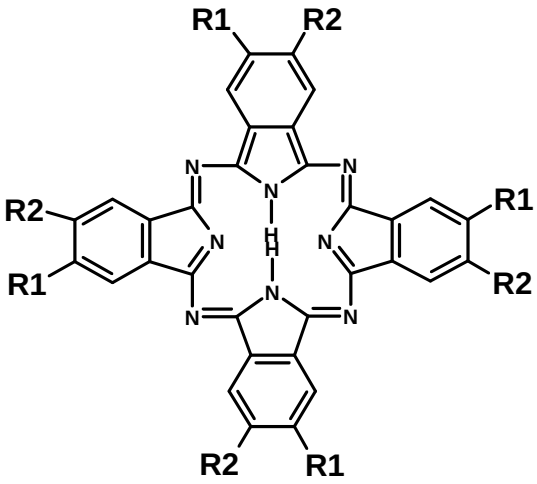

R1	Complexes	Reference
R1 = H, R2 = NO_2	Tetra	[35]
R1= H, R2 = OPh	Tetra	[35]
R1 = H, R2 = SPh	Tetra	[35]
R1 = H, R2 = t-Bu	Tetra	[35]
R1 = Cl, R2 = Cl	Octa	[35]

OPh = phenyloxy, SPh = thiophenyl, t-Bu = tertiary-butyl

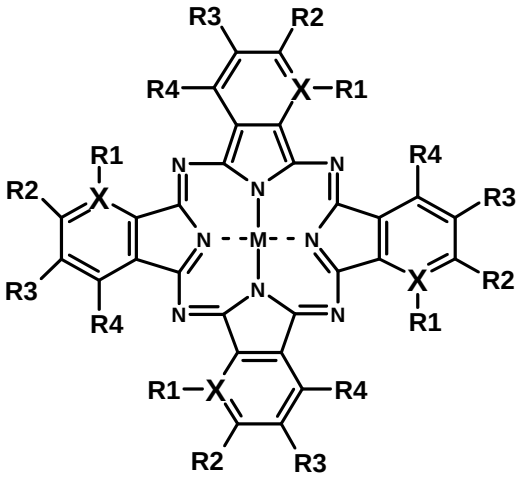

R1, R2 and R3	Complexes	X = N or C and Metal	Reference
R1 = R3 = R4= H, R2 = COOH	TCPcM	X = C M = Co	[36]
R2 = R3 = R4 = H, R1 = NO_2	3-TNPcM	X = C M = Fe	[36]
R1 = R3 = R4 = H, R2 = NO_2	4-TNPcM	X = C M = Fe	[36]
R1 = R4 = H, R2 = R3 =Cl	4,5-OCPcM	X = C M = Fe	[36]
R1 = R2 = R3 = R4 = H	TPPzM	X = N M = Fe	[36]

TCPc = tetracarboxyphthalocyanine, TNPc = tetranitrophthalocyanine, OCPc = octachlorophthalocyanine, TPPz = tetrapyridylporphyrazine

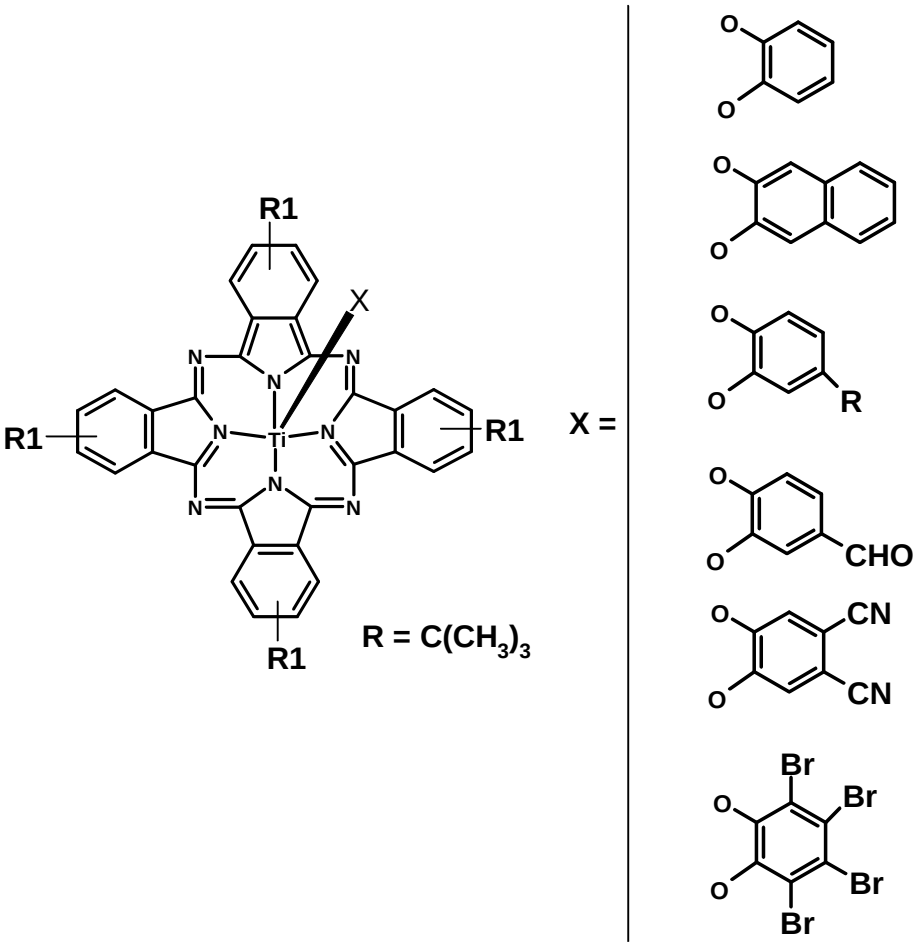

[37]

1.4.2 Syntheses of Peripherally Octasubstituted Phthalocyanines

Unlike tetrasubstituted phthalocyanines, octasubstituted phthalocyanines can easily be purified because only one isomer is obtained. 4, 5-Dichlorosubstituted phthalonitrile **(7)** is generally required to synthesise the phthalocyanine. New precursors can be synthesised by substituting different functional groups on the 4, 5 positions of the phthalonitrile. There are different methods of synthesising the precursors **(**disubstited phthalonitrile**)**, but only one method, developed by Wohrle *et al*. [38], will be discussed.

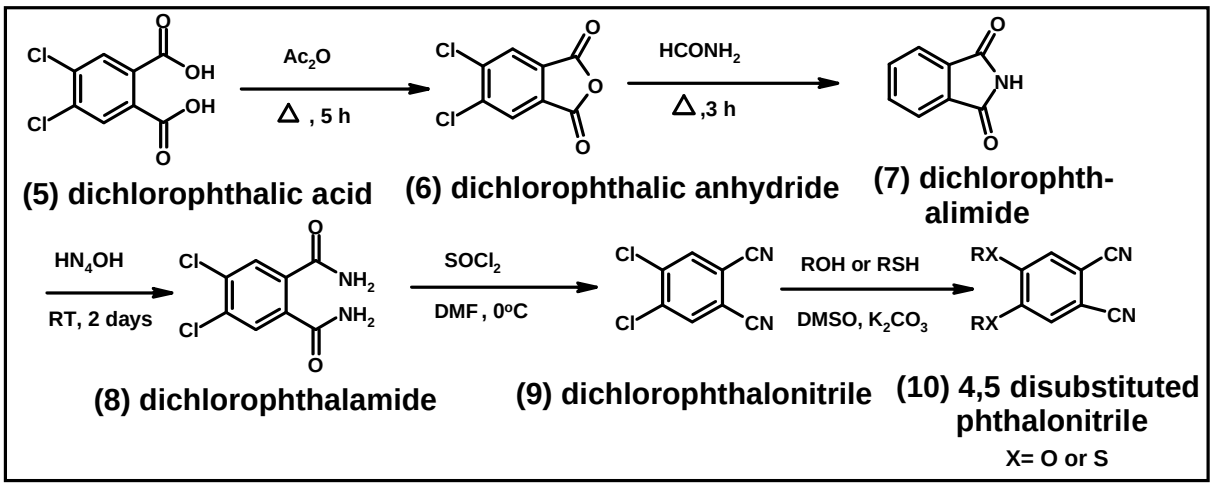

Scheme 1.4: Synthesis of disubstituted phthalonitriles.

Wohrle's method (**Scheme 1.4**) involves the use of commercially available 4, 5-dichloropthalic acid **(5)** followed by dehydration to dichlorophthalic anhydride **(6)** and the formation of dichlorophthalimide **(7)**. Formamide is used as a solvent and a source of ammonia during formation of the phthalimide **(7)**. Addition of ammonia solution results in the formation of dichlorophthalamide **(8)** which is dehydrated to form dichlorophthalonitrile **(9).** The 4, 5-dichlorophthalonitrile **(9)** undergoes nucleophilic displacement reaction with a variety of alcohols or thiols to give **(10)** [38]. 4, 5-Dichlorophthalonitrile can also be purchased. **Scheme 1.5** shows the formation of a

metallated MPc using precursor **(10)**, which is substituted with alkylthio or alkoxy derivatives.

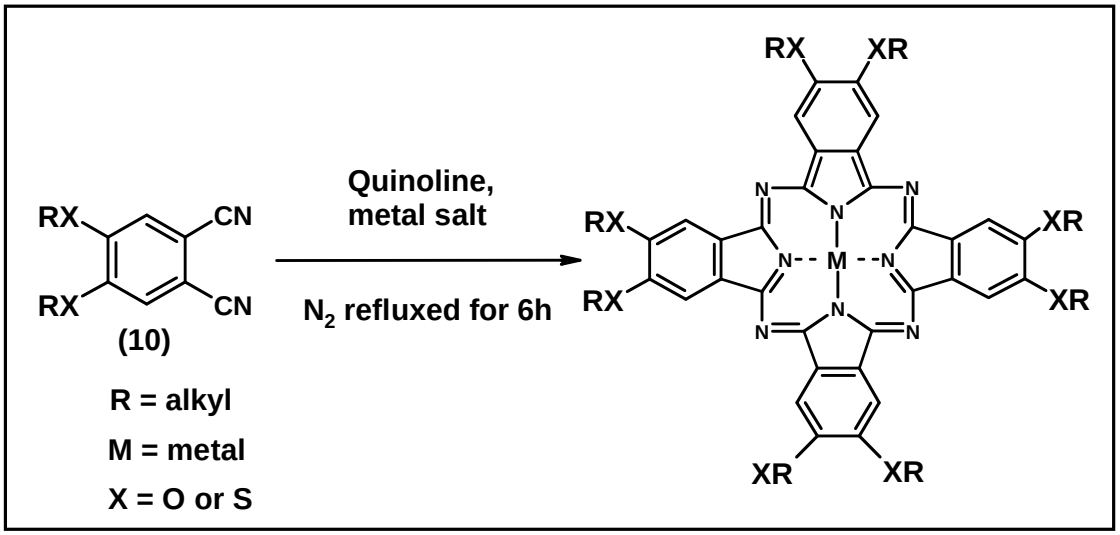

Scheme 1.5: Synthesis of metallated MPc using precursor (10).

In this work the synthesis of sulfur (S) substituted SnPc will be reported. **Table 1.3** shows a list of known MPcPc$(SR)_n$ (n = 4 or n = 8).

Table 1.3: A list of known MPc$(SR)_n$ (n = 4 or n = 8)

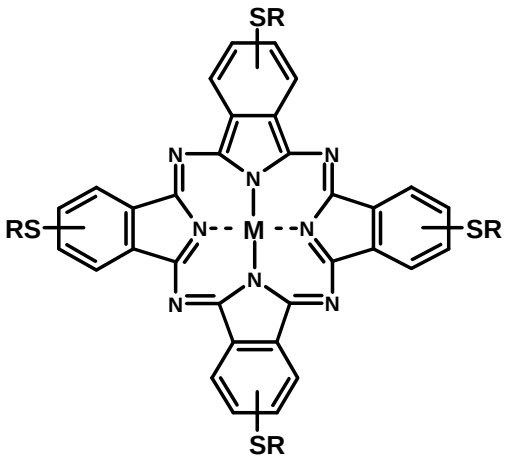

MTBMPcs, R =

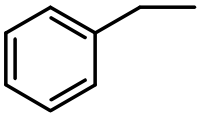

MTDMPcs, R = $C_{12}H_{25}$

Complexes[a]	**Reference**
$CoPc(SC_4H_9)_8$	[39]
$CoPc(SC_2H_4OH)_8$	[39]
$FePc(SC_4H_9)_8$	[40]
$FePc(SC_2H_4OH)_8$	[41]
CoTBMPc	[42]
CoTDMPc	[42]
FeTBMPc	[42]
FeTDMPc	[42]
MnTBMPc	[42]
MnTDMPc	[42]
NiTBMPc	[42]
NiTDMPc	[42]
ZnTDMPc	[42]
$ZnPc(SC_4H_9)_8$	[43]
α -$PbPc(SC_6H_{13})_8$	[44]
α -$ZnPc(SC_6H_{13})_8$	[44]
α -$InClPc(SC_6H_{13})_8$	[44]
α -$CuPc(SC_6H_{13})_8$	[44]
$TiOPc(SCH_2Ph)_4$	[45]
$TiOPc(SPh)_4$	[45]
α -$TiOPc(SCH_2Ph)_4$	[45]
α -$TiOPc(SPh)_4$	[45]

Complexes[a]	Reference
$TiPc(SC_5H_{11})_8$	[46]
$MnPc(SC_5H_{11})_8$	[46]

[a]MTBMPc = tetrabenzyl mercapto phthalocyanine, MTDMPc = tetradodecyl mercapto phthalocyanine.

1.4.3 Syntheses of Non-peripherally Octasubstituted Phthalocyanines

In this thesis Pc that are non-peripherally substituted with SR or C-C bonds were developed, hence the general synthesis for these Pcs are presented.

For the synthesis of 3,6-disubstituted phthalonitiles containing C-C bonds (alkyl substituted), [4+2] cycloadition reactions have been successfully developed [47, 48]. Fumaronitrile **(14)** is used as dienophile and heterocyclic systems (five membered) such as thiophene **(11)** or furan can be used as a source of diene **(Scheme 1.6).** To prepare 3, 6-disubstituted phthalonitile **(16)**, **(11)** is first reacted with BuLi/RBr (butylithium) to form 2, 5-dialkylthiophene-1 **(12).** Oxidation of the thiophene ring **(12)** to the1,1-dioxide **(13)** is required to break the aromaticity of this system which can then undergo Diels-Alder reaction with fumaronitrile **(14).** Compound **(13)** is known to form unstable cycloaddition adduct **(15)** with **(14).** Thermally or by treating with a non-nucleophilic base, **(15)** will self aromatize to yield **(16)**.

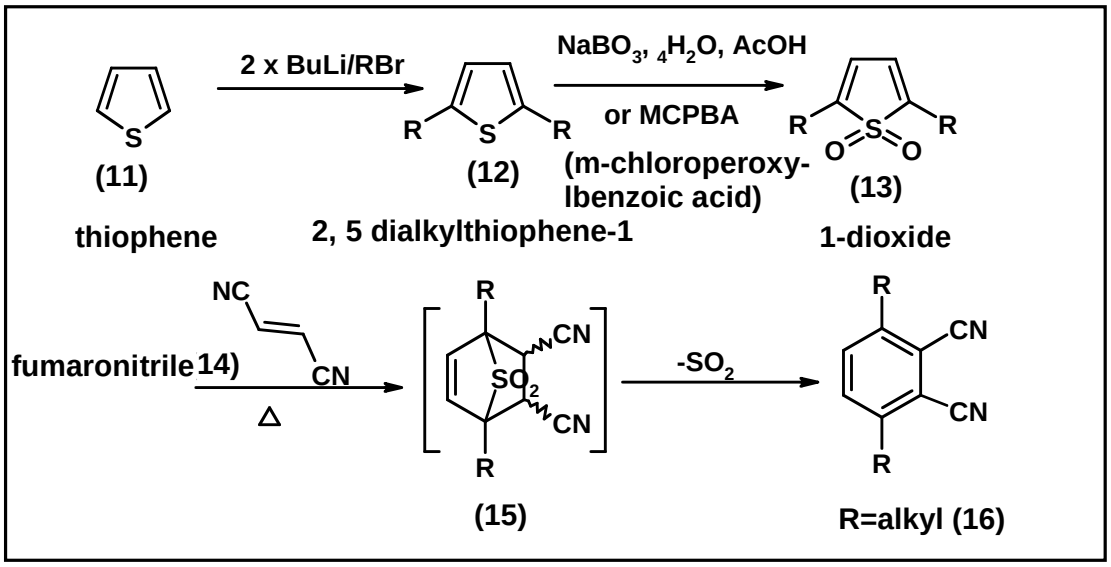

Scheme 1.6: Preparation of 3, 6-dialkylphthalonitriles.

Another synthetic route of 3,6-dialkylpthalonitriles **(19 to 21)** involves the use of 3,6-bis(trifluoromethanesulfonyloxy)phthalonitrile **(18)** as a precursor (**Scheme 1.7**). This method was developed by Cook's group [49, 50].

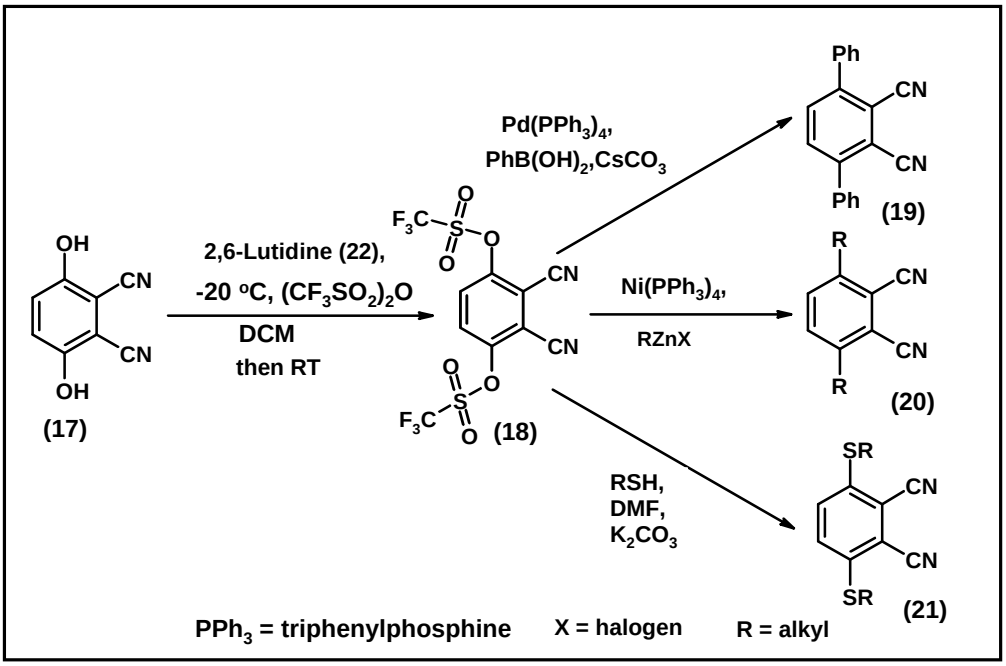

Scheme 1.7: Cross coupling reactions of aryl triflate. (DCM = dichloromethane, DMF = dimethylformamide, and RSH = thiol).

Compound **(18)** is synthesised by reacting 2,3-dicyanohydroquinone **(17)** with $(CF_3SO_2)_2O$, using 2,6-lutidine as a base and a solvent, **Scheme 1.8**. For the synthesis of 3,6-diphenyl **(19)** Suzuki [51] coupling is used.

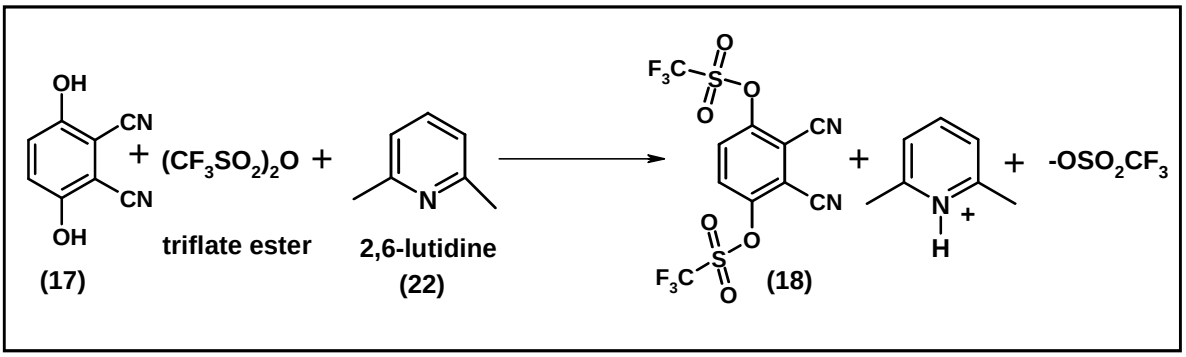

Scheme 1.8: Formation of an Aryl triflate (18).

The role of 2,6-lutidine **(22)** (a base) is to neutralize triflic acid generated by the reaction of **(17)** with triflate ester.

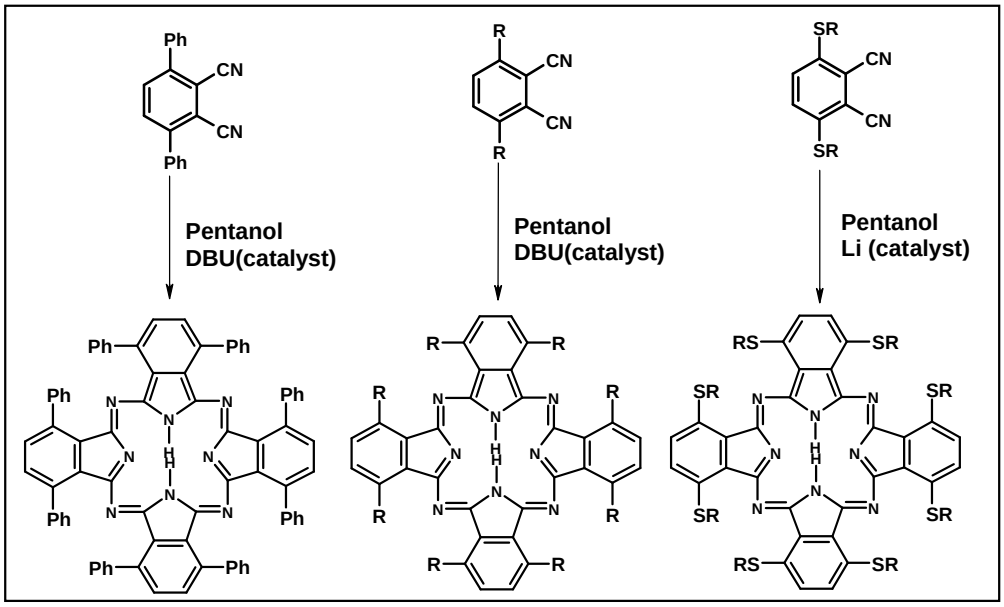

Scheme 1.9: Formation of a phthhalocyanine from precursor (19), (20), and (21).

Precursors **(19)**, **(20)** and **(21)** are refluxed in pentanol in the presence of DBU (1, 8-diazabicyclo-octane catalyst) or Li to form phthalocyanines (**Scheme 1.9**). These phthalocyanines have not been reported for SnPcs.

The method developed by Cook's group to make precursor **(20)** involves the use of Negishi coupling of a triflate **(18)** and an organozinc reagent to afford the dialkyl derivative **(20)** [52]. A Negishi coupling is a cross coupling reaction between an organometallic reagent RMX (M=Sn, Zn, Mg for example) and an organic halide or triflate in **Scheme 1.10** (as in **Scheme 1.8**), and is one of the most important methods for forming a new carbon-carbon σ bond. Negishi and co-workers [52] developed the first transition-metal catalysed cross-coupling reaction between an aryl halide and an organozinc reagent. However Cook *et al*. used the triflate method, which will be employed in this thesis (**Scheme 1.10**).

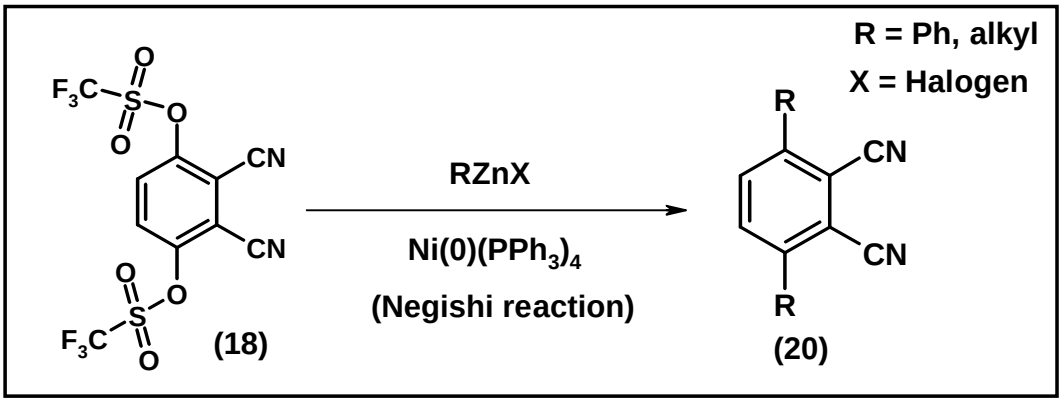

Scheme 1.10: Negishi coupling reaction.

Different functional groups can be incorporated into the organozincs used by Negishi (RZnX) [53, 54]. Due to the low-laying p orbitals of zinc, organozincs can undergo

smooth transmetallations with a variety of transition metal salts or complexes **(Scheme 1.11)**.

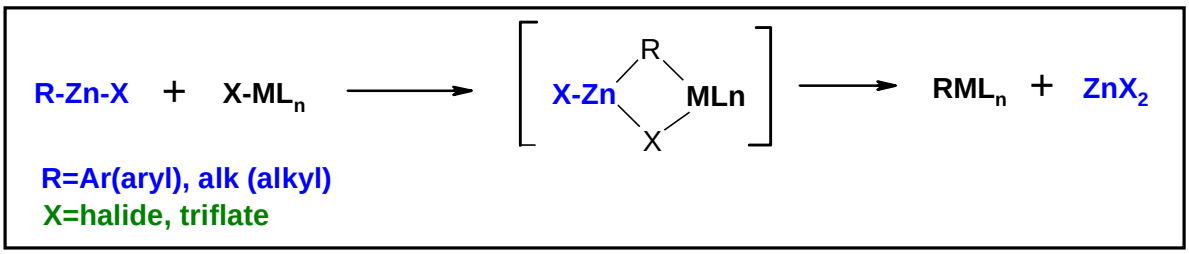

Scheme 1.11: Transmetallatiom of an Organozincs.

Nickel (0) is reactive towards oxidative insertion into carbon-triflate (**Scheme 1.10** or **Scheme 1.7**) bond. Among all PPh_3 stabilised Ni (0) catalysts, $(Ni(0)(PPh_3)_4)$ proved to be the most reactive catalyst. The latter is generated in situ by reaction of $NiCl_2$ $(PPh_3)_2$ complex with n-BuLi following a known procedure (**Scheme 1.12**) [55].

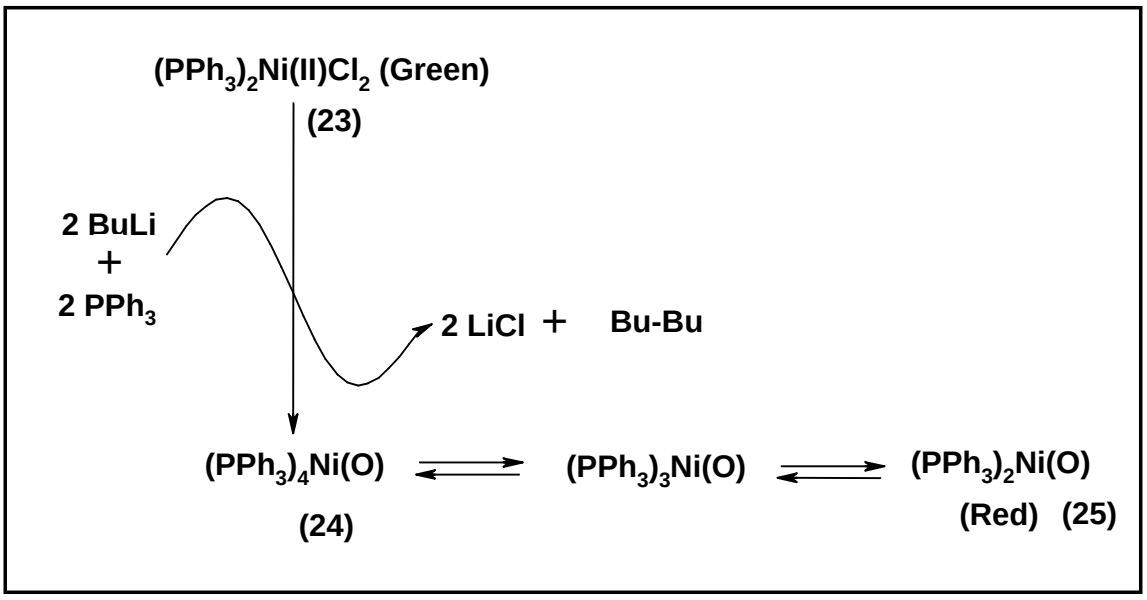

Scheme 1.12: In situ generation of (Ni $(PPh_3)_4$)) by reaction of $NiCl_2$ $(PPh_3)_2$ complex with n-BuLi.

It is thought that in this reaction the two chlorine atoms on the dihalodiphosphine nickel (II) complex **(23)** are easily displaced by n-BuLi to yield a stabilized nickel (0) catalyst,

tetrakis(triphenylphosphine) nickel (0) **(24)**. But the reactive species in the process is expected to be the bis(triphenylphosphine) nickel (0) **(25)** derived from **(24)**. The mechanism of this catalytic cycle has been described (**Scheme 1.12)** by Tamao *et al*. [56]. In **Scheme 1.13** the Negishi cycle is shown with a triflate ($Ar(OTF)_2$) instead of aryl halide.

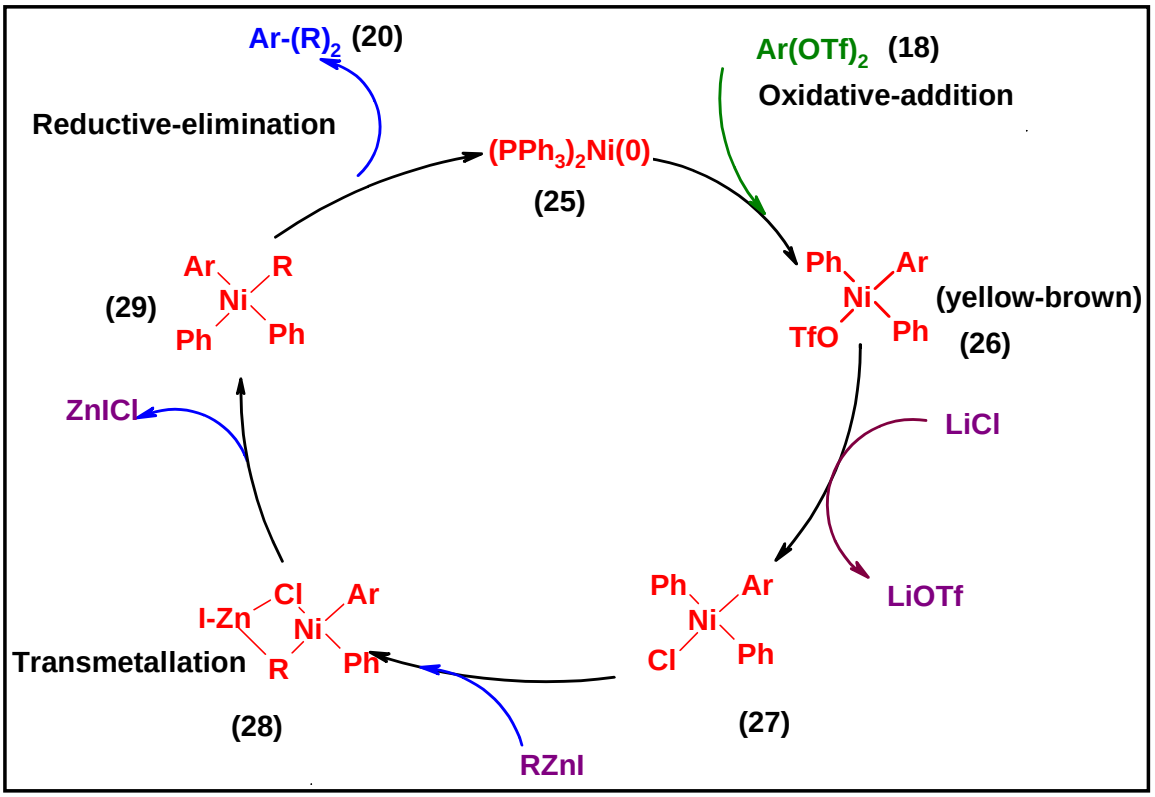

Scheme 1.13: Proposed catalytic cycle for the Negishi coupling reaction using triflate instead of halogen proposed by Negishi [49].

The nickel (0) complex **(25)** is known to be highly reactive towards organotriflates [57] or halides [58]. Anhydrous lithium chloride is added with the triflate as a co-catalyst, for three possible functions: avoiding biaryl formation [58], stabilizing the catalyst [59] and also accelerating the transmetallation step by replacing the inert M-O bond of **(26)** by an active M-Cl bond of **(27)** [60, 61].

Aim of the thesis:

The Negishi method (**Scheme 1.7**) will be employed to synthesise SnPcs containing C-C bonds with the substituents.

1.4.4 Syntheses of Water Soluble Phthalocyanines

A substantial number of water soluble phthalocyanines have been reported in literature. These phthalocyanines have been substituted at the peripheral positions with sulfonates [62], carboxylates [63], phosphates [64] and quaternarized amino groups [65]. Another type of water soluble phthalocyanines possesses hydrophilic groups as axial ligands coordinated to the central metal ion [66].

Water-soluble sulfonated Pc derivatives **(Scheme 1.14)** containing chloroaluminium, and zinc as a central metal have been studied extensively as photosensitisers for PDT [67]. The first example of water soluble sulfonated phthalocyanine (substituted CuPc) was reported in 1929 [8]. Two well known synthetic routes to sulfonated MPcs are those by Weber and Busch [68] and Abmroz *et al.* [69]. In the Weber and Bush, method monosodium salt of sulphonic acid (**30**) and metal salt are heated in nitrobenzene together with urea and ammonium molybdate as a catalyst to give tetrasulfonated Pc (**Scheme 1.14**).

Sulfo phthalonitriles results in the formation of water soluble Pcs known as tetra sulfonated metallophthalocyanine (MTSPc). However, direct sulfonation using oleum is often used (**Scheme 1.15**). Using this method offers no control over where sulfonation

occurs; therefore a mixture of isomers (mono-, di-, tri- and tetra) is obtained [70], $MPcS_{mix}$. By varying temperature and reaction time the degree of sulfonation can be controlled [71]. Water soluble phthalocyanines of Ge, Sn, and Si have been prepared this way [72]. To gain control, chlorosulfonylation (using chlorosulphuric acid) is used instead [73].

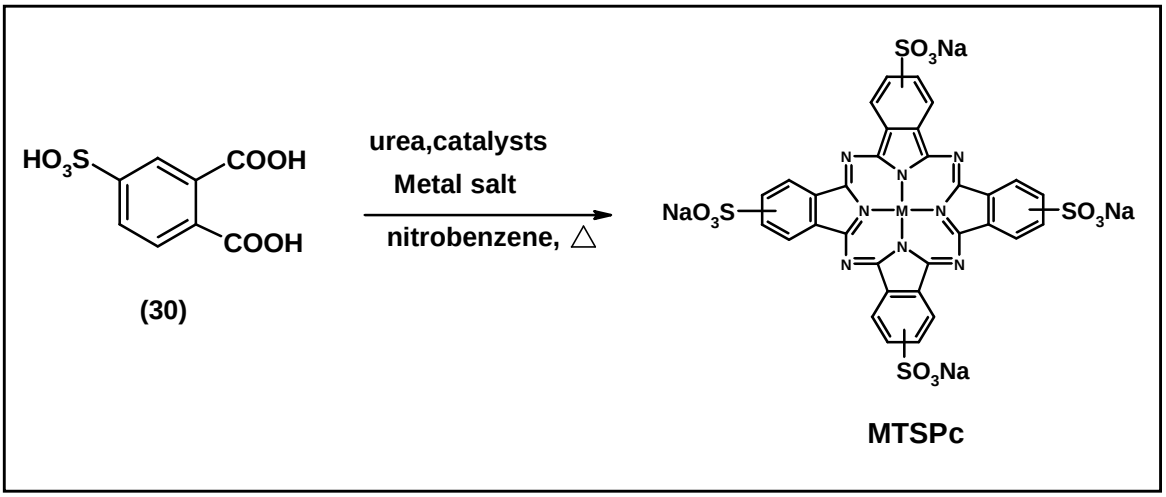

Scheme 1.14: Synthesis of tertra-sulphonated MPc from 4-sulphonic acid.

Even though MTSPcs are well known their synthesis by microwave is still uncommon and synthesis of SnTSPc by microwave is unknown, hence, in this thesis microwave synthesis of SnTSPc is reported.

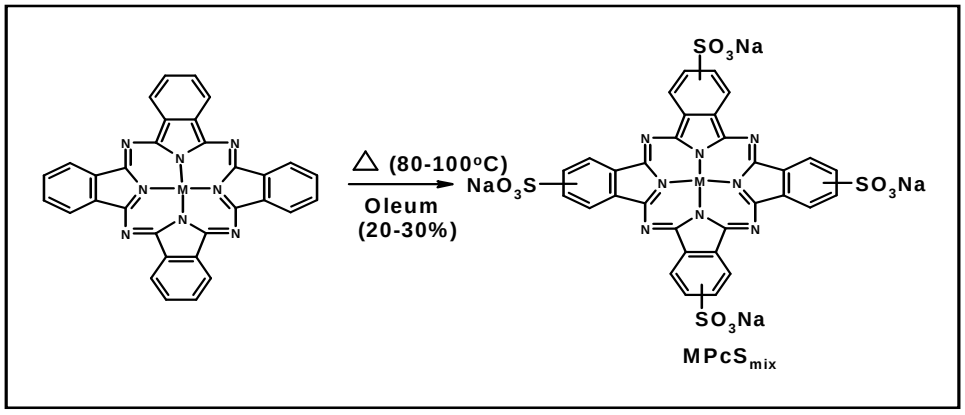

Scheme 1.15: Synthesis route of $MPcS_{mix}$.

More recently, microwave synthesis of tetrasulfonated MPcs was reported by Lui Mo *et al*. [74], in which the zinc, copper, cobalt and aluminum phthalocyanine complexes were synthesised.

It has been reported that the efficiency (in PDT) of $AlPcS_n$ (n = number of sulfonates) depended on the degree of sulfonation [67, 75]. $AlPcS_1$ and $AlPcS_2$ were shown to be more efficient photosensitisers than $AlPcS_4$. It has been shown that the cell uptake of the monomeric form is optimal for $AlPcS_n$ consisting of a mixture of differently substituted compounds [76]. For a series of sulfonated Pcs, their efficiency as PDT photosensitisers can be ordered from high to low as $AlPcS_2$ = $ZnPcS_1$ > $AlPcS_1$ >$AlPcS_4$ > $ZnPcS_2$ > $ZnPcS_4$ [77]. Separation of $AlPcS_2$ has been shown by HPLC to consist of at least eight regioisomers [78]. **Table 1.4** lists examples of MTSPcs, which have been synthesised by use of microwave radiation. The Synthesis of SnTSPc or SnTBC by microwave has not been reported prior to this work. In fact microwave synthesis of TBC has not been reported.

Table 1.4: List of microwave synthesised TSPc complexes

Complexes	**Referece**
H_2TSPc	[79]
ZnTSPc	[79]
CuTSPc	[79]
ClAlTSPc	[79]
CoTSPc	[79]

The problem with microwave synthesis is that, Pcs synthesised this way tend to posses a lot of impurities which can be difficult to remove for water soluble Pcs. The advantage of microwave synthesis is that a reaction that usually takes hours is completed within a matter of minutes.

Aims of project:

The aim of the project is to synthesise novel tin macromolecules (SnPc, SnTBTAP and SnTBC) that are water soluble and those that dissolve in organic solvents. These macromolecules will be characterized by using basic chemical characterization, which includes the use of elemental analysis, inductively coupled plasma (ICP) spectroscopy, nuclear magmetic resonance (NMR) spectroscopy, UV-vis spectroscopy, infrared (IR) spectroscopy and mass spectroscopy (MS).

1.5 Determination of Percentage Aggregation, Dimerization and Equilibrium Constants.

Since water soluble TSPcs and other macrocycles readily aggregate, the aggregation constants for SnTBC and SnTSPc will be evaluated in this work.

Percentage aggregation can be calculated by using **Equation 1.1:**

$$\%_{Agg} = \frac{Abs_{(TX)} - Abs}{Abs_{(TX)}} \times 100 \qquad 1.1$$

where $Abs_{(TX)}$ and Abs are the absorbances of the Q band maximum in the presence and absence of Triton X-100.

The dimerization constant (K_D) for the equilibrium represented by $2M \leftrightarrow D$ is defined by **Equation 1.2**:

$$K_D = \frac{[D]}{[M]^2} \qquad 1.2$$

where $[M]$ and $[D]$ are the molar concentration of the monomer and dimer, respectively.

The total concentration of MPc is given by **Equation 1.3**:

$$C_T = [M] + 2[D] \qquad 1.3$$

The Absorbance of a solution containing both the monomer and dimer is given by **Equation 1.4**:

$$Abs = (\varepsilon_M [M] + \varepsilon_D [D])l \qquad 1.4$$

where ε_M and ε_D are the molar extinction coefficient of the monomer and the dimer, respectively, and l, the optical path length. Substitution of **Equation 1.3** into **Equation 1.4** followed by rearrangement leads to **Equation 1.5** [80]:

$$Abs = \varepsilon_D C_T + \frac{[1-\sqrt{(1+8K_D C_T)}][\varepsilon_D/(2-\varepsilon_M)] + 2\varepsilon_D K_D C_T]}{4lK_D} \qquad 1.5$$

The value of ε_D and K_D can be determined by using non-linear least square fit procedure using MATLAB, Origin or other statistical software.

1.6 Photophysics

In order to use MPcs as photosensitizers, it is important to study their photophysical behaviour such as fluorescence lifetimes (τ_F) and quantum yield (Φ_F), and triplet lifetimes (τ_T) and quantum yield (Φ_T). Photophysics explains the processes of light absorption and energy transfer by a molecule, which results in net physical (not chemical) change. Photophysics deals with relaxation processes such as radiative and non-radiative pathways. Interaction of light with photosensitizers is a fundamental step in all photophysical and photochemical reactions.

A Jablonski diagram (**Figure 1.11**) is often used to illustrate how the excitation energy is dissipated within the molecule (photosensitizer) after absorption has taken place. Before excitation the molecules are in their ground state represented as $\mathbf{S_0}$. When photons are absorbed, electrons are promoted into higher energy valance orbitals resulting in an excited singlet state ($\mathbf{S_1}$). From the $\mathbf{S_1}$ the excited molecule will loose energy by emitting light (fluorescence, F) and by releasing heat to its surroundings through internal conversion (IC) and it may undergo intersystem crossing (ISC) into the triplet excited state ($\mathbf{T_1}$). In the triplet state the molecules may emit light (phosphorescence, P) and thus

return to its ground state (S_0) or give energy to another molecule through photosensitization.

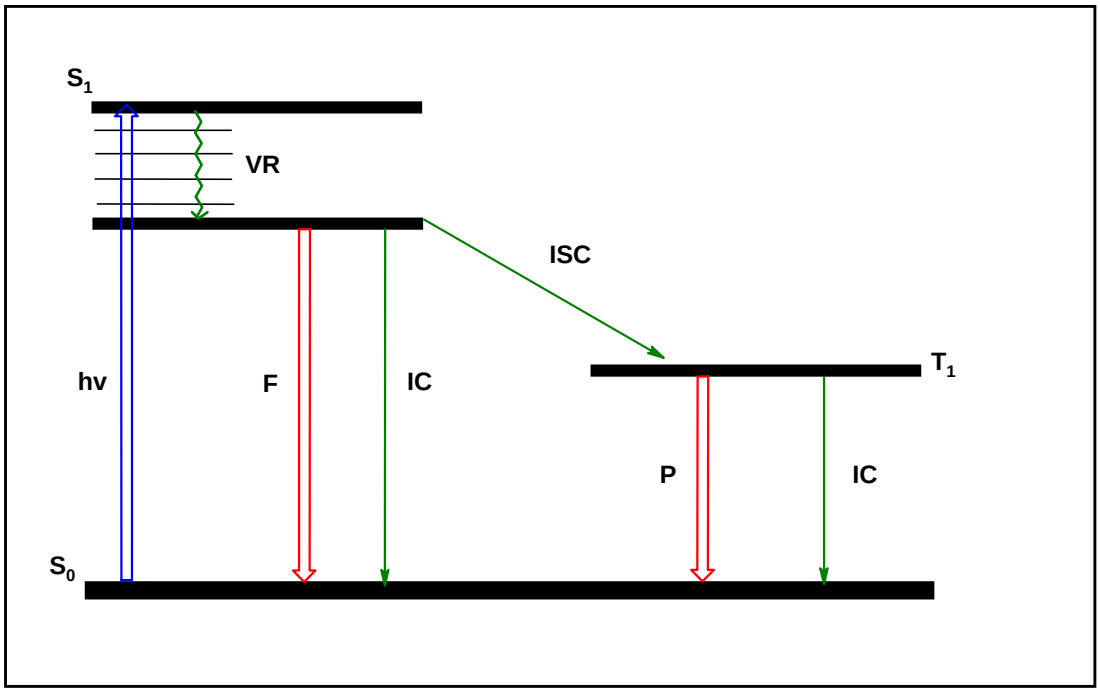

Figure 1.11: A Jablonski diagram showing transitions between the excited electronic state and the ground state. hv = absorption energy , F = fluorescence, IC = internal conversion, ISC = intersystem crossing, P = phosphorescence, S_0 = ground singlet state, S_1 = excited singlet state, T_1 = excited triplet state and VR = vibrational relaxation.

Figure 1.11 shows that there are three non-radiative deactivation processes, IC, ISC and vibrational relaxation (VR). When heavy atoms are present in the molecular structure or medium, ICS is encouraged, such that there is an increase in the population of the triplet state (T_1).

1.6.1 Fluorescence

Three processes govern fluorescence, that is, excitation of molecules, vibrational relaxation to the lowest excited state energy level, followed by the emission to the ground state (**Figure 1.11**). The emission spectrum is observed at longer wavelength with respect to the absorption spectrum (**Figure 1.12**) and it is a mirror image of the absorption spectrum.

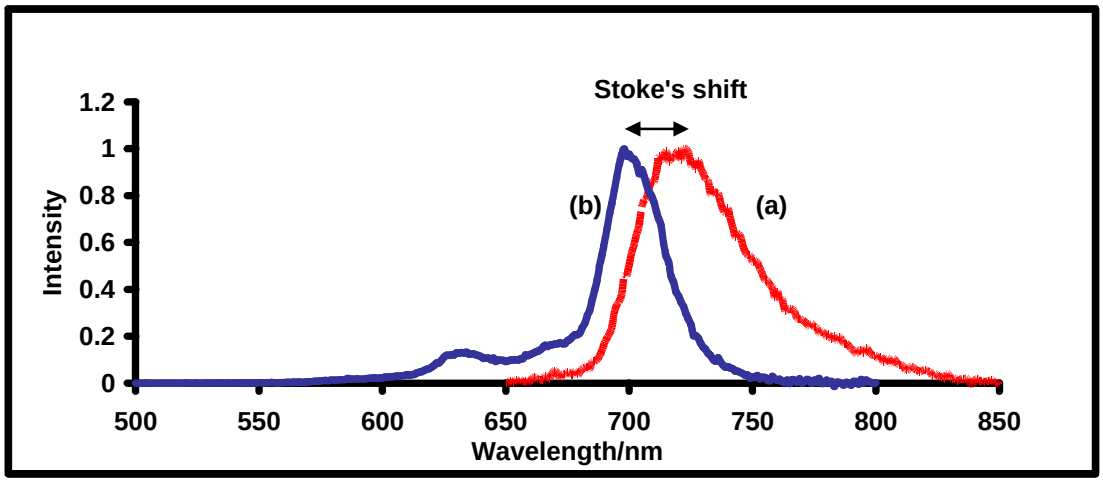

Figure 1.12: Typical fluorescence (a) and an emission (b) spectrum of a phthalocyanine.

Life time and Yields

The difference between the spectral position of the band maxima of absorbance and fluorescence is called the Stoke's shift (**Figure 1.12**). Several factors influence the magnitude of the Stoke's shift. A small Stoke's shift (less than 10 nm) is expected if the environment is rigid, such that little rearrangement is possible. In other words, the excited state has a similar geometry to that of the ground state (there is no change in the electronic energy levels).

An excitation spectrum is obtained when the emission spectrum is excited, which provides information about the absorption spectrum of the fluorescent molecules. The excitation spectrum should ideally resemble the absorption spectrum [81]. Apart from Stoke's shift, other parameters such as fluorescence quantum yield (Φ_F) and fluorescence lifetimes (τ_F) can be determined because they are in competition with other processes.

Fluorescence quantum yields

The quantum yield (Φ) represents and quantifies the efficiency of a photophysical or photochemical process (**Equation 1.6**).

$$\Phi = [\textbf{Number of events}] / [\textbf{Number of photons absorbed}] \qquad 1.6$$

Fluorescence quantum yield (Φ_F), the efficiency of the fluorescence process, is defined as the ratio of the number of photons emitted and number of photons absorbed. A comparative method is usually used when determining Φ_F values. This method involves using known Φ_F of well characterized standard samples (eg. ZnPc in dimethylsulfoxide (DMSO)) to find the Φ_F for the complex of interest using **Equation 1.7**.

$$\Phi_F = \Phi_{F(std)} \frac{F.A_{std}.\eta^2}{F_{std}.A.\eta_{std}^2} \qquad 1.7$$

where F and F_{std} are areas under the fluorescence curve of the sample and standard respectively, A and A_{std} are the respective absorbances of the sample and standard at the excitation wavelength while η and η_{std} are the refractive indices of the solvents used for the sample and standard respectively. Absorbance of 0.05 at the excitation wavelength of both sample and standard should be used to minimize re-absorption effects [82].

Fluorescence lifetimes

Fluorescence lifetime can be defined as the time it takes for a molecule to stay in the excited state before emitting a photon. This parameter represents the probability of finding a molecule in the excited state at a given time [81]. This parameter can be derived by letting n_0 represent the number of molecules in the ground state. An assumption that is made is that fluorescence is the only radiative pathway for the excited state molecule to return to the ground state. Therefore, at time t, the number of molecules emitting photons per second is proportional to n_t , which is the number of molecules in the excited state. This is represented by **Equation 1.8**:

$$\frac{dn}{dt} = -k_f n_t \qquad 1.8$$

where k_f is the fluorescence rate constant. Integrating **Equation 1.8** gives **Equation 1.9**.

$$\int \frac{dn}{n_t} = \int -k_t dt \qquad 1.9$$

From this integration step we obtain an equation that represents an excited state population that is dependent on time, shown in **Equation 1.10**.

$$n_t = n_0 e^{-k_t t} \qquad 1.10$$

This equation represents the average time that a molecule will stay in the excited state. The natural radiative lifetime (τ_0) is defined as the time required for all but $1/e$ (~ 37 %) of the excited state molecules to return to the ground state. This lifetime includes all relaxation processes, both radiative and non-radiative. The observed (radiative) life time (τ) specifically refers to the decay in fluorescence intensity, which is given by **Equation 1.11**:

$$I = I_0 e^{-t/\tau} \qquad 1.11$$

where I is the fluorescence intensity and, I_0 is the fluorescence intensity at t = 0 and τ is the observed fluorescence lifetime. If radiationless transitions are absent, the fluorescence lifetime and fluorescence rate constant are related by **Equation 1.12**:

$$\tau = \frac{1}{k_F} \qquad 1.12$$

From this expression, fluorescence quantum yield can be expressed in terms of the natural and observed lifetime, as shown in **Equation 1.13**:

$$\Phi_F = \frac{\tau}{\tau_0} \qquad 1.13$$

The value of τ_0 can be calculated from the absorption spectrum of the molecule using **Equation 1.14** [83]:

$$\tau_0 = \frac{3.417 \times 10^8}{v_{max}^2 . \eta^2 . A} \qquad 1.14$$

were v_{max} is the wavenumber of maximum absorption in cm^{-1}, η is the viscocity of the solvent and A is the area of the absorption band. From **Equation 1.14** we see that τ_0 is related to the absorption band area, therefore τ_0 can be estimated by using the absorbance and fluorescence spectra, using the modified Strickler-Berg equation, that is, **Equation 1.15** [84, 85]:

$$\frac{1}{\tau_0} = 2.88 \times 10^{-9} . \eta^2 \frac{\int \frac{F(\lambda)}{\lambda^2} . d(\lambda)}{\int F(\lambda) \lambda . d(\lambda)} \int \frac{\varepsilon(\lambda)}{\lambda} . d(\lambda) \qquad 1.15$$

where $F(\lambda)$ and $\varepsilon(\lambda)$ are the areas under the fluorescence and absorption spectra respectively. **Equation 1.14** can be used to evaluate the actual fluoresce lifetime values. A software package developed by Du *et al.* [86], called PhotochemCAD, can be used to calculate the fluorescence lifetime. This software package makes use of the Strickler-Berg equation [85]. **Table 1.5** shows known fluorescence quantum yields and lifetimes for SnPc complexes. **Table 1.5** shows that all fluorescence quantum yields are smaller than 0.1 and that there are very low flouresence life times. The presence of Sn in these complexes encourages intersystem crossing to the triplet state (due to the heavy atomic

effect or spin orbit coupling) thus resulting in a very low fluorescence quantum yield. Φ_F and τ_F for SnTBC and SnTSPc were not found in the literature, hence they are reported in this work. These parameters are important for predicting the efficiency of the fluorescence of Pcs (for example, for imaging purposes).

Table 1.5: List fluorescence quantum yield and lifetimes of SnPc complexes.

Complexes [a]	**Solvent**	Φ_F	τ_F (μs)	**Reference:**
$SnPcS_{mix}$	PBS 7.4	0.05	-	[62]
$(Estrone)_2SnPc$	DMSO	0.02	2.2	[87]
$(Cl)_2SnOPPc$	DMSO	0.04	0.3	[87]
$(Cl)_2SnOMPPc$	DMSO	0.06	0.4	[87]
$(Cl)_2SnOEPc$	DMSO	0.01	0.2	[87]
$(I)_2SnOPPc$	DMSO	0.04	0.4	[87]

[a]**OPPc = octa(phenoxy)phthalocyanine, OMPPc = octa(o-methyl-phenoxy)-phthalocyanine and OEPc = octa(esterone)phthalocyanine**.

Fluorescence quenching

When porphyrin-like substances (for example, chlorophyll and MPc) absorb energy, a fair percentage of this energy may be lost as fluorescence. Prevention (quenching) of this fluorescence may result in the excitation energy being redirected and made available for chemical use. In this thesis, quenching of bovine serum albumin (BSA) fluorescence by

SnTSPc and SnTBC by BSA is investigated, because these Pcs will definitely encounter BSA in the blood, when used for PDT. Further more, fluorescence quenching of BSA by MPc is used to determine the binding constant between BSA and MPc. The study of BSA binding to TSPcs has not received much attention and the study of the binding of BSA to TBCs has not been done.

Fluorescence quenching refers to processes that lead to a reduction of fluorescence intensity of a given system. There are two basic types of fluorescence quenching mechanisms, dynamic and static quenching. Dynamic quenching involves nonradiative deactivation of the excited state upon collision with other molecules [88]. Static quenching is a process that leads to a reduction in the observed fluorescence intensities due to the formation of a ground state complex [81]. This work concentrates only on the dynamic quenching.

In the absence of quenching, the fluorescence quantum yield, Φ_F, is given by **Equation 1.16**:

$$\Phi_F = \frac{k_F}{k_{ic} + k_{ics} + k_F} \qquad 1.16$$

where k_F, k_{ic} and k_{ics} are fluorescence, internal conversion and intersystem crossing rate constants. In the presence of a quencher, the quenching rate constant (k_Q)and the concentration of quencher are included, shown in **Equation 1.17**.

$$\Phi_F^Q = \frac{k_F}{k_{ic} + k_{ics} + k_F + k_Q[Q]} \qquad 1.17$$

When **Equation 1.16 and 1.17** are combined, the ratio of the quantum efficiency in the absence and presence of quencher is given by **Equation 1.18.**

$$\frac{\Phi_F}{\Phi_F^Q} = 1 + \frac{k_Q[Q]}{k_{ic} + k_{ics} + k_F} = 1 + \tau_0 k_Q[Q] \qquad 1.18$$

Equation 1.18 can be expressed in terms of fluorescence lifetime:

$$\frac{\tau_0}{\tau} = 1 + \tau_0 k_Q[Q] = 1 + K_{SV}[Q] \qquad 1.19$$

where τ_0 and τ are the fluorescence lifetimes in the absence and presence of quencher and K_{SV} is the Stern-Volmer quenching constant. **Equation 1.19** is generally used in the form of **Equation 1.20.**

$$\frac{I_0}{I} = K_{SV}[Q] + 1 \qquad 1.20$$

where

$$K_{SV} = \tau_F k_Q \qquad 1.21$$

A plot of I_0 / I versus $[Q]$ will give a Stern-Volmer constant as the slope. The effectiveness of quenching and accessibility of the fluorophores to the quencher in

bimolecular quenching is determined from the bimolecular constant (k_Q) determined from K_{SV} using **Equation 1.21**. According to Einstein-Smoluchowski approximations [88], k_Q value for diffusion controlled quenching is approximated to be $1\times10^{10}\,M^{-1}s^{-1}$ at room temperature. If a large value of k_Q is observed, it indicates that some type of interaction between the flourophore and the quencher occurs and a small k_Q is indicative of steric shielding of the fluorophore [88]. **Table 1.6** lists the quenching and binding constants of $MPcS_{mix}$ found in literature. This work studies the interaction of SnTSPc and SnTBC with BSA by determining their binding and biomolecular constants.

Table1.6: Quenching and binding data for MPcSmix complexes in PBS 7.4.

Complex	$K_b/10^{-6}M^{-1}$	n	$K_{SV}^{BSA}/10^{-4}M^{-1}$	$k_Q/10^{-12}M^{-1}s^{-1}$	
$AlPcS_{mix}$	17.21	1.4	11.45	11.40	[89]
$SiPcS_{mix}$	1.29	1.3	6.90	6.90	[89]
$GePcS_{mix}$	0.81	1.1	4.54	4.54	[89]
$ZnPcS_{mix}$	0.10 (0.34)	1.0	7.36 (6.72)	7.36 (6.72)	[89]
$SnPcS_{mix}$	0.08 (0.21)	1.0	1.98 (3.19)	1.98 (3.19)	[89]

1.6.2 Binding of Sulphonated Metallophthalocaynine ($MPcS_4$) Complexes to Bovine Serum Albumin (BSA)

Albumin is known to be the most abundant protein found in the circulatory system and constitutes about 80% to colloid osmotic blood pressure [90]. The investigation of

albumin interaction or binding property with porphyrin-like drugs has received considerable interest [91, 92]. BSA has been extensively characterized [93, 94] and for this reason it is well suited for studies involving the binding of albumin and porphyrin-like drugs. When Pcs are used for PDT, after an injection one way or another they will encounter serum proteins in the blood which influence drug distribution. Serum albumin are known to display effective drug delivery functions, therefore, a study of their binding to porphyrin-based drugs is of significance. The quenching of fluorescence observed when BSA binds with a tetrapyrrolic compounds, can provide a means of studying the interaction between these compounds and BSA. The binding constants and stoichiometry of the complex formed can also be determined [95].

The basic reaction between an MPc complex and BSA is represented as **Equation 1.22**:

$$BSA + nMPc \rightarrow BSA:(MPc)_n \qquad 1.22$$

The expression for the binding constant (K_b) in the above equation is given by **Equation 1.23:**

$$K_b = \frac{[BSA:(MPc)_n]}{[BSA][MPc]^n} \qquad 1.23$$

The number of binding sites on a BSA molecule can be estimated by rewriting **Equation 1.23** as **Equation 1.24:**

$$K_b = \frac{[F_0 - F]}{[F - F_\infty][MPc]^n} \qquad 1.24$$

where F_0 is the fluorescence intensity of BSA in the absence of MPc; F, the fluorescence intensity of BSA in the presence of MPc; F_∞, the fluorescence intensity of BSA saturated with MPc; and n, the number of binding sites on a BSA molecule. By taking the logs of both sides of **Equation 1.24** and rearranging gives **Equation 1.25**:

$$\log[\frac{(F_0 - F)}{(F - F_\infty)}] = \log K_b + n\log[MPc] \qquad 1.25$$

Plots of $\log[\frac{(F_0 - F)}{(F - F_\infty)}]$ versus $\log[MPc]$ should give a straight line with slope n and intercept $\log K_b$. Some examples of n and K_b values for BSA binding are given in **Table 1.6**.

1.6.3 Triplet Lifetimes and Quantum Yields

Triplet excited states are generated and studied by the use of a technique known as flash photolysis. The technique makes use of a short and intense pulse from a laser source to generate transient chemical species at the excited state. **Figure 1.13**, shows a typical triplet decay curve following laser flash photolysis. From this curve one could determine the triplet quantum yield and life time of the compound under study.

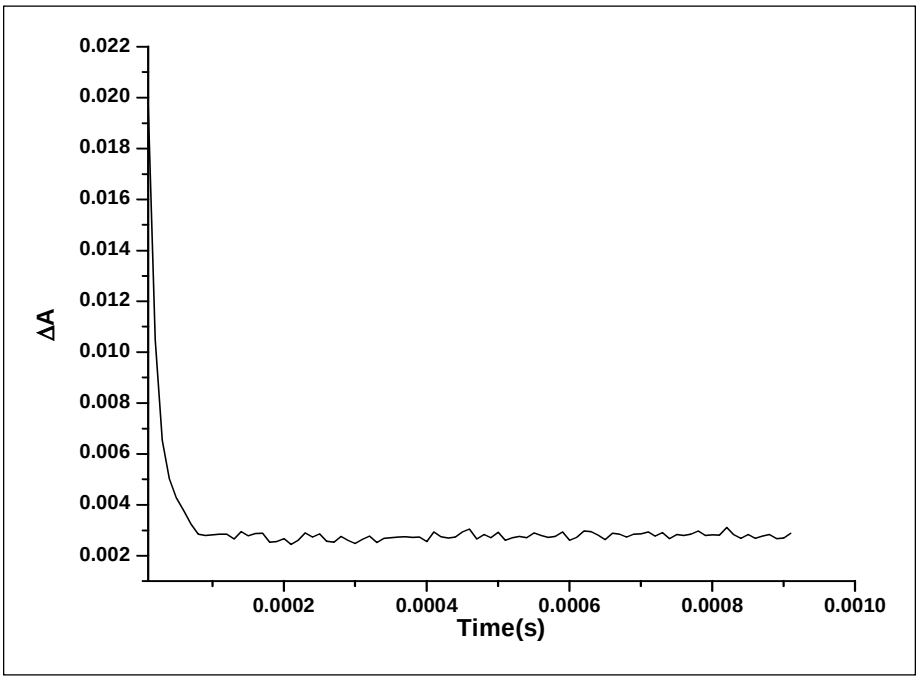

Figure 1.13: Typical transient spectrum (triplet decay curve) following laser flash photolysis.

Triplet quantum yield (Φ_T) and triplet lifetime (τ_T) measurements depend on maximum absorption of the triplet state, which occurs near 500 nm for most phthalocyanines. The triplet absorption is due to the transition from the lowest triplet state of a molecule to a higher triplet state (**Figure 1.14).**

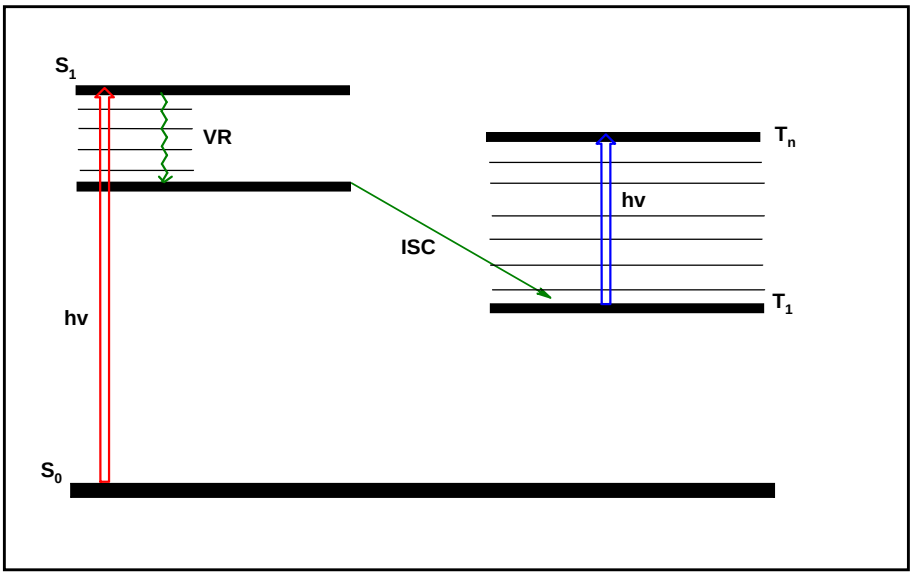

Figure 1.14: Jablonski diagram showing transition from T_1 to T_n state.

Triplet quantum yield is defined as the probability of a sensitizer to convert absorbed quanta of light to the T_1 state. This photophysical parameter can be determined by using a comparative method [96]. The method involves using known Φ_T and triplet extinction coefficient (ε_T), at a given wavelength, of well characterized standard to find Φ_T for the sample of interest using **Equation 1.26**.

$$\Phi_T = \Phi_T^{Std} \frac{\Delta A_T^{Sample} . \varepsilon_T^{Std}}{\Delta A_T^{Std} . \varepsilon_T^{Sample}} \qquad 1.26$$

where ΔA_T^{Sample} and ΔA_T^{Std} are the changes in the triplet state absorbance of the sample and standard respectively, and ε_T^{Sample} and ε_T^{Std} are the triplet state extinction coefficients of the sample and standard respectively. The values of ε_T are determined by making use of the singlet depletion method. Singlet depletion method requires one to measure the change in

absorbance (ΔA_s) where there is an absorption from the ground state [97]. The triplet state extinction coefficient (ε_T) of a sample is given by **Equation 1.27**:

$$\varepsilon_T = \frac{(\Delta A)_T . \varepsilon_S}{(\Delta A)_S} \qquad 1.27$$

where ε_s is the molar extinction coefficient of the ground state molecule in its singlet state (ΔA_T). The triplet lifetimes (τ_T) can be determined by fitting the triplet decay data by using a first order kinetic function. **Table 1.7** shows triplet quantum yield and lifetimes of known Sn macrocycles. From the table we see that SnPP has the highest Φ_T and τ_T in the list. Generally, it is expected that these compounds should have high triplet quantum yields and short lifetimes (due to the encouraged intersystem crossing by the heavy Sn), but sometimes this behavior does not happen as expected.

Table 1.7: **Triplet quantum yield and lifetimes of known Sn macrocycles**

Complexes	**Solvent**	Φ_T	τ_T (μs)	**Reference**
$SnPcS_{mix}$	PBS 7.4	0.59	2.52	[62]
SnPP	PO_4 buffer, pH 7.4	0.68	162	[87]
$(Estrone)_2SnPc$	DMSO	0.08	18	[87]
$(Cl)_2SnOPPc$	DMSO	0.19	30	[87]
$(Cl)_2SnOMPPc$	DMSO	0.45	32	[87]
$(Cl)_2SnOEPc$	DMSO	0.15	10	[87]
$(I)_2SnOPPc$	DMSO	0.19	32	[87]

OPPc = octa(phenoxy)phthalocyanine, OMPPc = octa(o-methyl-phenoxy)-phthalocyanine, OEPc = octa(esterone)phthalocyanine and PP = photoporphyrin.

Aim of thesis:

Photophysical properties (dimerisation constants, fluorescence quantum yields, fluorescence lifetimes, triplet quantum yields and triplet lifetimes) of the newly synthesised tin complexes of the macromolecules will be investigated. The interaction properties of water soluble macromolecule with BSA (together with their binding constant and bimolecular constant) will be studied.

1.7 Electrochemistry

In this work the new TBTAP complexes are characterized by electrochemistry and spectroelectrochemistry, hence, we need to discuss these techniques. Also cyclic voltammetry (CV) will be used to characterize self assembled monolayer (SAMS) of thiol substituted Pcs.

1.7.1 Cyclic Voltammetry

Voltammetric analysis employs the three-electrode system containing the working (also known as the indicator or sensing electrode), the reference electrode (R.E) and the counter electrode (C.E.) **(Figure 1.15)**. The working electrode, W.E. is where electrochemical reaction takes place. The counter electrode completes the electric circuit of the cell. The potentiostat maintains a potential difference, ΔE, between the R.E. and W.E. and supplies the current, i, needed for affecting the changes occurring at W.E..

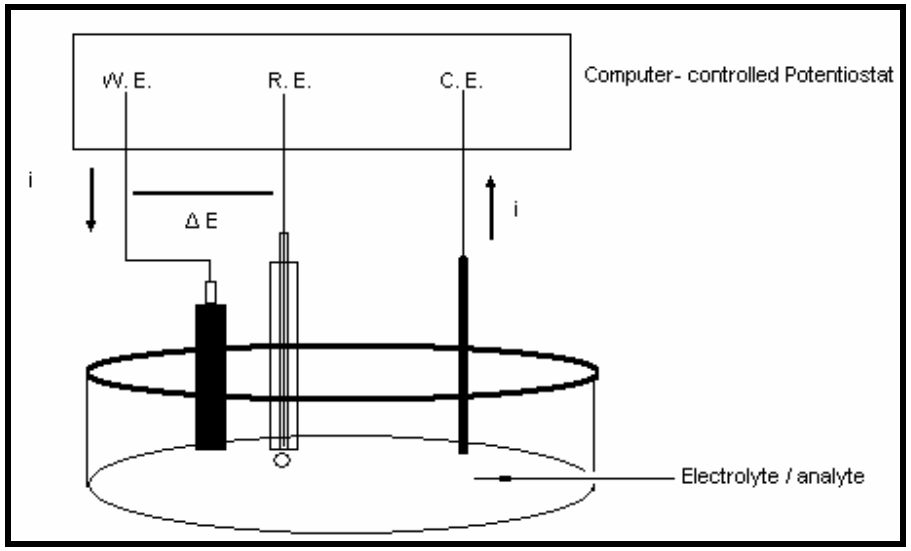

Figure 1.15: A diagrammatic representation of a conventional three-electrode cell, showing the working (WE), reference (RE) and counter electrodes (CE).

In voltammetric analysis, a varying potential is applied to the electrochemical cell until oxidation or reduction of the analyte occurs and there is a sharp rise in the current to give a peak current (I_p). The height of the I_p is directly proportional to the concentration of the target analyte. The plot of current versus potential is called a voltammogram **(Figure 1.16)**. The potential at which the I_p is observed is the peak potential (E_p). If the potential is reversed the technique is called cyclic voltammetry (**Figure 1.16**)

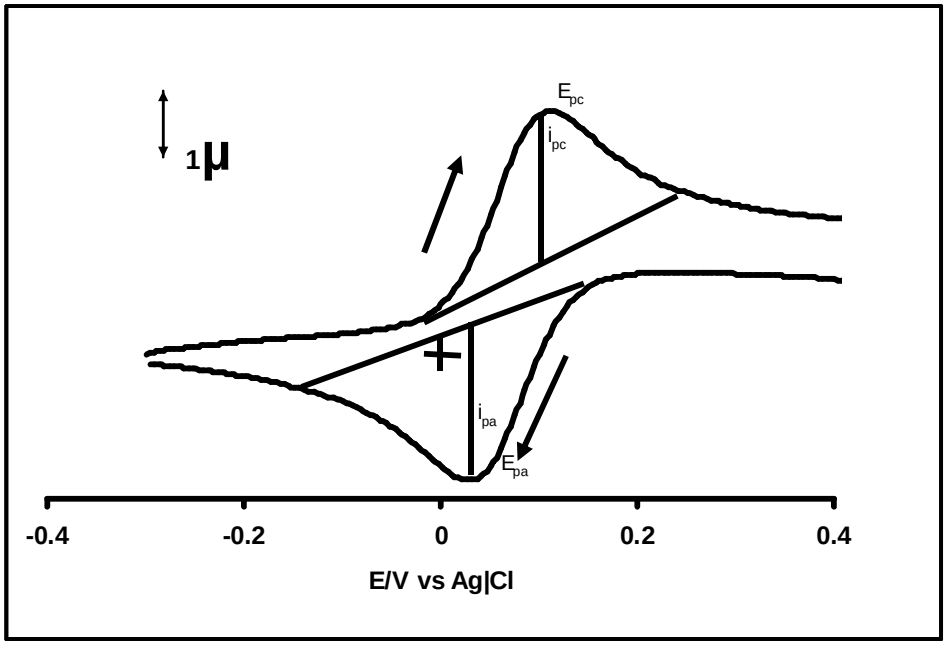

Figure 1.16 A typical cyclic voltammogram(CV)

$E^{\circ'}$ is the formal redox potential, situated between E_{pc} and E_{pa}, which is approximately equal to the half-wave potential ($E_{1/2}$), given by **Equation 1.28.**

$$E^{\circ'} = 1/2(E_{pa} + E_{pc}) \qquad 1.28$$

From the peak separation one can determine the number of electrons (n), using **Equation 1.29**

$$\Delta E_p = E_{pa} - E_{pc} = RT/nF \text{ and at } 25^{\circ}C \approx 0.059/n \qquad 1.29$$

Randles-Sevcik equation is used to describe the peak current (i_p), as outlined in **Equation 1.30**

$$i_p = (2.69x10^5)n^{3/2}AD^{1/2}Cv^{1/2} \qquad 1.30$$

where i_p = peak current in Ampere

n = electron stoichiometry

A = electrode surface (cm^2)

D = diffusion coefficient (cm^2/s)

C = concentration (mol/cm^3)

v = scan rate (V/s)

According to **Equation 1.30** i_p will increase as $v^{1/2}$ increases and it is directly related to the concentration. A linear plot of $v^{1/2}$ versus i_{pc} or i_{pa} indicates diffusion controlled mass transfer. The relationship between i_p and concentration is very important in studies concerning electrode mechanism. For a simple reversible system the value of the ratio of i_{pc} and i_{pa} is expected to be near unity for simple reversible systems: **Equation 1.31**

$$\frac{i_{pa}}{i_{pc}} = 1 \qquad 1.31$$

Applications of Cyclic Voltammetry

Cyclic voltammetry (CV) is used in this work to study electrochemical reactions and for characterization of self assembled monolayer (SAMs) of thiols and MPc SAMs on gold electrodes. In this work $Cl_2SnPc(SR)_8$ and $Cl_2SnPc(SR)_4$ complexes ($R = C_{12}H_{25}$) will be used for the formation of SAMs. When this technique is used to study electrochemical reactions, it provides a fast and simple way of obtaining information about the electron transfer, stability of electrolysed (oxidized or reduced) analyte, adsorption process and electrode kinetics and mechanisms [98, 99]. Faradaic processes are known to be easily blocked by SAMs, this property of SAMs can be studied or monitored using CV. This blocking ability of SAMs is known to depend on the terminal functional groups of SAMs [100]. Ferricyanine solutions $[Fe(CN)_6^{3-/4-}]$ are usually used to study this blocking behavior of SAMs. Ferricyanine is a highly reversible system and this reversibility can be affected by modifying the electrode with SAMs. This reversible system can either be inhibited or enhanced by the SAMs [101]. Other systems such as ferric ammonium sulfate ($FeNH_4(SO_4)_2$) solution can be used to characterize SAMs. However, this is a slow electron transfer system [101] compared to ferricyanine and shows a redox couple due to $[Fe(H_2O)_6]^{3+}/[Fe(H_2O)_6]^{2+}$.

1.7.2 Square Wave Voltammetry

For an investigation of redox reactions that may otherwise be impossible with CV, square wave voltammetry (SWV) is used, because it is a more sensitive electroanalytical

technique compared to cyclic voltammetry. Osteryoung square wave voltammetry (OSWV) invented in the 1950's (by the Osteryoungs) [102] is the most popular square wave voltammetry technique used to date. In this technique, currents signals are sampled at two points, the difference of which is plotted as a function of applied potential. The resulting peak-shaped voltammogram is symmetrical about the half wave-potential and the peak current is proportional to the concentration. This technique offers several advantages such as optimal peak separation, greater analysis speed, lower electroactive species consumption and lower detection limits of up to 10^{-8} M.

1.7.3 Spectroelectrochemistry

In spectroelectrochemistry two disciplines are merged together, electrochemistry and spectroscopy. A typical electrochemical cell that is used is called an OTTLE (Optically Transparent Thin Layer Electrode) cell. This cell houses a redox active compound of interest, which can be oxidized or reduced and the product monitored in situ by spectroscopic techniques [103]. MPc redox processes may take place at the central metal atom or at the ring, CV alone cannot give information on the nature of these redox processes. Redox processes for MPc complexes occurring at the central metal or ring often result in colour changes, with ring redox processes showing more drastic colour changes [104].

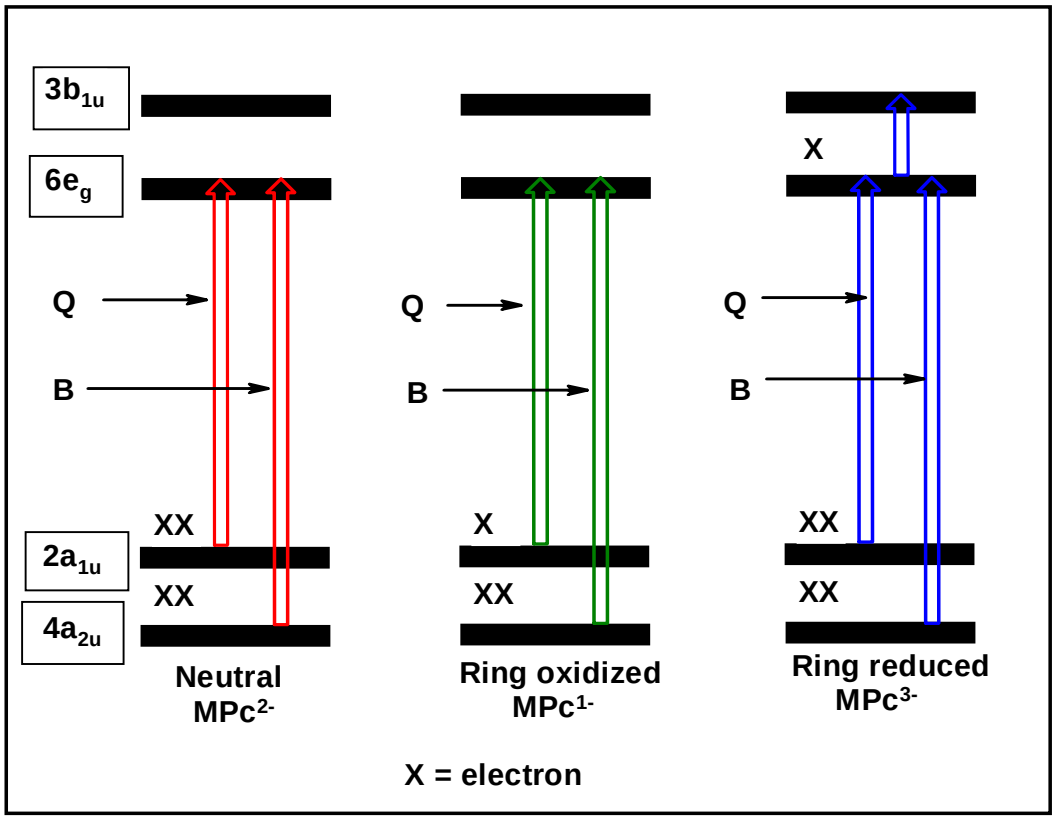

Figure1.17: Energy level diagrams of neutral, one-electron ring reduced and one-electron ring oxidized MPc complex.

Monitoring spectral changes as MPc is oxidized or reduced (**Figure 1.17**), can give information about the nature of the redox process. For example, a shift in the Q-band is due to oxidation or reduction of the central metal [105] and the collapse of the Q-band with a simultaneous formation of a new band at the 500-600 nm region is due to oxidation or reduction of the ring [106]. In this work spectroelectrochemistry and electrochemistry of tin macrocycles are studied.

Aim of thesis:

Electrochemistry (cyclic voltametric) and spectroelectrochemistry of the newly synthesised macrocycles and SAMs will be investigated.

1.7.4 Electrochemical Impedance Spectroscopy (EIS)

Electrochemical impedance spectroscopy (EIS) is an important tool that is used to characterize or study materials and electrochemical processes. Materials whose external parameter or property has an influence on the conductivity of an electrochemical system can be studied by use of impedance spectroscopy [107]. EIS has vast applications, such as characterization of thin films, corrosion and kinetics studies.

1.7.4.1 Basics of Impedance Spectroscopy

Electrochemical impedance spectroscopy makes use of a three electrode set up, similar to a voltammetric analysis cell set up (**Figure 1.15**). In performing a basic EIS experiment, a general approach involves applying an electrical stimulus (known as the voltage or current) to the electrode and observing the response (the resulting current or voltage). The overall electronic response is due to the microscopic process taking place throughout the cell. The spectroscopic processes include transport of electrons through the electronic conductor and the movement of charged particles towards the electrode through a concentration gradient. The flow rate of the charged particles depends on the ohmic resistance, electrolyte and on reaction rates at the electrode-electrolyte interfaces [108].

In ESI spectroscopy a general stimulus used to measure impedance is a single-frequency sinusoidal voltage signal. The response measured is the phase shift and amplitude, or real and imaginary parts, of the resulting current at that particular frequency using fast Fourier transform (FFT) analysis of the response. FFT analysis converts measurements in the

time domain into the frequency domain. The results or response can be related to the physical and chemical properties of the material [107].

Impedance is a complex resistance and differs from ordinary Ohm's law resistance (R) which is defined in terms of ratio between voltage (V) and current (I) (**Equation 1.32**)

$$R = \frac{V}{I} \qquad 1.32$$

Impedance (Z) is defined as a ratio of the alternating potential and the alternating-current signal:

$$Z(\omega) = \frac{E(t)}{I(t)} = \frac{E_m}{I_m} e^{j(\alpha-\beta)} = \frac{E_m}{I_m} e^{j\theta} = |Z| e^{j\theta} \qquad 1.33$$

where

$$E(t) = E_m e^{j(\omega t+\alpha)} \qquad 1.34$$

and

$$I(t) = I_m e^{j(\omega t+\beta)} \qquad 1.35$$

with $j^2 = 1$

where **Equations 1.34** and **1.35** represent a sinusoidal wave with amplitude of potential E_m and current I_m and an angular frequency ω where $\omega = 2\pi f$ (f in Hz), t is time and α and β in rads are phase angles (**Figure 1.18 (a)**). From **Equation 1.33** it can be seen that

impedance is dependent on frequency and has a phase angle θ. This impedance (**Equation 1.33**) can be presented as a vector in the complex plane with modulus $|Z| = E_m / I_m$ and argument $\theta = \alpha - \beta$. The resistance Z' (real part) and reactance Z'' (the imaginary part) are the x and y axis of the complex plane (**Figure 1.18 (b)**).

$$Z(\omega) = Z'(\omega) + jZ''(\omega) \qquad 1.36$$

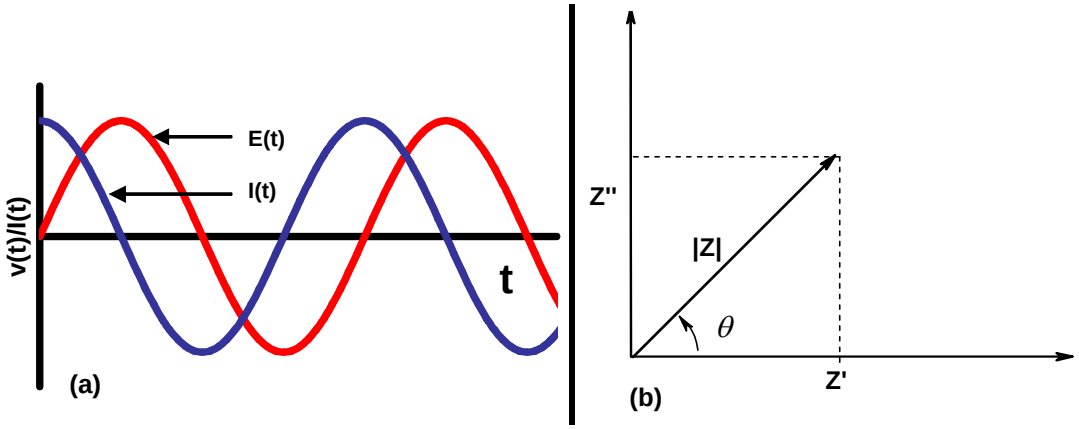

Figure 1.18: (a) Applied sinusoidal voltage and resulting sinusoid current response (b) vector representation of real (Z') and imaginary (Z'') part of impedance (Z).

1.7.4.2 Measurements and Characterization of Material-electrode System

Impedance Spectroscopy (IS) is becoming a popular analytical tool in material research and development because simple electrical measurements can be made and the results can often be correlated with the material variables. These variables include: mass transport [109], rates of chemical reactions [110], corrosion [111], dielectric properties [112], and defects [113]. A flow diagram of a general characterization procedure using EIS is represented in **Figure 1.19**. Experimentally obtained impedance data for a given electrode-materials system may be analyzed by using electrical equivalent circuits. These circuits (RC circuits) consist of simple elements such as resistance (R) and

capacitance (C) which are connected to model the electrochemical processes [107, 108]. The resistance in the equivalent circuit represents the electrical conductivity of the electrolyte (bulk resistance) and the capacitance (double-layer capacitance) caused by the charge which is in excess at the electrode-electrolyte interface. The most commonly used equivalent circuit in EIS is the Ershler-Randles circuit [107]. This circuit is equivalent to an electrode to which a chemical reaction, $O + ne^- \leftrightarrow R$, occurs (**Figure 1.20**).

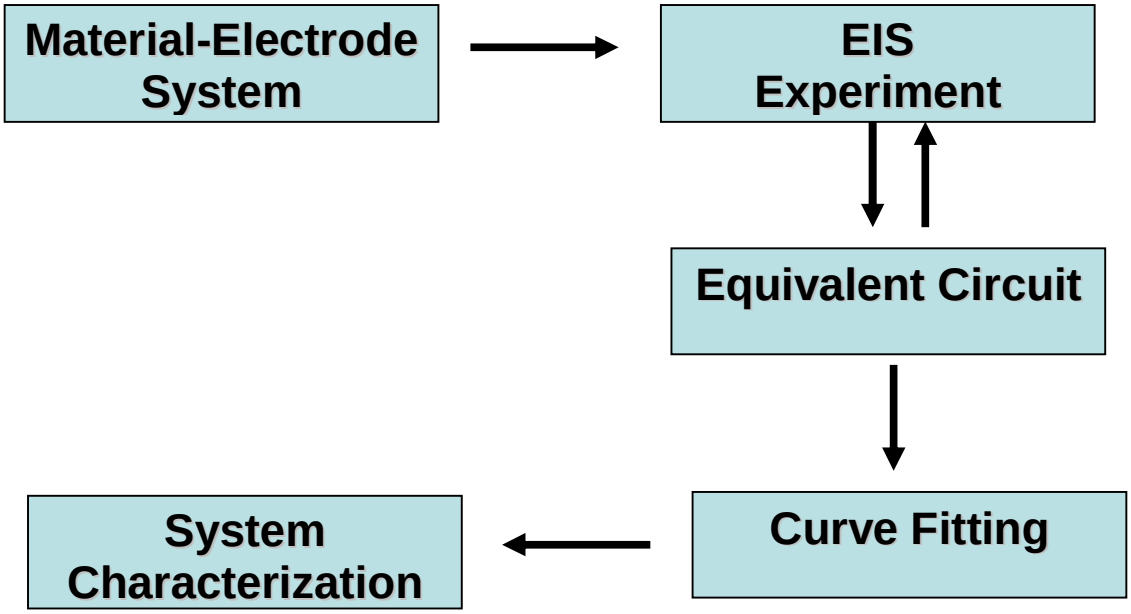

Figure 1.19: Flow diagram for the measurement and characterization of a material-electrode system.

In Randles equivalent circuit the electrolyte resistance (R_E) is connected in series to the parallel connections of charge transfer resistance (R_{CT}) and the double layer capacitance (C_d). Randles equivalent circuit also takes into account the fact that the reaction rate might be controlled by the transport phenomenon of electroactive species [107], by having an extra component called Warburg impedance (Z_W). This component is connected in series with the charge transfer resistance.

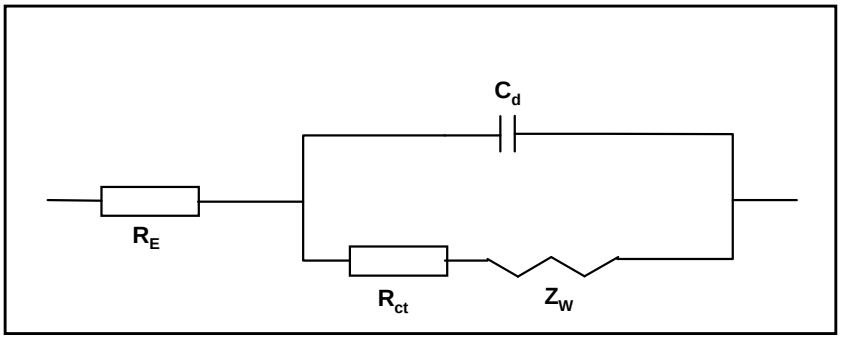

Figure 1.20: Ershler-Randles circuit for the electrochemical system with diffusion-limited behaviour.

Impedance data is graphically represented as a Nyquist and Bode plots. Nyquist plot, is a plot of the imaginary part (-Z'', y-axis) versus the real part (Z', x-axis) of impedance (**Figure 1.21**). In this representation of impedance data there is no clear indication of the dependence of impedance and phase angle to frequency. For this reason Bode plots are used to monitor the real part of impedance and phase angle (θ) as a function of frequency. Therefore, Bode data representation is a plot of the phase angle (θ) and the logarithm of impedance magnitude (log Z) versus the logarithm of the frequency (log f) (**Figure1.22**).

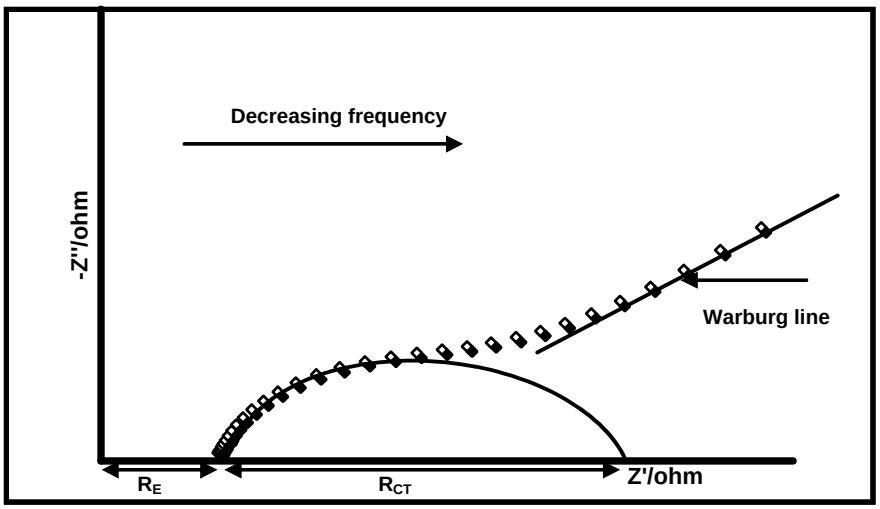

Figure 1.21: Nyquist plot for the electrochemical system with diffusion-limited behavior.

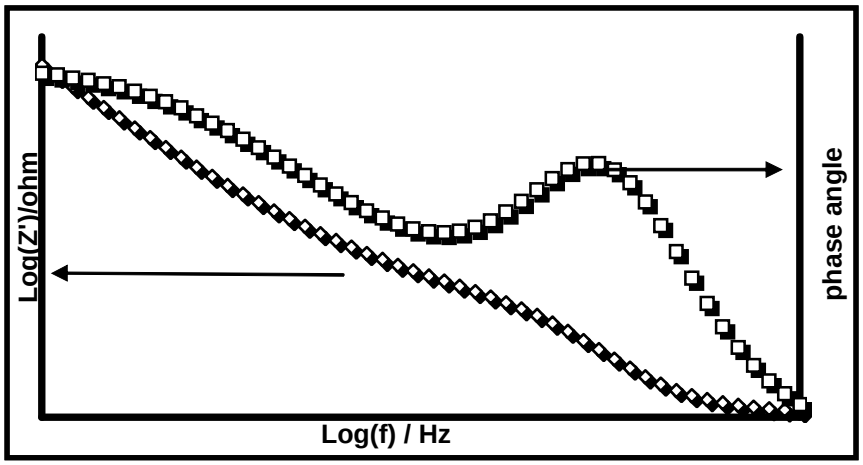

Figure 1.22: Bode plot for the Randles equivalent circuit with diffusion-limited behavior.

1.7.4.3 The Use of Impedance Spectroscopy to Study the Blocking Properties of SAM towards Electron Transfer.

Self-assembled monolayer of thiol substituted phthalocyanine (like alkane thiols) on gold, are remarkable structures because the monolayer can survive the voltammetry experiments in aqueous electrolyte [114, 115]. The monolayer strongly blocks electrode processes like gold oxidation in acidic electrolyte and electron transfer with otherwise reversible redox couples (eg. $Fe(NH_4)(SO_4)_2$) [115]. However, the blocking properties of SAM are not perfect, because in most cases the coated electrode exhibits behavior resembling a microarray electrode. A microarray electrode is an electrode containing small active sites embedded in an insulating plane [116]. The active sites in the monolayer are identified as pinholes. Pinholes are a result of imperfect adsorption of thiol substituted derivatives [116]. At the pinholes electrolytes and redox couples have access to the gold substrate.

Theoretical treatment assumes that microarrays are evenly spaced array of disc shape micro electrodes of uniform radii embedded in an insulating plane (**Figure 1.23**).

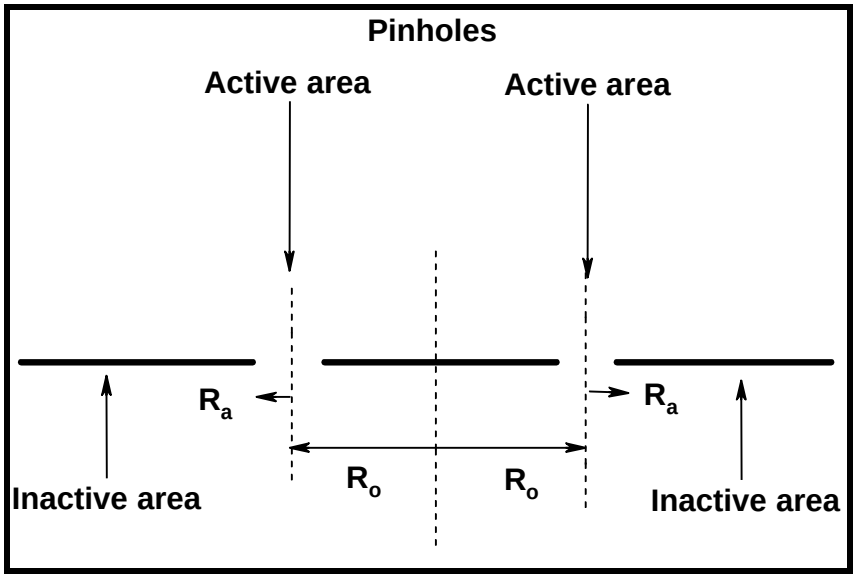

Figure 1.23: Microarray parameters.

The surface coverage θ (note that in impedance θ is used both as surface coverage and angle) can easily be calculated from the data obtained from an EIS experiment by using **Equation 1.37**.

$$\theta = 1 - (\frac{R_o}{R_{ct}}) \qquad 1.37$$

where R_o is a charge transfer resistance of a bare electrode and R_{ct} is a charge transfer resistance of the modified electrode. According to Amatore *et al*. [117], θ should not be derived from **Equation 1.37** when its value is close to one (θ>0.9), due to fact that there are a large number of pinholes on SAMs. In this case, the coverage can be estimated from a model based on a pinhole size and spacing. The fraction of pinhole area (1 - θ) can

be related to the size of pinholes (r_a) and distance between pinholes (r_b) by **Equation 1.38** [118].

$$1-\theta=\frac{r_a^2}{r_b^2} \qquad 1.38$$

From the plot of $Z_f^{'}$ versus $\omega^{-1/2}$ the r_a and r_b may be obtained using **Equation 1.39** to **1.41**[118]:

$$r_b=\frac{\gamma(1-\theta)}{\sigma\sqrt{0.72/D}} \qquad 1.39$$

$$r_a=\frac{r_b}{\sqrt{(1-\theta)}} \qquad 1.40$$

and

$$\sigma=\frac{\sqrt{2}(RT/F)}{FAc\sqrt{D}} \qquad 1.41$$

where σ is the Warburg coefficient; γ is the intercept of $Z_f^{'}$ versus $\omega^{-1/2}$ plot in the low frequency region; A is the electrode geometrical area in cm^2; c is the redox species concentration in mol cm^{-3}; and D is the diffusion coefficient of the redox species in cm s^{-1}.

1.8 Summary of Thesis Aims:

i) The aim of the project is to synthesise novel tin macromolecules (SnPcs, SnTBTAP and SnTBC: **Figure 1.24)** that are water soluble and those that dissolve in organic solvents. These macromolecules will be characterized by elemental analysis, inductively coupled plasma (ICP) spectroscopy, nuclear magmetic resonance (NMR) spectroscopy, UV-vis spectroscopy, infrared (IR) spectroscopy and mass spectroscopy (MS).

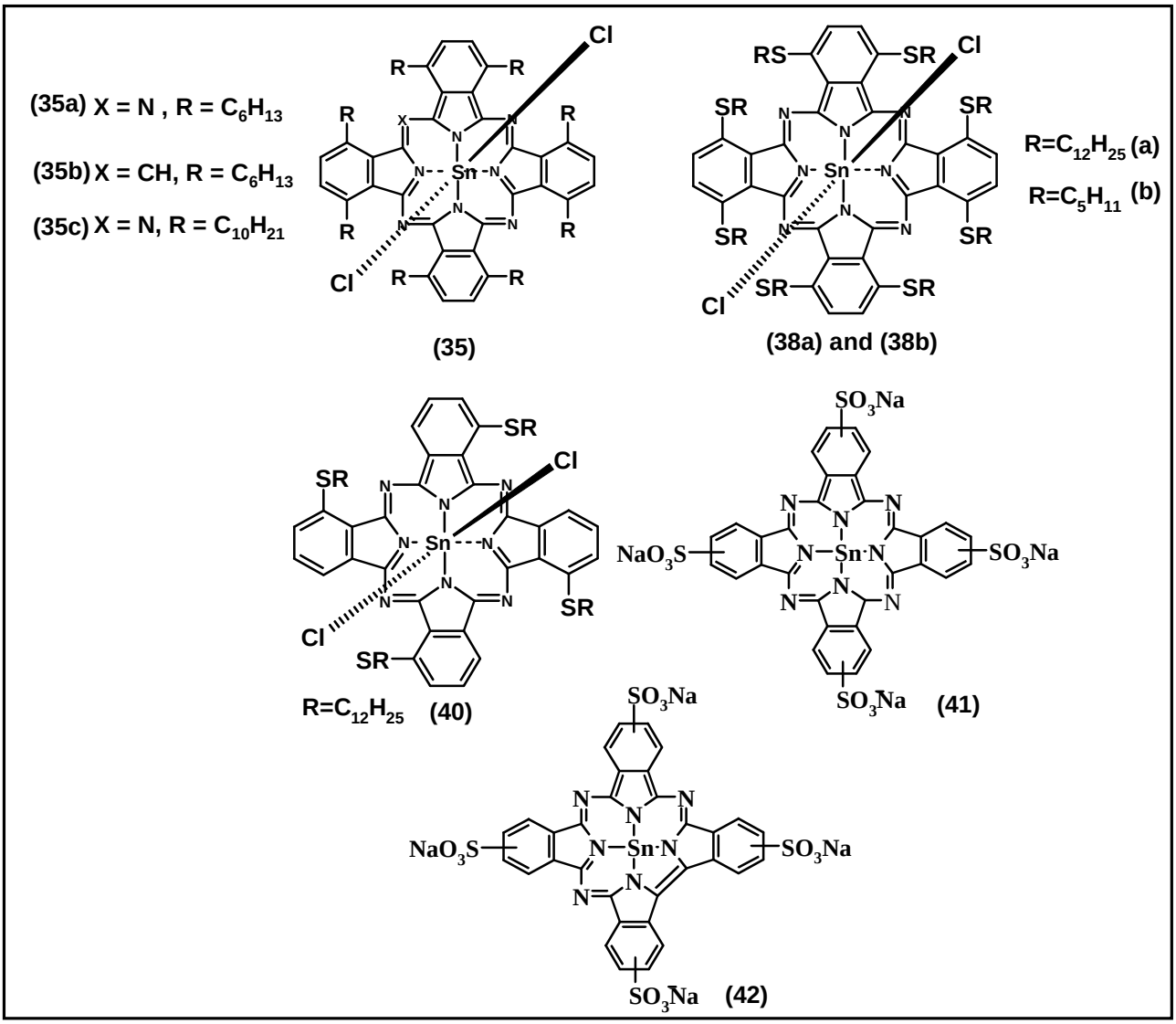

Figure 1.24: Molecules that are studied in this thesis.

ii) Photophysical properties (dimerisation constant, fluorescence quantum yield, fluorescence lifetimes, triplet quantum yield and triplet lifetimes) of the newly synthesised tin macromolecules will be investigated. The interaction properties of water soluble macromolecules with BSA (together with their binding constants and biomolecular constants) will be studied.

iii) The self assembled monolayer study of α substituted $Cl_2SnPc(SC_{12}H_{25})_4$ and $Cl_2SnPc(SC_{12}H_{25})_8$ on gold electrode will be investigated by the use of EIS. Electrochemical characterization of $Cl_2SnPc(SC_{12}H_{25})_4$ and $Cl_2SnPc(SC_5H_{12})_8$ will also be investigated.

CHAPTER TWO: EXPERIMENTAL

2.1 Materials

Acetone, dimethylformamide (DMF), dichloromethane (DCM), tetrahydrofuran (THF), toluene, hydrogen peroxide, sulfuric acid, potassium hydroxide pallets where obtained from SAARCHEM, 1.8-diazabicyclo[5, 4, 0] undec-7-ene (DBU), 3-nitrophthalic acid, 2, 3-dicyanohydroquinone, triflic anhydride, dibromoethane, p-toluenesulfonyl chloride, ferricyanide ($K_3Fe(CN)_6$), ferrocyanide ($K_4Fe(CN)_6$), potassium chloride, dodacanethiol, potassium cabornate, buffer tablets, cerium chloride, tin(II)chloride and tetraethylammonium perchlorate (TEAP), were purchased from Sigma-Aldrich. 2, 6-Lutidine, iododecane, iodohexane, bis(triphenylphosphine)nickel(II) dichloride and lithium chloride were from Alfa Aesar. Triphenylphosphine, Zn dust and n-butyllithium (2.5 M hexane) were procured from Lancaster. Trifluoromethanesulfonic acid anhydride and trimethylsilyl chloride were from Apollo. Hexyl iodide and decyl iodide (for making $C_6H_{13}ZnI$ and $C_{10}H_{21}ZnI$, respectively) according to reference [49] were from Aldrich. Glacial acetic acid and Li metal were obtained from commercial suppliers. Column chromatography was performed on silica gel 60 (0.04-0.063 mm). DMF was stored over alumina, distilled and stored dry over molecular sieves before use.

2.2 Equipment

Cyclic (CV), square wave (SWV) voltammetry and Impedance data were obtained with Autolab potentiostat PGSTAT 30 (Eco Chemie, Utretch, The Netherlands) driven by the General Purpose Electrochemical Systems data processing software (GPES, software version 4.9, Eco Chemie), using a conventional three-electrode set-up with glassy carbon electrode (GCE, 3 mm diameter) as a working electrode, platinum wire as counter electrode and Ag|AgCl wire as pseudo-reference electrode. The potential response of Ag|AgCl pseudo-reference in aqueous conditions was less than the Ag|AgCl (3M KCl) by 0.015 V. Electrochemical experiments were performed in dry chloroform containing tetrabutylammonium tetrafluoroborate ($TBABF_4$) as a supporting electrolyte. Prior to scans, the working electrode was polished with alumina paste on a Buehler felt pad, followed by washing with deionised water and rinsing with methanol and chloroform.

Spectroelectrochemical data were recorded using a home-made optically transparent thin-layer electrochemical (OTTLE) cell. The OTTLE cell was connected to a BioAnalytical Systems (BAS) CV 27 voltammograph. UV/Vis spectra were recorded on a Cary 500 UV-Vis/NIR spectrophotometer.

Electrochemical impedance spectroscopy (EIS) experiments were performed on an Autolab potentiostat PGSTAT 30, controlled by FRA software which was used for the acquisition and analysis of the impedance data. EIS experiments were recorded in the frequency range between 100 mHz to10 KHz at a formal potential of 150 mv ($E_{1/2}$ of

$Fe(CN)_6^{3-/4-}$ redox couple on bare gold electrode) and with an amplitude 5mV sinusoidal modulation.

Fluorescence excitation and emission spectra, were recorded on a Varian Eclipse spectrofluoremeter using 1 cm pathlength cuvettes at room temperature. IR spectra (KBr pellets) were recorded on a Perkin-Elmer spectrum 2000 FTIR spectrometer. ^{1}H-NMR spectra were recorded using a Bruker EMX 400 MHz NMR spectrometer or at 300 MHz using a Varian Gemini 2000 spectrometer. Elemental Analyses were performed at the University of Cape Town. Sn elemental analyses was performed using inductively coupled plasma (ICP) Thermo Electron iCAP 6000 ICP. MS data were recorded on a Shimadzu KRATOS Maldi MS instrument.

Microwave irradiations were carried out in a Defy DM206T microwave oven at a power of 1000W. Triplet absorption and decay kinetics were recorded on a laser flash photolysis system (**Figure 2.1)**, the excitation pulses were produced by an Nd: YAG laser (Quanta-Ray, 1.5 J / 90 ns) pumping a dye laser (Lambda Physic FL 3002, Pyridin 1 in methanol). The analyzing beam source was from a Thermo Oriel xenon arc lamp, and a photomultiplier tube was used as detector. Signals were recorded with a two-channel digital real-time oscilloscope (Tektronix TDS 360); the kinetic curves were averaged over 256 laser pulses.

Photo-irradiations for photodegradation studies were done using a General electric Quartz line lamp (300W). A 600 nm glass cut off filter (Schott) and a water filter were used to

filter off ultraviolet and infrared radiations respectively. An interference filter (Intor, 670 nm with a band width of 40 nm) was additionally placed in the light path before the sample. Light intensities were measured with a POWER MAX 5100 (Molelectron detector incorporated) power meter and were found to be 7 x 10^{16} photons $s^{-1}.cm^{-2}$.

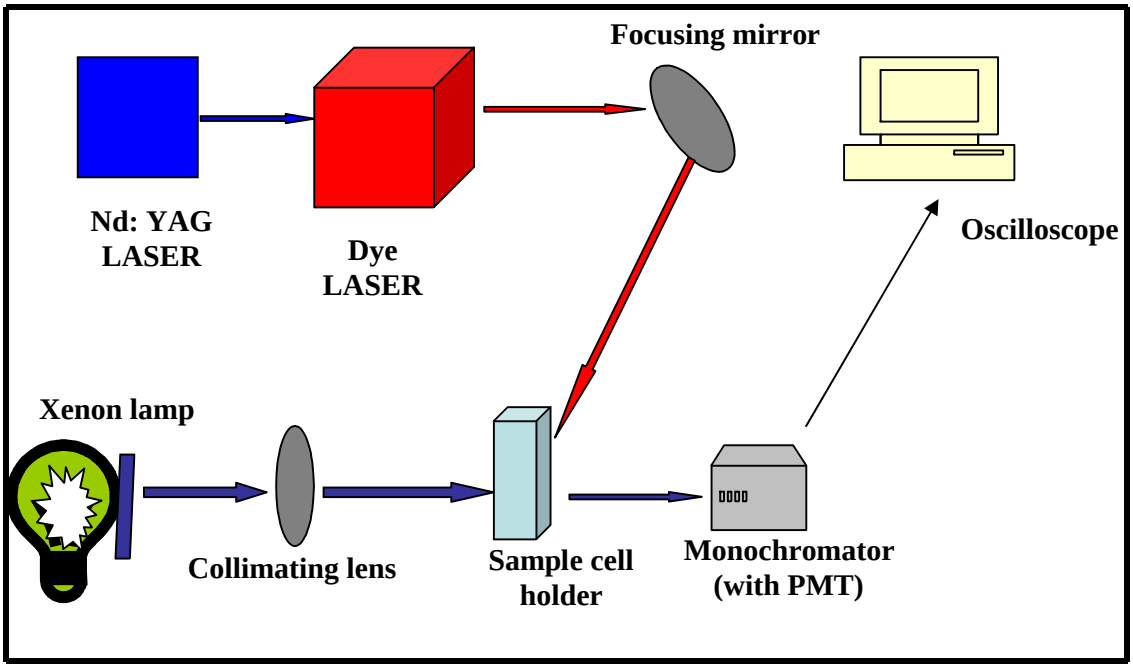

Figure 2.1: Flash photolysis system.

2.3 Synthesis

2.3.1 Nonperipheral and peripherally substituted phthalonitrile synthesis

2.3.2 Preparation of 3, 6-bis(trifluoromethanesulfonyloxy) phthalonitrile (18): Scheme (Scheme 3.1).

Following a literature methods [49], 2, 3-Dicyanohydroquinone **(17)** (1 g, 6.1 mmol) was dissolved in a mixture of DCM (60 mL) and 2, 6-lutidine (3mL) under argon, and the resulting brown solution was cooled to -20 °C. A solution of trifluoromethanesulfonic acid anhydride (2.5 mL, 15 mmol) in DCM (10 mL) was added dropwise at -20 °C. The resulting solution was allowed to warm up to RT and stirred overnight (as slowly as possible). The reaction was filtered off by suction and washed with cold methanol. The crude product obtained was recrystallised from dichloromethane/methanol to afford the titled compound **(18)** as white plates; Yield: 1.85g (71%); IR[(KBr) v_{max} / cm^{-1}]; 3110, 2364 ($C-C$), 2337, 2250 ($C \equiv N$), 1473, 1437, 1227, 1131, 954, 840, 808, 700, 665, 598, 505, 337; δ_H (300 MHz, $CDCl_3$) 7.87 (2H, s, H_{arom}).

2.3.3 Preparation of activated zinc dust (Scheme 3.2).

Following a literature method [119], zinc dust (200 g) was stirred in 2% solution of hydrochloric acid (500 mL) for 2 minutes and the acid removed (decanted). The resulting dust was stirred sequentially with a 2% solution of hydrochloric acid (500 mL), water (3 x 500 mL) and absolute ethanol (2 x 350 mL). The dust was allowed to settle before the solution was decanted. Finally, the zinc was washed with diethyl ether (350 mL), filtered

and dried under vacuum for 24 h. The resulting dust was stored under vacuum over phosphorous pentoxide.

2.3.4 Preparation of hexylzinc iodide (Scheme 3.3).

Activated zinc dust from **Scheme 3.2,** (60g, 0.92 mol) and THF (40 mL) were mixed in a flask. Dibromoethane (3.2 mL, 38 mmol) was added via syringe, and the mixture was heated to boiling. The reaction was allowed to cool and heated again. This process was repeated once more, and trimethylsilyl chloride (4.8 mL, 38 mmol) was added. The mixture was heated again, and allowed to cool. The rubber septum was replaced by a pressure-equalising addition funnel charged with iodohexane (46 mL, 312 mmol) in THF (60 mL), and the reaction was heated to 40-45 °C. The iodohexane was added dropwise over 30 minutes and the resultant mixture stirred for 12h at 40 °C (under reflux). The reaction was cooled and the excess of zinc allowed to settle (4h). The resulting grey zinc reagent was transferred via a syringe to a storage vessel. The remaining zinc was washed with THF (40 mL), allowed to settle and transferred into the storage vessel to afford hexylzinc iodide in THF (194 mL, at 1.44 M assuming a 90 % conversion).

2.3.5 Phthalonitrile synthesis (Scheme 3.4).

Preparation of 3, 6-dihexylphthalonitrile (20a) and 3, 6-didecylphthalonitrile (20b) Negishi coupling (Scheme 3.4).

Following a literature method [22], both 3, 6-dihexylphthalonitrile **(20a)** and 3, 6-didecylphthalonitrile **(20b)** are synthesised as described below, but **(20b)** was donated by Cook's group. Bis(triphenylphosphine)nickel (II) dichloride (465 mg, 0.05 mol) and triphenylphosphine (375 mg, 0.1 mol) were stirred in THF (30 mL). n-Butyllithium (0.9, 0.1 mol, 2.5 M in hexane) was added to afford a blood red slurry. 3, 6-Bis(trifluoromethanesulfonyloxy) phthalonitrile **(18)** (3 g, 7 mmol) and lithium chloride (0.9 g, 21 mmol) were added as solids under a fast stream of argon, and the resulting pale brown solution was cooled to -78 °C. Hexylzinc iodide in THF (21 mmol, 15 mL of a 1.44 M solution of THF) was added dropwise via a syringe and the resulting red solution was warmed to RT over ca. 1 h. The reaction was stirred over night. A 10 % solution of hydrochloric acid (10 mL) was carefully added and the mixture extracted with ethyl acetate (2 x 30 mL). The combined organic layers were successively washed with a 10% solution of hydrochloric acid (20 mL), a 5% solution of sodium hydroxide (20 mL), brine (20 mL), dried over $MgSO_4$, filtered and concentrated under reduced pressure. The resulting oily brown residue was purified by chromatography (dry loading with ethyl acetate) over silica using 24:1 mixture of petroleum ether/diethyl ether (thin layer chromatography (TLC) developed using petroleum ether/diethyl ether 9:1). **(20a)** was isolated as a yellow solid; Yield: 0.8g (41%): IR[(KBr) $v_{\max} / cm^{-1}$]: 2929 ($C-C$), 2858, 2363, 2333, 2228 ($C \equiv N$), 1702, 1560, 1460, 1420, 1375, 1294, 1234, 1170, 1100, 838,

718, 638, 447; δ_H (300 MHz, $CDCl_3$) 7.47 (2H, s, H_{arom}), 2.86 (4H, t, Ar-CH_2-), 1.67 (4H, m, Ar-CH_2-CH_2-), 1.34 (12H, m, $H_{aliphatic}$), 0.90 (6H, t, CH_3-).

3, 6-didecylphthalonitrile (20b)

IR[(KBr) v_{max} / cm^{-1}]: 2920 ($C-H$), 2849($C-H$), 2363, 2342, 2228 ($C \equiv N$),1702, 1560, 1463, 1375, 1300, 1230, 1170, 1122, 1002, 890, 853, 721, 646, 503, 468; δ_H (300 MHz, $CDCl_3$) 7.47 (2H, s, H_{arom}), 2.86 (4H, t, Ar-CH_2-), 1.67 (4H, m, Ar-CH_2-CH_2-), 1.34 (28H, m, $H_{aliphatic}$), 0.90 (6H, t, CH_3-).

Synthesis of 3, 6-Bis(4-methylphenylsulfonyloxy) phthalonitrile (31) (Scheme 3.5)

Following a literature method [120], p-toluenesulfonyl chloride (10.32g, 0.054mol) was added to a suspension of 2, 3-dicyanohydroquinone (4g, 0.025mmol) and potassium carbonate (13.8g, 0.1mmol) in acetone (30mL). The temperature of the flask rose and stabilized after 2 minutes. The mixture was then heated to reflux and stirred for 2 hours. TLC (eluting: CH_2Cl_2) indicated that all the starting material (2, 3-dicyanohydroquinone) has completely reacted. The mixture was allowed to cool to room temperature, and was poured into water (200mL) and the mixture stirred for 1 hour. Filtration gave the title compound **(31)** as a colourless solid. Yield: 9.52g (80%), IR[(KBr) v_{max} / cm^{-1}]: 3432, 3239, 3085, 2243, 2226 ($C \equiv N$), 1504, 1449, 1315, 1279, 1204, 1174, 1142($S=O$), 1021, 1004, 979, 934, 847, 749, 694, 638, 614.

3, 6-Di(pentanethiol)-4, 5-dicyanobenzene (21a) (Scheme 3.6).

1-Pentanethiol (0.69, 6.6 mmol) was dissolved in dry DMF (15 ml) under a nitrogen atmosphere and **(18)** (0.7g, 1.65 mmol) was added. The mixture was stirred for 15 min and finely ground anhydrous potassium carbonate (2g, 14.5 mmol) was added portionwise for 2h while stirring. The mixture was stirred under a nitrogen atmosphere for 12h, the mixture was then poured into ice water and stirred for 30 min. 4, 5-didodecanephthalonitrile was extracted with DCM and washed with 5% sodium carbonate solution (2 x 50 ml). The solution was further treated with water (2 x 250 ml) and the resulting yellow oil was concentrated under reduced pressure and recrystallised from ethanol. Yield: 0.36g(78%), IR[(KBr) v_{max} / cm^{-1}]: 3084, 2951, 2930, 2864, 2378 (C-H), 2225 ($C \equiv N$), 1444, 1283, 1202, 1181, 1173, 1145, 877, 847, 827, 725 ($C - S$), 547, 447. ^{1}H-NMR ($CDCl_3$): δ ppm 7.49 (2H, s, Ar-H), 2.99 -3.02 (4H, t, -CH_2), 1.63 -1.71 (4H, m, -CH_2), 1.37 -1.46 (4H, m, -CH_2), 1.28 -1.36 (4H, m, -CH_2), 0.91-0.88 (6H, t, -CH_3).

3, 6-Di(dodacanethiol)-4, 5-dicyanobenzene (21b)

Compound **(21b)** was prepared as described above for compound **(21a)** using **(31)** (2g, 14.5 mmol), pentanethiol (6.0g, 58 mmol) and potassium carbonate (5g, 36.2 mmol).Yield: 5.74(75%), IR[(KBr) v_{max} / cm^{-1}]: 3084, 2951, 2930, 2864, 2378 (C-H), 2225 ($C \equiv N$), 1444, 1283, 1202, 1181, 1173, 1145, 877, 847, 827, 725 ($C - S$), 547, 447. ^{1}H-NMR ($CDCl_3$): δ ppm 7.49 (2H, s, Ar-H), 2.99 -3.02 (4H, t, -CH_2), 1.63 -1.71 (4H, t, -CH_2), 1.37 -1.46 (4H, m, -CH_2), 1.28 -1.36 (32H, m, -CH_2), 0.88 -0.91 (6H, t, -CH_3).

3-Didodecanethiol-4, 5-dicyanobenzene (33) (Scheme 3.7).

3-Nitrophthalonitrile **(32)** was purchased from Aldrich and used as received. Under a blanket of nitrogen, dodecanethiol (2.18g, 10.8 mmol) and 3-nitrophthalonitrile **(32)** (1.0g, 5.3 mmol) were dissolved in dry DMF (15ml). Anhydrous K_2CO_2 (2g, 14.5 mmol) was added portion-wise for 2h, after 12h (total reaction time) the mixture was poured into ice water and stirred for 30 min. 3-Didodecanephthalonitrile was extracted with DCM and washed with 5% sodium carbonate solution (2 x 50 ml). The solution was further treated with water (2 x 250 ml) and the resulting yellow oil was concentrated under reduced pressure and recrystallised from ethanol. Yield: 1.21g (70%), IR[(KBr) v_{max} / cm^{-1}]: 3071, 2922, 2851, 2585, 2364 (C-H), 2335, 2230 ($C \equiv N$), 1702, 1562, 1458, 1346, 1262, 1223, 1109, 930, 899, 870, 722($C - S$), 680, 526; ^{1}H-NMR ($CDCl_3$): δ ppm 7.58 -7.64 (2H, m, Ar-H), 7.30 (1H, s, Ar-H), 3.07 -3.10 (2H, t, -CH_2), 1.76 -1.78 (2H, t, -CH_2), 1.46 -1.64 (2H, m, -CH_2), 1.28 -1.29 (16H, m, -CH_2), 0.84 -0.93 (3H, t, -CH_3).

2.3.6 Tin phthalocyanines synthesis (Scheme 3.8).

Metal-free (34a) 1, 4, 8, 11, 15, 18, 22, 25-octahexylphthalocyanine, (34b) 2^1, 2^4, 7^1, 7^4, 12^1, 12^4, 17^1, 17^4–octahexyltetrabenzo-5, 10, 15-triazaporphyrin and (34c) 1, 4, 8, 11, 15, 18, 22, 25-octadecylphthalocyanine (Scheme 3.8).

Complexes (**34a)**, (**34b) and (34c)** were synthesized using the lithium base catalysed method but with excess lithium as follows: 3, 6-dihexylphthalonitrile (**20a**) (0.7g, 2.35 mmol) was dissolved in hot 1-pentanol (15 mL) in open atmosphere. Lithium metal was added in portions (0.28 g, 6eq) at room temperature and the yellow suspension was

heated under reflux for 24 h under an atmosphere of Ar. The dark green mixture was cooled down to room temperature. Glacial acetic acid (30 mL) was added and the mixture was stirred at RT for 30 minutes, precipitated out with methanol and filtered. The green solid (0.29g) was purified by column chromatography over silica. Two different complexes (**34a)** and (**34b)** were isolated using cyclohexane as eluent. Complex (**34b)** in which one of the aza nitrogen atoms as been replaced by C-H group, was eluted first, followed by the normal phthalocyanine derivative (**34a**).

Complex (**34c)** was synthesized as for complex (**34a)** except (**20b)** was employed instead of (**20a)** using the same amounts of reagents.

34a: δ_H ($CDCl_3$): 7.8 (8H, H_{arom}), 4.4 (16H, t, -CH_2-Ar), 2.1 (16H, m, Ar-CH_2-CH_2-), 1.3 (48H, m, $H_{aliphatic}$), 0.90 (24H, t, CH_3-), -0.2 (2H, s, inner protons).

34b: δ_H ($CDCl_3$): 11.4 (1H, s, methine), 8.18 (8H, H_{arom}), 4.7(16H, t, -CH_2-Ar) 2.30 (16H, m, Ar-CH_2-CH_2-), 1.52 (48H, m, $H_{aliphatic}$), 0.90 (24H, t, CH_3-), -0.35 (2H, s, inner proton).

34c: δ_H ($CDCl_3$): δ_H (300 MHz, $CHCl_3$), 7.8 (8H, H_{arom}), 4.4(16H, t, -CH_2-Ar), 2.1 (16H, m, Ar-CH2-CH2-), 1.3 (112H, m, $H_{aliphatic}$), 0.90 (24H, t, CH3-), -0.2 (2H, s, inner protons).

1, 4, 8, 11, 15, 18, 22, 25-Octahexylphthalocyanine tin (IV) dichloride (35a) (Scheme 3.8)

Complex **(34a)** (0.25g, 0.21 mmol) and $SnCl_2$ (0.040 g, 0.21mmol) were dissolved in hot pentanol refluxed at 150°C for 90 min. The green product obtained was concentrated under reduced pressure and precipitated out with cold methanol. The green product was

recrystallized from THF and methanol. Yield: 0.19g, 70%. M.p. 170 ^{o}C; δ_H ($CDCl_3$), 8.19 (8H, H_{arom}), 4.6(16H, t, -CH_2-Ar), 2.28 (16H, m, Ar-CH_2-CH_2-), 1.40 (48H, m, $H_{aliphatic}$), 0.9 (24H, t, CH_3-). Calcd. for $C_{80}H_{112}N_8Sn(Cl)_2$: C, 69.94: H, 8.16: N, 8.16 %: Found C: 69.77 H: 8.29 N: 7.69 %: IR [(KBr) ν_{max} / cm^{-1}]: 3246, 2923 (C-H), 2855, 2364, 2326, 1701, 1354, 1543, 1561, 1459, 1420, 1327, 1215, 1157, 1086, 893, 825, 742, 546,419. UV/Vis (THF), λ_{max} / nm ($\log\varepsilon$)]: 736 (5.34), 699 (4.65), 660 (4.73), 364 (4.89).

2^1, 2^4, 7^1, 7^4, 12^1, 12^4, 17^1, 17^4–octahexyltetrabenzo-5, 10, 15-triazaporphyrin tin(IV) dichloride (35b) (Scheme 3.8).

The synthesis and purification procedure was as outlined for **(35a)**, except (**34b)** was employed instead of (**34a)**. The amounts of reagents employed were: **(34b)** (0.04g, 0.034 mmol) and $SnCl_2$ (0.004g, 0.034 mmol) in pentanol (3ml). Yield: 0.024g, 60%; δ_H ($CDCl_3$), 11.4 (1H, s, methine), 8.18 (8H, $H_{arom,}$), 4.7 (16H, t, -CH_2-Ar), 2.30 (16H, m, Ar-CH_2-CH_2-), 1.52 (48H, m, $H_{aliphatic}$), 0.90 (24H, t, CH_3-). MS (ESI). m/z: Calc. 1373.7, found 1372 $[M-1]^+$, 1337 [M-Cl]. IR [(KBr) ν_{max} / cm^{-1}]: 3278, 2939 (C-H), 2924 (C-H), 2854, 2359, 2332, 1732, 1652, 1573, 1537, 1539, 1506, 1455, 1427, 1329, 1270, 1226, 1161, 1089, 893, 814, 741, 668, 497, 418. UV/Vis [(THF, λ_{max} / nm ($\log\varepsilon$)]: 727(5.15), 701(4.95), 660(4.63), 637(4.62), 425(4.71), 372(4.83)

1, 4, 8, 11, 15, 18, 22, 25-Octadecylphthalocyanine tin(IV) dichloride (35c)

The synthesis and purification procedure for **(35c)** was as out lined for **(35a)**, except (**34c)** was employed instead of (**34a).** The amounts of reagents employed were: (**34c**) (0.1g, 0.25 mmol) and $SnCl_2$ (0.014g, 0.0613 mmol) in pentanol (20 ml). Yield: 0.075g, 68%; δ_H ($CDCl_3$), 8.19 (8H, H_{arom}), 4.7 (16H, t, -CH_2-Ar), 2.30 (16H, m, Ar-CH_2-CH_2-), 1.30 (112H, m, $H_{aliphatic}$), 0.90 (24H, t, CH_3-). Calcd. for $C_{112}H_{176}N_8Sn(Cl)_2$ C, 73.82: H, 9.67: N, 6.15 %: Found C: 73.49 H: 9.83 N: 5.25 %. IR [(KBr) ν_{max} / cm^{-1}]: 3417, 2944 (C-H), 2919 (C-H), 2849, 2352, 1644, 1591, 1504, 1454, 1327, 1217, 1154, 1086, 894, 744, 418. UV/Vis[(THF, λ_{max} / nm ($\log\varepsilon$)]; 736(5.34), 701(4.64), 661(4.68), 429.6(4.46), 365(4.80), 324(4.78).

1, 4, 8, 11, 15, 18, 22, 25-Octadecylphthalocyanine Zn(II) (36) (Scheme 3.9).

The synthesis and purification procedure for **(36)** was as out lined for **(35a)**, except zinc acetate was employed instead of tin chloride**.** The amounts of reagents employed were: (**34c**) (0.04g, 0.034 mmol) and zinc acetate (0.0075g, 0.034 mmol) in pentanol (3ml). Calcd. for $C_{112}H_{176}N_8Zn$, C, 79.78: H, 10.37: N, 6.60 %: Found C: 78.06 H: 10.53 N: 6.44 %. IR [(KBr) ν_{max} / cm^{-1}]: 3417, 2944 (C-H), 2919 (C-H), 2849, 2352, 1644, 1591, 1504, 1454, 1327, 1217, 1154, 1086, 894, 744, 418. UV/Vis[(THF, λ_{max} / nm ($\log\varepsilon$)]; 700(5.28), 665(4.53), 629(4.56), 334(4.86).

Metal-free 1, 4, 8, 11, 15, 18, 22, 25,-octathiododecylphthalocyanine (37a) (Scheme 3.11).

In refluxing pentanol (10 ml), (**21a)** (0.5g, 0.95 mmol) and DBU (1.70 g, 11.17 mmol) were added. The solution was heated to reflux for 1hour and $CeCl_3$ (41mg, 0.16 mmol) was added to afford a black coloured precipitate. Reflux was continued for a further 4 hours. Reaction was then cooled down and the solvent removed under reduced pressure, followed by titration with cold methanol to precipitate the product. The black precipitate was dissolved in DCM and passed through a silica column, DCM was used as the eluting solvent to afford (**37a).** Yield: 0.74g (37%), $C_{128}H_{208}N_8S_8$: Found: C, 72.46; H, 10.13 N, 4.97, S, 12.51%: Calculated C, 72.69; H, 9.84; N, 5.3; S, 12.12 %.UV/Vis [($CHCl_3$, λ_{max} / nm] 806, 713, 357.

Metal-free 1, 4, 8, 11, 15, 18, 22, 25,-octapentylthiophthalocyanine (37b) (Scheme 3.11).

Compound (**37b)** was prepared as described above for compound (**37a),** using compound **(21b)** (0.30g, 0.95 mmol), DBU (1.70 g, 11.17 mmol) and $CeCl_3$ (41mg, 0.16 mmol). Compound **(37b)** was purified as described above for compound **(37a).** Yield: 0.55g (40%), $C_{72}H_{96}N_8S_8$: Found: C, 64.87; H, 7.47 N, 7.71, S, 20.44%: Calculated C, 64.80; H, 6.87; N, 8.01; S, 18.3 %.UV/Vis [($CHCl_3$, λ_{max} / nm] 806, 713, 357.

1, 4, 8, 11, 15, 18, 22, 25,-octathiododecylphthalocyanine tin(IV) dichloride (38a) (Scheme 3.11).

Complex (**37a)** (0.44g, 0.19 mmol) and $SnCl_2$ (0.04 g, 0.21 mmol) were dissolved in hot pentanol (10 ml), refluxed at 150°C for 90 min to afford the titled compound (**38a**). Compound **(38a)** was concentrated under reduced pressure and precipitated out with cold methanol. The purple product was recrystalised from DCM and methanol. Yield: (0.384g, 80%); δ_H ($CDCl_3$), 8.0 (8H, s, H_{arom}), 3.5 (16H, t, Ar –SCH_2-), 2.1 (16H, m, Ar-SCH_2-CH_2-), 1.2-1.65 (144H, m, $H_{aliphatic}$), 0.80 (24H, t, CH_3-); $C_{128}H_{208}N_8S_8SnCl_2$: Found: C, 68.38; H, 9.46 N,4.67, S, 11.85%: Calculated C, 67.40; H, 9.12; N, 4.90; S, 10.34 % , [IR (KBr pellets) ν_{max}/cm^{-1}] 316, 2922 ($C-H$), 2851 ($C-H$), 1587, 1539, 1505, 1454, 1410, 1369, 1333, 1080, 945, 864, 774, 734, 667 ($C-S$), 544, 498, 518;[UV/Vis, $CHCl_3$, λ_{max}/nm ($\log\varepsilon$)]: 918(5.00), 805(4.62), 635(4.02), 355(34.56).

1, 4, 8, 11, 15, 18, 22, 25,-octapentathiododecylphthalocyanine tin(IV) dichloride (38b) (Scheme 3.11).

Compound (**38b)** was prepared as described above for compound (**38a)** using **(37b)** instead of **(37a).** Amounts of reagents were: Complex **(37b)** (0.45 g, 0.32 mmol), $SnCl_2$ (0.061 g, 0.32 mmol) and pentanol (15 ml). Yield: (0.38g, 80%); δ_H ($CDCl_3$), 8.0 (8H, s, H_{arom}), 3.5 (16H, t, Ar –SCH_2-), 2.1 (16H, m, Ar-SCH_2-CH_2-), 1.2-1.65 (32H, m, $H_{aliphatic}$), 0.80 (24H, t, CH_3-); $C_{72}H_{96}N_8S_8SnCl_2$: Found: C, 57.28; H, 6.47 N, 46.93 %: Calculated C, 56.99; H, 6.33; N, 7.39 %, [IR (KBr pellets) ν_{max}/cm^{-1}]; 3057, 2953 ($C-H$), 2922 ($C-H$), 2358, 2336, 1865, 1791, 1730, 1652, 1556, 1538, 1505, 1456,

1320, 1278, 1217, 1186, 1142, 1077, 939, 808, 736, 668 ($C-S$), 577, 499, 418; [UV/Vis, $CHCl_3$, λ_{max}/nm]: 918, 805, 635, 355.

Metal free 1, 10, 19, 28,-tetrathiododecylphthalocyanine (39) (Scheme 3.12).

Compound (**39)** was synthesised and purified the same way as for (**(37a)** and **(37b))** except (**33)** instead of (**21)** was employed. The amounts of reagents were: **(33)** (1.00g, 3.05 mmol), DBU (1.70 g, 11.17 mmol), $CeCl_3$ (41mg, 0.16 mmol) and pentanol (20 ml). Yield: 1.56g, 34%, $C_{80}H_{112}N_8S_4$: Found: C, 72.72; H, 8.80 N, 6.57, S, 9.79%: Calculated C, 73.17; H, 8.54; N. 8.54; S, 9.76 %UV/Vis [($CHCl_3$, λ_{max}/nm ($\log\varepsilon$)] 73, 704, 668, 637, 455, 350.

1, 10, 19, 28,-tetrathiododecylphthalocyanine tin (IV) dichloride (40) (Scheme 3.12).

Complex **(40)** was synthesized and purified the same way as for complex **(38a)** except **(39)** instead of **(37a)** was employed. Amounts of reagents were: Complex **(39)** (0.50 g, 0.45 mmol), $SnCl_2$ (0.086 g, 0.45 mmol) and pentanol (15 ml). Yield: (0.45g, 76%); δ_H ($CDCl_3$), 9.3 (4H, m, H_{arom}), 8.4 (8H, s, H_{arom}), 3.7 (8H, m, Ar-SCH_2-), 1.2-2.2 (80H, m, $H_{aliphatic}$), 0.90 (12H, t, -CH_3); $C_{80}H_{112}N_8S_4SnCl_2$: Found: C, 62.93; H, 7.60 N, 7.80, S, 8.56%: Calculated C, 63.96; H, 7.46; N. 7.46; S, 8.53 %, [IR (KBr pellets) ν_{max}/cm^{-1}] 3435, 2923 ($C-H$), 2852($C-H$), 1589, 1562, 1464, 1384, 1338, 1313, 1233, 1184.3, 1150, 1107, 1082, 1039, 911, 798, 759, 732 ($C-S$), 593; U/Vis, $CHCl_3$: 918, 805, 635, 355; UV/Vis, $CHCl_3$, $\lambda_{max}/nm(\log\varepsilon)$:769(6.06), 687(5.58), 506(5.37), 355(6.00).

2.3.7 Microwave synthesis of water soluble tin phthalocyanine

Sn^{II}TSPc: Tetrasulphonated tin(II) phthalocyanine (41) (Scheme 3.10)

4-sulfophthalic acid **(30)** (16 g, 32.3 mmol) in the presence of ammonium molybdate (0.17 g, 014 mmol), **(30)** was thoroughly mixed with urea (14.4 g, 260 mmol) and $SnCl_2$ (0.55 g, 4.1 mmol) in a ratio of 1:8, **Table 2.1**. The mixture was placed in a microwave oven and irradiated at 1000 W for 5 min. The completeness of the reaction was determined using thin layer chromatography (TLC). The complex was purified by following literature methods [68] in addition to Soxhlet extraction of impurities using methanol and ethanol.

IR (KBr, cm^{-1}): 3434, 3130, 2835, 2366, 1740, 1662, 1593, 1593, 1471, 1431, 1360, 1121, 858, 825, 776 (C-S), 618, 598, 558, 437. ^{1}HNMR (400 MHz, D_2O): 7.63 (d, 4-H, Pc-H), 7.86 (d, H-4, Pc-H'), 7.98 (s, 4-H, Pc-H). λ_{max}(nm) (log ε) (water/Triton X 100): 330 (1.60), 383 (1.04), 609 (0.83), 678 (4.01) nm. Sn elemental analyses for $SnC_{32}H_{12}N_8S_4O_{12}Na_4$: Calcd. 11.58%. Found 11.68%.

Sn^{II}TSTBC: Tetrasulphonated tin α,β,γ-tetrabenzcorrole (42) (Scheme 3.10).

This complex was synthesized and purified as described above for SnTSPc **(41)**, except that different amounts of 4-sulfophthalic acid **(30)** (4g, 8.1 mmol), and urea (1.5 g, 24.3 mmol) and $SnCl_2$ (0.55 g, 4.1 mmol) were employed. IR (KBr, cm^{-1}): 3303, 2914, 2833, 2352, 1726, 1661, 1582 (C=C-C), 1481, 1405, 1363, 1192, 1126, 1072, 1042, 836, 754 (C-S), 670, 641, 573, 471. ^{1}HNMR (400 MHz, D_2O): 7.63 (d, 4-H, Pc-H), 7.86 (d, H-4, Pc-H'), 7.98 (s, 4-H, Pc-H). λ_{max}(nm) (log ε) (water/Triton X 100): 461 (5.05), 604

(1.55), 628 (1.46), 676 (3.05) nm. Sn elemental analyses for $SnC_{32}H_{12}N_7S_4O_{12}Na_4$: Calcd. 11.42%. Found 11.54%.

2.4 Photophysics

2.4.1 Fluorescence quantum yield

A comparative method was used to determine the fluorescence quantum yield, this method required the use of a fluorescence quantum yield value of ZnPc (standard) in DMSO (Φ_F = 0.2 [121]). The solution of the standard and the MPc investigated where prepared such that the absorbance of each is approximately 0.05 at the wavelength of excitation. The areas under the curves of emission spectra were measured. The refractive indices correction of the solvents where used for different solvents of MPc and standard.

2.4.2 Fluorescence quenching with BSA

Fluorescence quenching was carried out by addition of increasing concentration of the quencher, MPc. i.e.; $0, 6.72\times10^{-9}$, $1.34\times10^{-8}, 2.69\times10^{-8}$ and $5.38\times10^{-8}M$ of a fixed BSA concentration, i.e. $5.4\times10^{-8}M$. BSA fuorescence spectra were recorded at each MPc concentration and the dependence of the emission intensity on quencher concentration were given by Stern-Volmer (SV) equation, **Equation 1.20**. The ratio F_0/F was plotted against quencher concentration [Q].

2.5 Preparation of self-assembled monolayers of $SnPc(SC_{12}H_{25})_8$ and $SnPc(SC_{12}H_25)_4$ on gold electrode.

The gold electrode was cleaned before coating using established procedure [122, 123], by first polishing with a SiC-emery paper (Type 2400 grit), followed by polishing with alumina on a Buehler felt pad and then rinsing with ethanol. Finally the electrode was etched for about 2 minutes in a "Pirhana" solution (3:1 mixture of concentrated H_2SO_4 and 30% H_2O_2) and rinsing with distilled deionised Millipore water from Milli-Q-water Water System (Millipore corp., Bedford, MA, USA) followed by ethanol. Removal of gold oxides on the surface was finally established by placing the electrode in 0.5 mol dm^{-3} H_2SO_4 and scanning the potential between - 0.5 and 1.0 V vs Ag/AgCl at a scan rate of 100 mVs^{-1}. Following this pretreatment the electrode was rinsed with chloroform and immediately placed in 5 ml of chloroform solution of the thiol substituted MPc's (concentration = 10 μM) and varying the immersion time. The electrode was thoroughly rinsed with chloroform prior to electrochemical experiments.

Publications

Some of the results presented in this thesis have been published in the following journals and are not referenced further:

1. Microwave Syntheses and Photophysics of New Tetrasulfonated Tin(II) Macrocycles, **S. Khene**, A. Ogunsipe, E. Antunes and T. Nyokong, *J. Porphyrins Phthalocyanines*, **11**, 2007, 109-117.
2. Electrochemical and photophysical characterization of non-peripherally octaalkyl-substituted dichlorotin(IV) phthalocyanine and tetrabenzotriazaporphyrin compounds, **S. Khene**, A. N. Cammidge, M. J. Cook, and T. Nyokong, *J. Porphyrins Phthalocyanines* (**In press**)
3. Synthesis, Electrochemical studies of tetra- and octa-substituted dodecyl-mercapto tin phthalocyanines in solution and as self assembled monolayers (SAMs), **S. Khene**, T. Nyokong, Electrochim. Acta (**Submitted for publication**)
4. T. B. Ogunbayo, **S. Khene** and T. Nyokong, Pd ion binding of tetra and octa-substituted alkylthio phthalocyanine (**In preparation**).

CHAPTER THREE: SYNTHESIS AND CHARACTERISATION

3.1 Synthesis and Spectroscopic Properties

3.1.1 Phthalonitriles

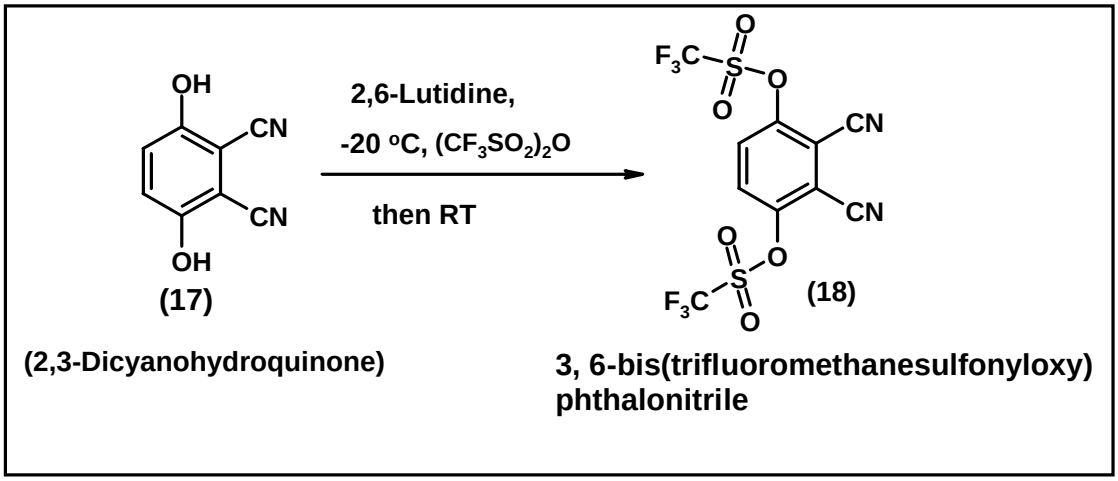

Scheme 3.1: Preparation of 3, 6-bis(trifluoromethanesulfonyloxy) phthalonitrile.

Before the reaction shown in **Scheme 3.1**, is started everything must be completely dry, from your starting material to your glassware (flame dried under vacuum), because any trace of water will considerably affect the yield and the desired product **(18)** might be difficult to obtain. The role of 2,6-lutidine is to neutralize triflic acid generated by the reaction and also to prevent further attack of 2,6-lutidine. 3,6-Bis(trifluoromethanesulfonyloxy) phthalonitrile **(18)** is used as an organic triflate precursor (in the Negishi coupling reaction) because it can be prepared from a readily available dicyanohyroquinone **(17)** according to **Scheme 3.1**. The CN band in the IR spectrum of **(18)** was observed at 2250 cm^{-1}. The protons in the ^{1}H-NMR spectrum of the two aromatic (Ar) protons of **(18)** appeared as a singlet integrating for 2 at 7.87 ppm.

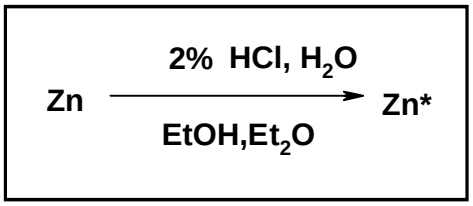

Scheme 3.2: Preparation of zinc dust.

Commercially obtained zinc powder is usually about 90% pure and requires an acid treatment to remove surface oxide which reduces its activity, according to **Scheme 3.2**. In **Scheme 3.2,** 2% HCl is used to remove the surface oxide followed by washing with ethanol then diethyl ether to remove excess water from the activated zinc. The activated zinc is then vacuum dried and stored under argon.

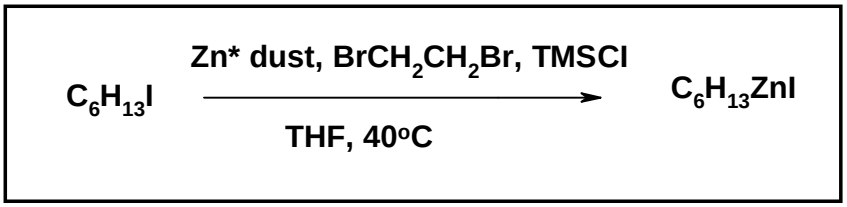

Scheme 3.3: Preparation of hexylzinc iodide. TMSCl = trimethylchlorosilane.

Hexylzinc iodide is used as an organometallic reagent (in a Negishi coupling reaction) in which the hexyl group will be coupled to **(18)**, forming a new carbon-carbon sigma bond, and thus forming compound **(20), Scheme 3.4**. Due to the low-lying p orbitals of zinc, organozincs can undergo smooth transmetallations with a variety of transition metal salts or complexes, such as $NiCl_2(PPh_3)_2$, **Scheme 1.11**.

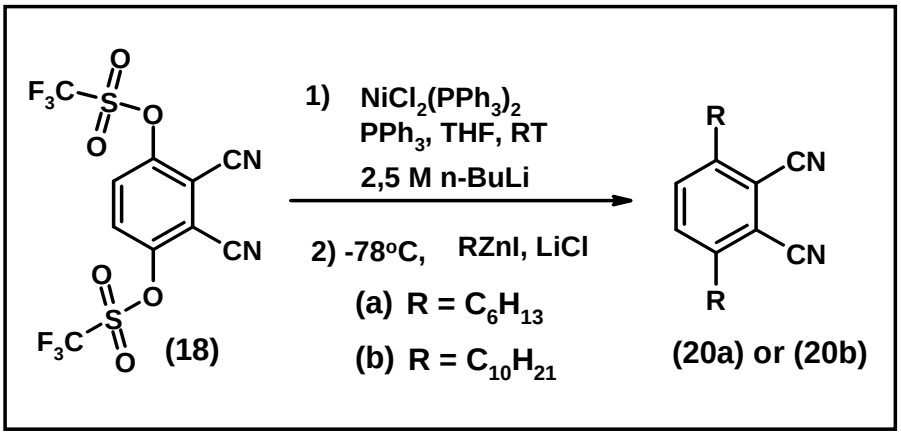

Scheme 3.4: Preparation of 3, 6-dihexylphthalonitrile (20a) and 3, 6-didecylphthalonitrile (20b). PPh3 = triphenyl phosophine.

In the conversion of **(18)** to **(20a)** and **(20b)** following the Negishi catalytic cycle (**Scheme 1.10)**, nickel(0) is used because it is known to be reactive towards oxidative insertion into carbon-triflate bond. Among all PPh_3 stabilised Ni(0) catalysts, ($Ni(0)(PPh_3)_4$) proved to be the most reactive catalyst [55]. The latter is generated in situ by reaction of $NiCl_2(PPh_3)_2$ complex with n-BuLi following a known procedure [55]. Anhydrous lithium chloride is added as a co-catalyst, for three possible functions: to avoid biaryl formation [58], stabilize the catalyst $NiCl_2(PPh_3)_2$ [59] and also accelerate the transmetallation step by replacing the inert M-O bond of **(26)** by an active M-Cl bond of **(27)** [60, 61] (see **Scheme 1.13)**. Hexylzinc iodide is added drop wise at -78°C because the reaction is highly exothermic. Satisfactory yields were obtained for the synthesis of **(20a)** and **(20b).** The CN band in the IR spectrum for both **(20a)** and **(20b)** were observed at 2228 cm^{-1}. The C-H band for both **(20a)** and **(20b)** were observed between 2920 and 2849 cm^{-1}. The ^{1}H-NMR spectrum of the two aromatic protons of **(20a)** appeared as a singlet at 7.47 ppm, CH_2 protons appeared as triplets and multiplets,

integrating for 4 at 2.86 ppm (Ar-CH_2- protons) and 16 between 1.67 and 1.34 ppm ($H_{aliphatic}$) and the CH_3 protons appeared as a triplet integrating for 6 at 0.90 ppm. The ^{1}H-NMR spectrum of the two aromatic protons of **(20b)** appeared as a singlet at 7.47 ppm, CH_2 protons appeared as triplets and multiplets, integrating for 4 at 2.86 ppm (Ar-CH_2-protons) and 32 between 1.67 and 1.34 ppm ($H_{aliphatic}$) and the CH_3 protons appeared as a triplet integrating for 6 at 0.90 ppm.

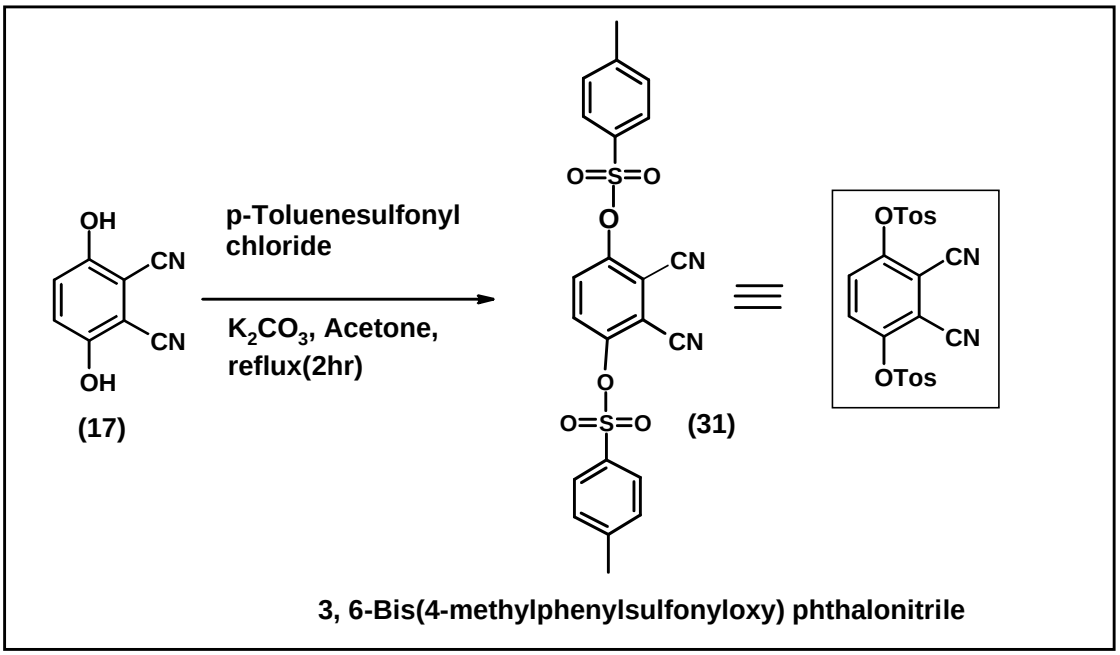

Scheme 3.5: Synthesis of 3, 6-bis(4-methylphenylsulfonyloxy) phthalonitrile.

3, 6-Bis(4-methylphenylsulfonyloxy) phthalonitrile **((31), Scheme 3.5)** is used in this work in order to make a precursor that is substituted with thiol substituents at the 3,6 position of the phthalonitrile **(Scheme 3.6).** The tosyl group at the 3,6 position of **(31)** is electron-withdrawing which makes it an excellent leaving group and thus makes substitution of thiol derivatives relatively easy. Compound **(31)** is preferred over compound **(18)** for this type of substitution simply because synthesis of **(31)** takes only 2

hours and reaction conditions are very relaxed compared to **(18)**. Compound **(31)** was not used for the Negishi coupling because it is not reactive enough compared to **(18)**. Compound **(18)** is more reactive due to fluorine substituents which are electron withdrawing, therefore increasing the overall electron withdrawing capability of the triflate group. Compound **(31)** is reactive enough for substitution of thiols and not for Negishi coupling using nickel catalyst. The CN band in the IR spectrum of **(31)** was observed at 2226 cm^{-1}.

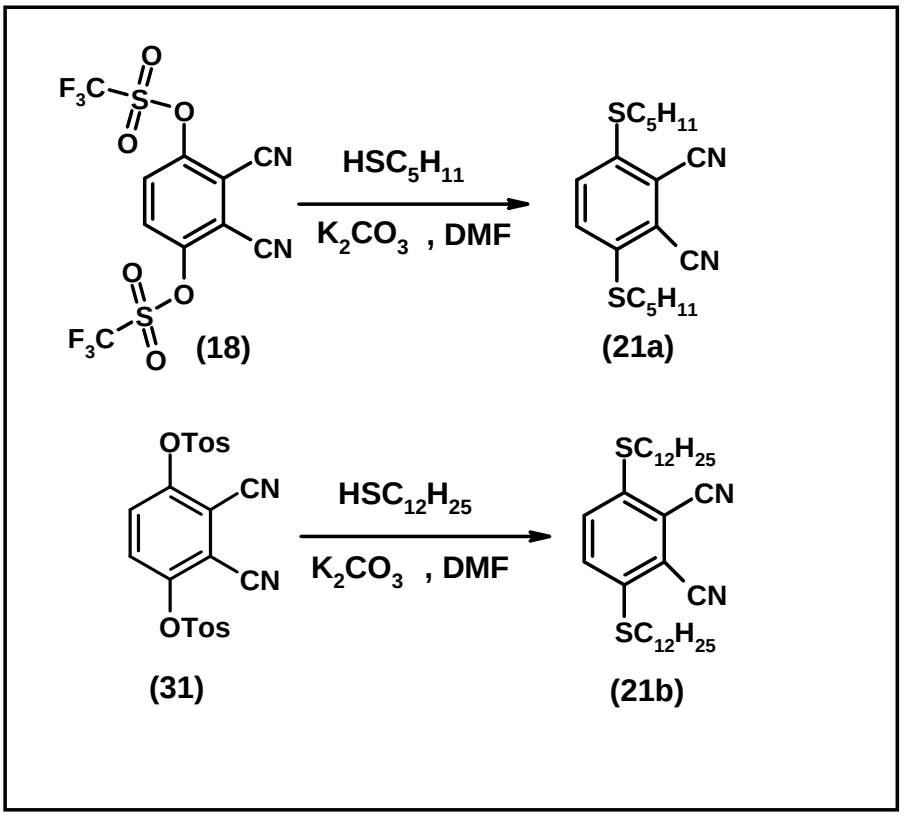

Scheme 3.6: Synthesis of 3, 6-Di(pentanethiol)-4, 5-dicyanobenzene (21a) and 3, 6-Di(dodacanethiol)-4, 5-dicyanobenzene (21b).

Both **(18)** and **(31)** precursors were used for the synthesis of thiol substituted phthalonitriles (**Scheme 3.6**). Precursor **(18)** was used to synthesise **(21a)** and precursor

(31) to synthesise **(21b)**. Synthesis of **(21a)** and **(21b)** was achieved by base (K_2CO_3) catalysed nucleophilic substitution of triflate and tosyl groups in **(18)** and **(31)** using pentanethiol and dodecylthiol respectively, **Scheme 3.6**. Satisfactory yields were obtained for the synthesis of compound **(21a)** and **(21b)**. The CN band in the IR spectrum for both **(21a)** and **(21b)** were observed at 2225 cm^{-1}. The C-H and C-S band in the IR spectrum for both **(21a)** and **(21b)** were observed at 2378 cm^{-1} and 725 cm^{-1}. The protons in the ^{1}H-NMR spectrum of the two aromatic protons of **(21a)** appeared as a singlet integrating for 2 at 7.49 ppm, the CH_2 protons appeared as a triplet and multiplets, integrating for 4 between 2.99-3.02 ppm (Ar-SCH_2- protons) and 12 between 1.71 and 1.28 ppm ($H_{aliphatic}$) and the CH_3 protons appeared as a triplet integrating for 6 between 0.88-0.91 ppm. The protons in the ^{1}H-NMR spectrum of the two aromatic protons of **(21b)** appeared as a singlet integrating for 2 at 7.49 ppm, the CH_2 protons appeared as a triplets and multiplets, integrating for 4 between 2.99-3.02 ppm (Ar-SCH_2- protons) and 40 between 1.71 and 1.28 ppm ($H_{aliphatic}$) and the CH_3 protons appeared as a triplet integrating for 6 between 0.91-0.88 ppm.

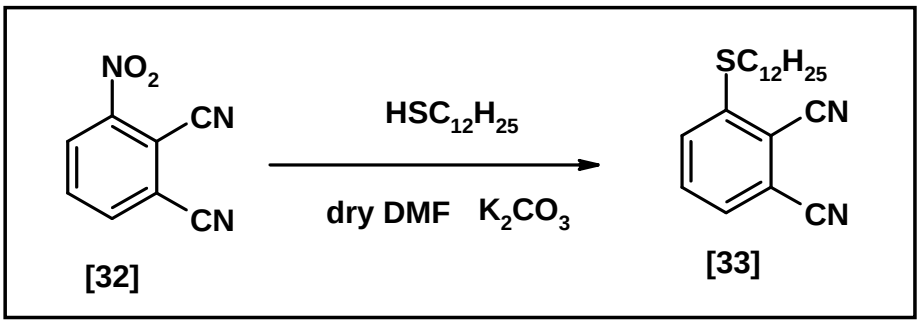

Scheme 3.7: Synthesis of 3-Didodecanethiol-4, 5-dicyanobenzene (33).

3-Nitrophthalonitrile **(32)** was purchased from Aldrich and used as received. The synthesis of compound **(33)** follows the same synthetic procedure as for **(21a)** and **(21b).** The CN band in the IR spectrum for **(33)** was observed at 2230 cm^{-1}. The C-H and C-S band in the IR spectrum were observed at 2364 cm^{-1} and 722 cm^{-1}. The protons in the ^{1}H-NMR spectrum of the two aromatic protons (Ar-H) of **(33)** appeared as a singlet and a multiplet between 7.64 and 7.30 ppm, the CH_2 protons appeared as a triplets at 3.07-3.10 ppm (Ar-SCH_2-) integrating for 2 and at 1.76-1.78 ppm (-CH_2) integrating for 2. Multiplets were observed at 1.46-1.64 ppm (-CH_2) integrating for 2 and at 1.28-1.29 ppm (-CH_2) integrating for 16 and the -CH_3 protons appeared as a triplet integrating for 6 between 0.84-0.93 ppm.

Table 3.1 is a summary list of the metallophthalocyanine (MPc) complexes studied in this thesis.

Table 3.1: List of metallophthalocyanine (MPc) complexes studied in this thesis

MPc and H_2Pc Complexes	**MPc Complex Number**	**Q band maxima λ_{abs} /nm**
α -$H_2Pc(C_6H_{13})_8$	**(34a)**	**695, 729 (THF)**
α -$H_2Pc(C_{10}H_{21})_8$	**(34c)**	**695, 729 (THF)**
α -$H_2Pc(SC_{12}H_{25})_8$	**(37a)**	**807 ($CHCl_3$)**
α -$H_2Pc(SC_5H_{11})_8$	**(37b)**	**807 ($CHCl_3$)**
α -$H_2Pc(SC_{12}H_{25})_4$	**(39)**	**703, 733 ($CHCl_3$)**
α - $Cl_2Sn(IV)Pc(C_6H_{13})_8$	**(35a)**	**735 (THF)**
α - $Cl_2Sn(IV)TBTAP(C_6H_{13})_8$	**(35b)**	**700, 727 (THF)**
α - $Cl_2Sn(IV)Pc(C_{10}H_{21})_8$	**(35c)**	**735 (THF)**
α -$ZnPc(C_{10}H_{21})_8$	**(36)**	**700 (THF)**
α - $Cl_2Sn(IV)Pc(SC_{12}H_{25})_8$	**(38a)**	**919 (THF)**
α - $Cl_2Sn(IV)Pc(SC_5H_{11})_8$	**(38b)**	**919 (THF)**
α - $Cl_2Sn(IV)Pc(SC_{12}H_{25})_4$	**(40)**	**769 (THF)**
β -$Sn(II)Pc(SO_3Na)_4$	**(41)**	**680 (water:methanol)**
β -$Sn(II)TBC(SO_3Na)_4$	**(42)**	**457, 680 (water:methanol)**

3.1.2 Alkyl Substituted Metallophthalocyanine Complexes

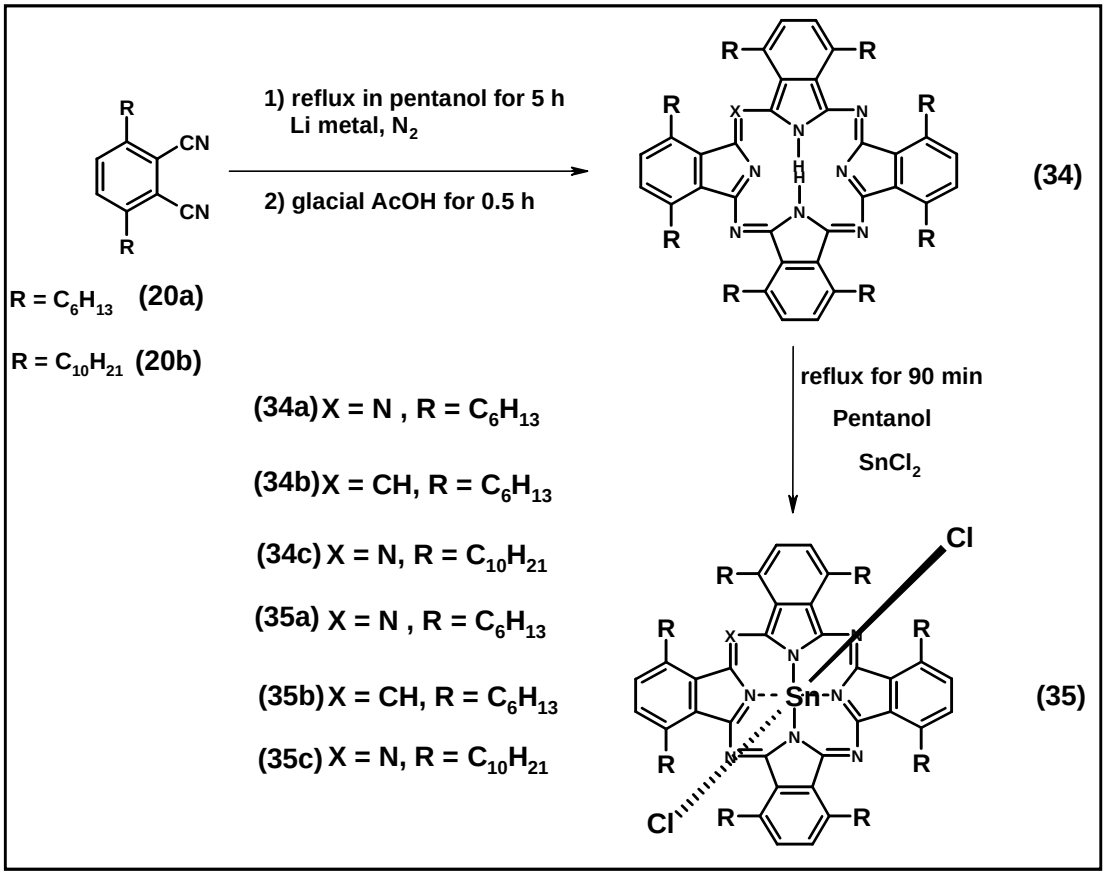

Scheme 3.8: Synthesis of tin phthalocyanines.

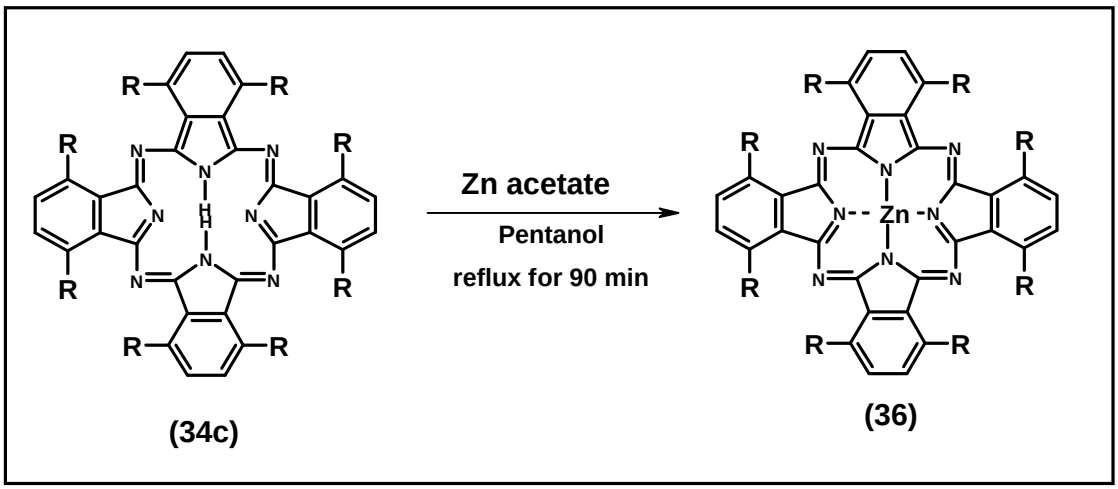

Scheme 3.9: Synthesis of 1, 4, 8, 11, 15, 18, 22, 25-Octadecylphthalocyanine Zn(II) (36).

The metal-free phthalocyanine complexes **(34a)**, **(34b)** and **(34c)** were synthesised following the reported method by Cook's group [22]. These complexes were synthesised by heating under reflux the corresponding alkyl substituted phthalonitrile derivatives (**(20a)** and **(20b), Scheme 3.8**) with lithium metal (strong base), in 1-pentanol for 24h under an Ar atmosphere, to obtain a mixture of complex **(34a)** and **(34b)**. Two different complexes **(34a)** and **(34b)** were isolated using cyclohexane as eluent with $R_f = 0.51$ and $R_f = 0.24$ **(Figure 3.1).** Complex (**34b)** is eluted first, followed by the normal phthalocyanine derivative (**34a**).

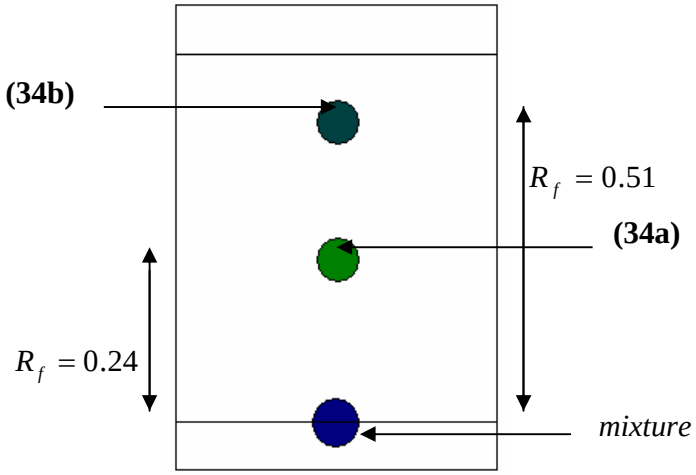

Figure 3.1: TLC separation of complexes (34a) and (34b).

The metallated phthalocyanine complexes **(35a), (35b)** and **(35c),** were synthesised by the metallation of metal-free analogues with $SnCl_2$ metal salt. This reaction took about 90 minutes to reach completion. UV/vis spectroscopy (in DCM) was used to monitor the reaction by observing a collapse of the split Q-band for complexes **(35a)** and **(35c),** while **(35b)** remained split. **Figure 3.2** shows typical UV/vis spectra of metal-free **(34c)** (with split Q band) and metallated **(35c)** (with one Q band)**.**

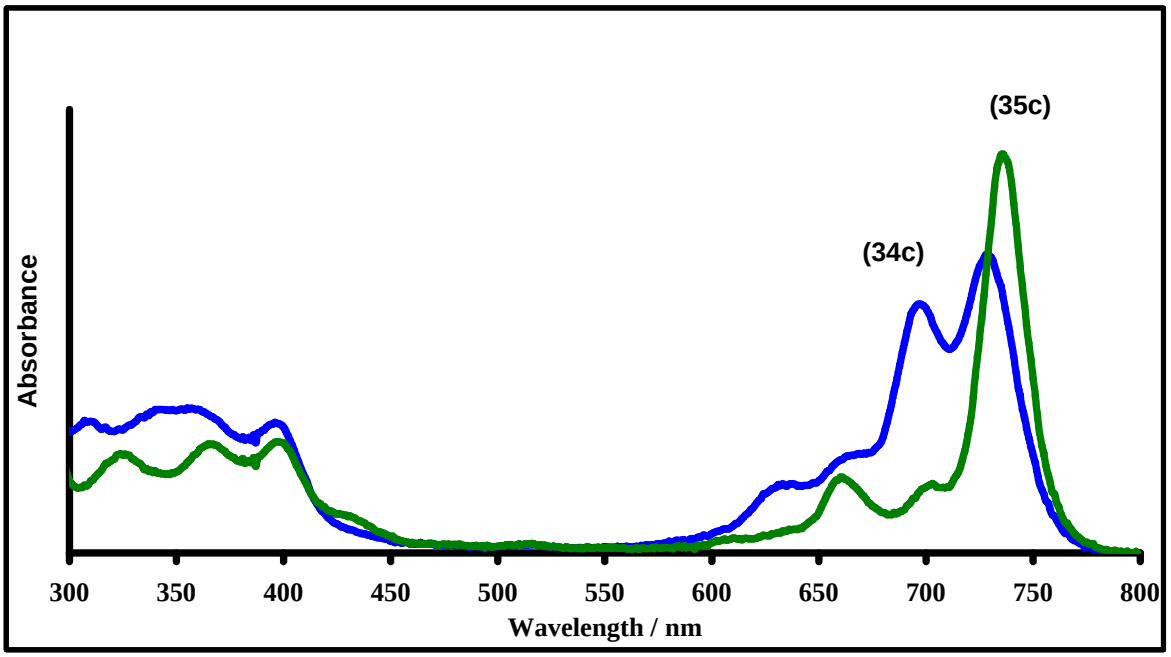

Figure 3.2: Absorption spectra of metallated (35c) and unmetallated phthalocyanine (34c) in DCM ~1 x 10^{-5} M.

In general, the synthesis of SnPc complexes using $SnCl_2$ may result in the formation of Sn(II)Pc or Cl_2Sn(IV)Pc species depending on the amount of $SnCl_2$ used in the reaction [124,125]. With excess $SnCl_2$, Sn(II)Pc derivatives are formed. In this work a ratio of 1:1 ($SnCl_2$: **(34a)**, **(34b)** or **(34c)**) was employed, resulting in the formation of the Cl_2Sn(IV)Pcs ((**35a)** and (**35c)**) and the corresponding dichlorotin metallated TBTAP (**35b**). Elemental analyses (mass spectrum for **35b**) and spectroscopic characterization confirmed the formation of these complexes. The ^{1}H NMR spectra showed appropriate resonances for each complex. Triazaporphyrin (**35b**) showed a signal for the methine proton on the carbon (replacing the nitrogen) at 11.4 ppm.

Figure 3.4 shows the ground state electronic absorption spectra of the complexes **(35a)** to **(35c)**. The Q band for the triazaporphyrin **(35b)** is split with maxima at 702 and 730 nm in toluene, **Figure 3.4**, as expected for a macrocycle with lower symmetry than that of the Pc ring. Mack *et al*. [27] have calculated the electronic energy levels for TBTAP molecules; a splitting in the lowest unoccupied molecular orbital (LUMO) leads to split Q and B bands [27].

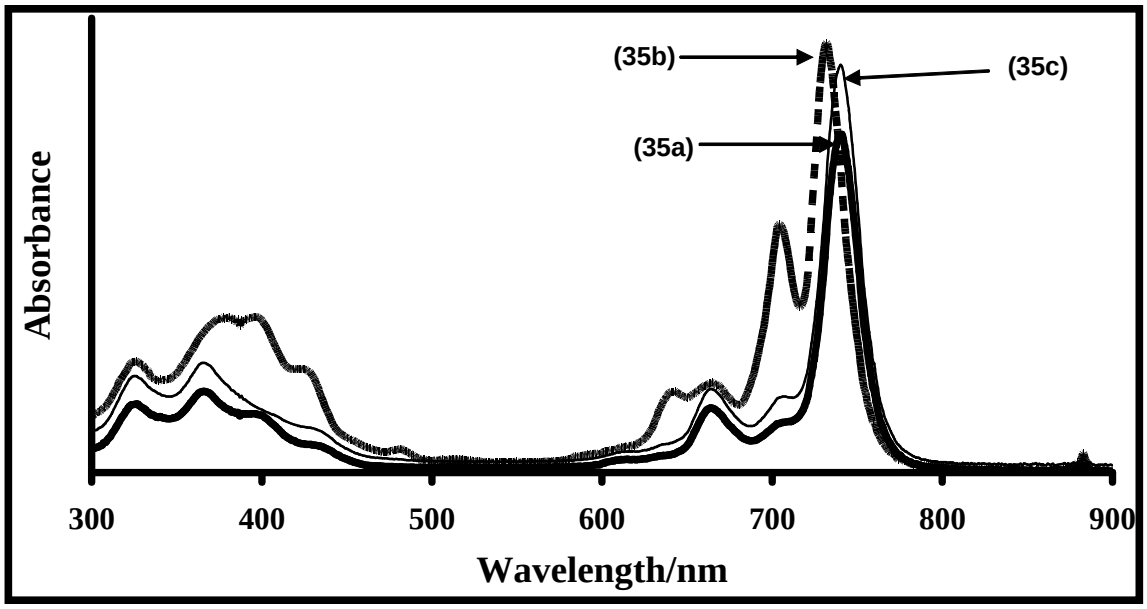

Figure 3.3: Ground state electronic absorption spectra of complexes 35a to 35c in toluene. Concentration = ~ 1. x 10^{-6} M.

The ground state electronic spectra of **(35a)** and **(35c)** were identical, with the Q band at 736 nm in toluene (**Figure 3.3**). The Q bands for (**35a)** and (**35c)** are typical for monomeric symmetric MPc complexes. Compared to the $ZnPc(C_{10}H_{21})_8$ counterpart, complex **(35c)** $[Cl_2SnPc(C_{10}H_{21})_8]$, is red-shifted by 35 nm in THF (**Table 3.1)** and 32 nm in toluene. For all complexes, Beer's law was obeyed both in toluene and THF up to molar concentrations of 1 x 10^{-5} M **(Figure 3.4).** Complexes **(35a)** to **(35c)** did not

dissolve in more polar solvents such as DMSO. For complex **(35b)**, decreasing the concentration did not result in the disappearance of one of the peaks, confirming that the presence of two peaks in the Q band region is not merely due to aggregation.

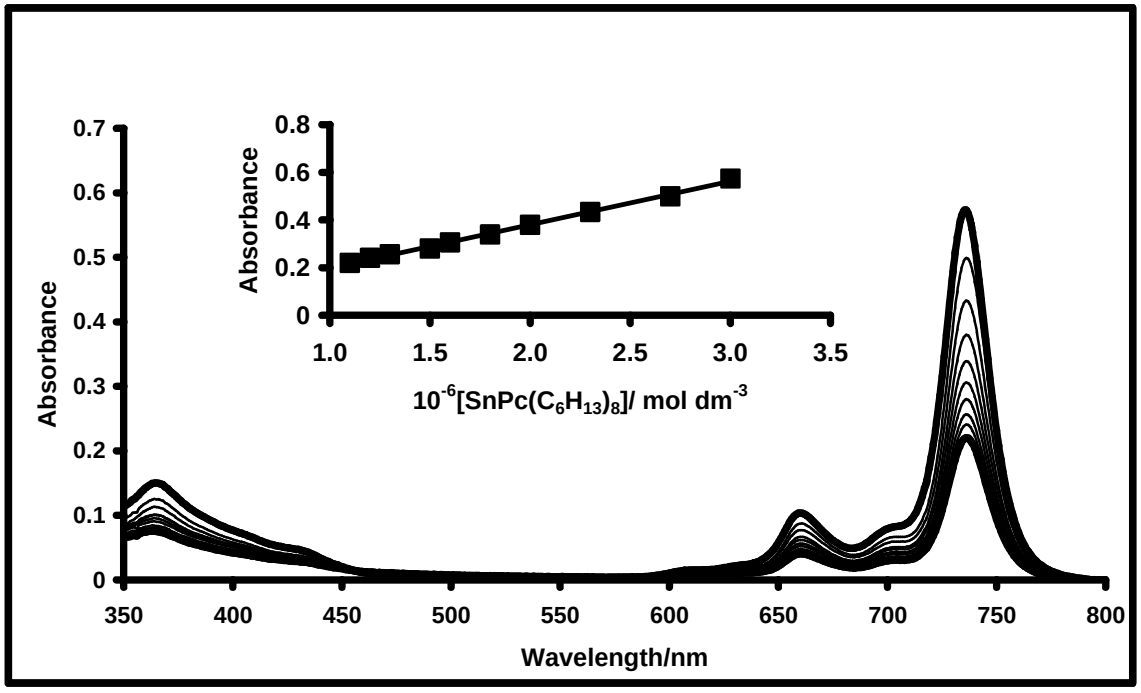

Figure 3.4: Variation of absorbance with concentration and Beer's law behaviour for α -Sn(IV)Pc(C_6H_{13})$_8$ (35a).

For complexes **(35a)** and **(35c)**, fluorescence spectra were mirror images of the absorption spectra (**Figure 3.5a**) and the latter was similar to the excitation spectra, confirming that the nuclear configurations of the ground and excited states are similar, and are not affected by excitation. For complex **(35b)**, the fluorescence spectrum showed only one peak (**Figure 3.5b**), and not two observed for both excitation and absorption spectra. This behaviour is typical of phthalocyanine complexes with low symmetry such as unmetallated Pcs [126], which fluoresce with only one main peak, assigned as the 0-0 transition of the fluorescence [126]. The observation of one peak in the fluorescence of

complex **(35b)** is thus similar to that of the D_{2h} symmetry unmetallated Pcs. The observed Stokes shifts were small as is typical of MPc complexes, **Table 3.2**.

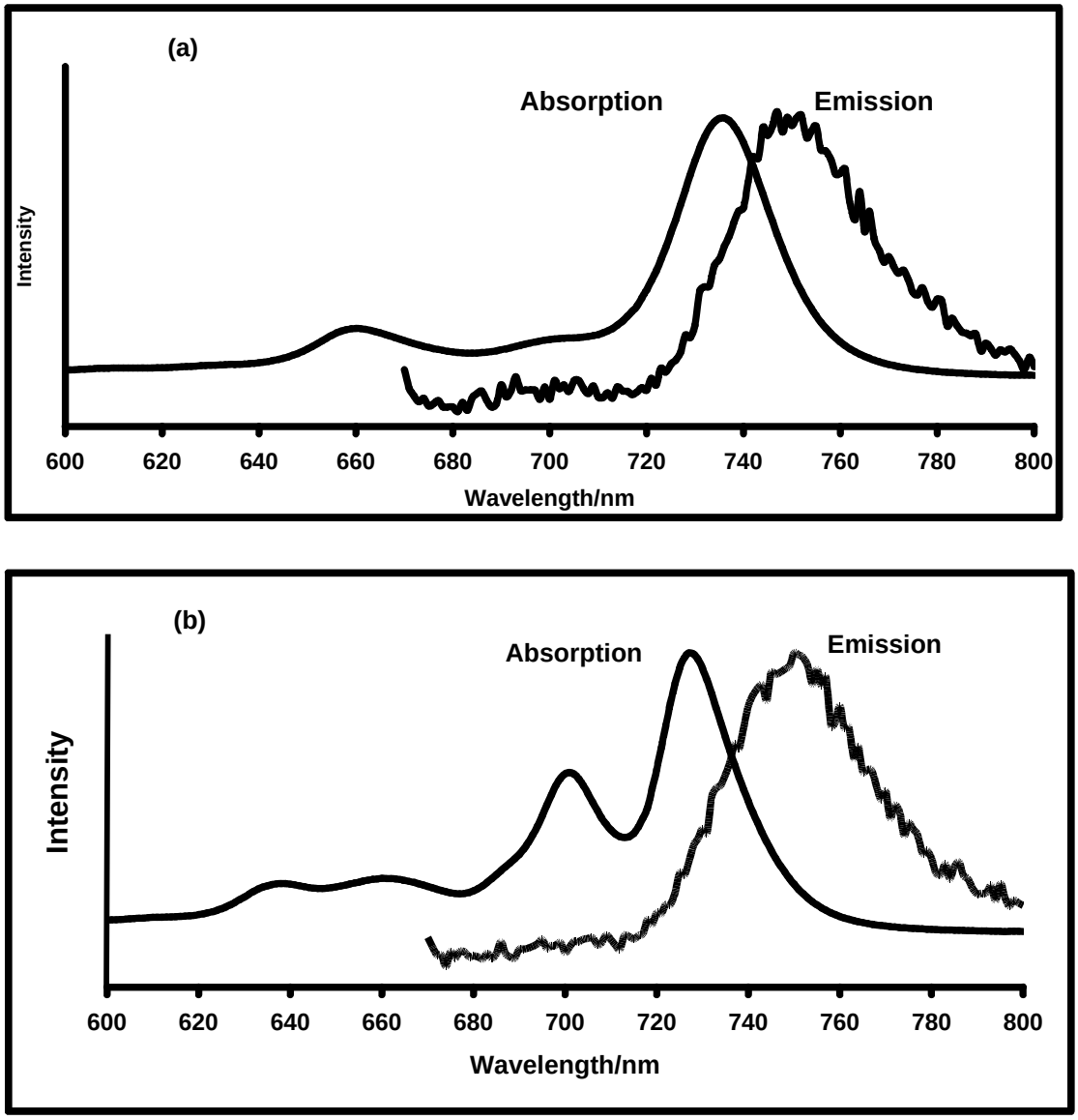

Figure 3.5: Fluorescence emission and ground state absorption spectra of (a) (35a) and (b) (35b) in toluene. Excitation at 665 nm.

Table 3.2: Stokes shift of complexes (35a) to (35c) in THF. Values in parentheses, ( ), were obtained in toluene.

Complexes in THF	**$\lambda_{abs.}$ nm**	**λ_{em} nm**	**Stokes Shift nm**
$ZnPc(C_{10}H_{21})_8$ **(36)**	700 (704)	712 731	12 (27)
(35a)	735 (736)	750 (750)	15 (14)
(35b)	700, 727 (702, 730)	734 750)	7 (20)
(35c)	735 (736)	750 (750)	15 (14)

3.1.3 Sulphonated Metallophthalocyanine Complexes

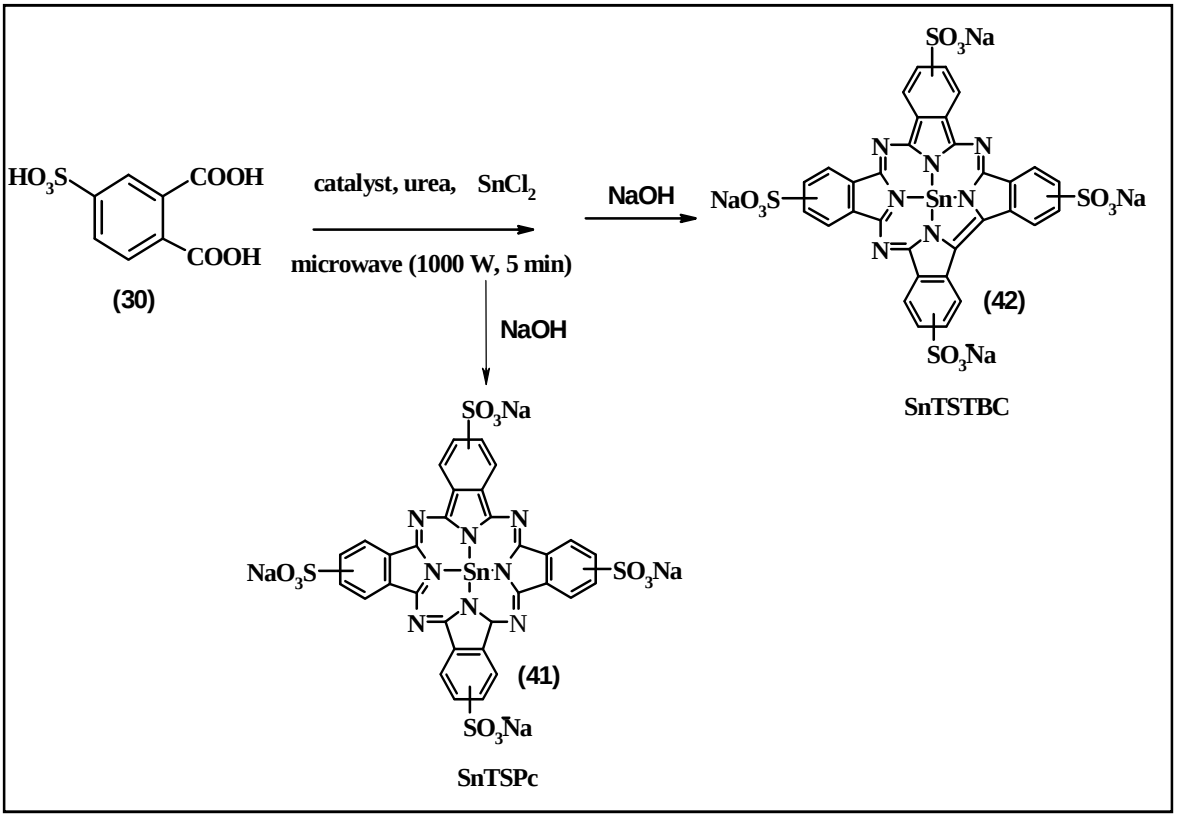

Scheme 3.10: Synthesis of SnTSTBC (42) and SnTSPc(41).

The aim in this work was to synthesize SnTSPc **(41)** using microwave irradiation, but surprisingly SnTSTBC **(42)** was formed, depending on the ratio of the reagents, as shown in **Table 3.3**. UV/Vis, IR, ^{1}H NMR and Sn elemental analyses were employed to characterize the complexes. The complexes were found to be pure by NMR spectroscopy discussed below. However, the Sn elemental analyses further ascertained the purity, especially from $SnCl_2$ starting material, which cannot be confirmed by ^{1}H NMR.

Table 3.3: Equivalents employed for microwave synthesis.

4-sulfophthalic acid (30)	**Urea, g/mmol**	**Ratio 4-sulfophthalic acid to urea**	**Compound**
12g / 24.4 mmol	0.5g/8.12 mmol	3:1	No reaction
4g/8.1 mmol	1.5g/24.3 mmol	1:3	SnTSTBC **(42)**
16g/32.5 mmol	14.4g/ 260 mmol	1:8	SnTSPc **(41)**

^{1}H NMR spectra showed appropriate resonances for both molecules which integrated correctly. The ring protons were observed at the same positions for the two complexes: 7.63, 7.86 and 7.98 ppm each integrating for 4 protons, making a total of 12 protons per complex (8 protons at non peripheral positions and 4 protons at peripheral).

The resonances were observed as two doublets and a singlet, the splitting could be due to the isomeric nature of the complexes. Both complexes are expected to have positional isomers due to the presence of a single substituent on the peripheral position. Peripherally tetrasubstituted MPc complexes contain positional isomers in a statistical ratio of 1:1:2:4 (for 2,9,16,23-, 2,10,16,24-, 2,9,17,24- and 2,9,16,24-isomers). The isomers are difficult to separate.

The IR data showed the presence of C-S bonds due to the sulfo ring substituents at 776 and 754 cm^{-1}, respectively for SnTSPc **(41)** and SnTSTBC **(42)**.

The UV-Vis spectra of MTSPc complexes are well known [69] and are often employed in characterization. Metallobenzcorrole (MBC) complexes have distinct UV-Vis spectra

with a sharp peak at ~ 450 nm [23, 30], and can be employed in characterization. The formation of the MBC complexes occurs when the MPc molecules no longer retain a Pc moiety. MBC does not have the fourth azomethine nitrogen, **Scheme 3.10**. The MBC complexes has been reported [23, 30] to occur on reduction of $Cl_2M(IV)Pc$ (M = Ge) with sodium borohydride. The mechanism for the formation TBC from reduction of MPc complexes has not been proved experimentally [23]. It is however believed [30] that in the presence of excess metal chloride, the bridge nitrogen of the Pc is eliminated forming TBC. Thus the evidence so far leads to the understanding that the Pc forms first and it is then reduced to TBC. The presence of chloride seems to be essential for the formation of TBC [23, 30]. In this work, a number of ratios of 4-sulfophthalic acid to urea were tested only three are shown in **Table 3.3**. The SnTSTBC **(42)** species was formed when ratios of 4-sulfophthalic acid to urea were less than 1:8, (but equal to 1:3 or more), suggesting that this complex is an intermediate towards the formation of an MPc complex, since the SnTSTBC **(42)** is formed when there is less urea.

Aggregation lowers the photoactivity of molecules through dissipation of energy by aggregates, hence it is not desirable in MPc complexes for applications in for example photodynamic therapy as photosensitisers. Aggregation in sulphonated MPc complexes is characterised by the presence of two main bands (instead of one for monomeric species) in the visible region. The lower energy band is due to the monomer (~ 670 nm), and the higher energy (~ 630 nm) band is due to the aggregated species. As observed in **Figure 3.6**, SnTSTBC **(42)** and SnTSPc **(41)** are extensively aggregated in aqueous solution. The aggregating tendencies of sulphonated MPcs in aqueous solution is well known in

literature [105, 127], and is believed to be as a result of association between the peripheral substituents, which hold adjacent rings together in space. The peak due to the aggregated species was observed at concentrations as low as 1 x 10^{-7} M. Beer's law was obtained at concentrations lower than this value for both complexes. The addition of a surfactant, Triton X-100 resulted in disaggregation (**Figure 3.6**), which further shows that these complexes are aggregated in aqueous solution. However, the spectrum of SnTSTBC **(42)** is still broad after addition of Triton X 100, suggesting either that it is not fully disaggregated or that there is loss of symmetry in this molecule.

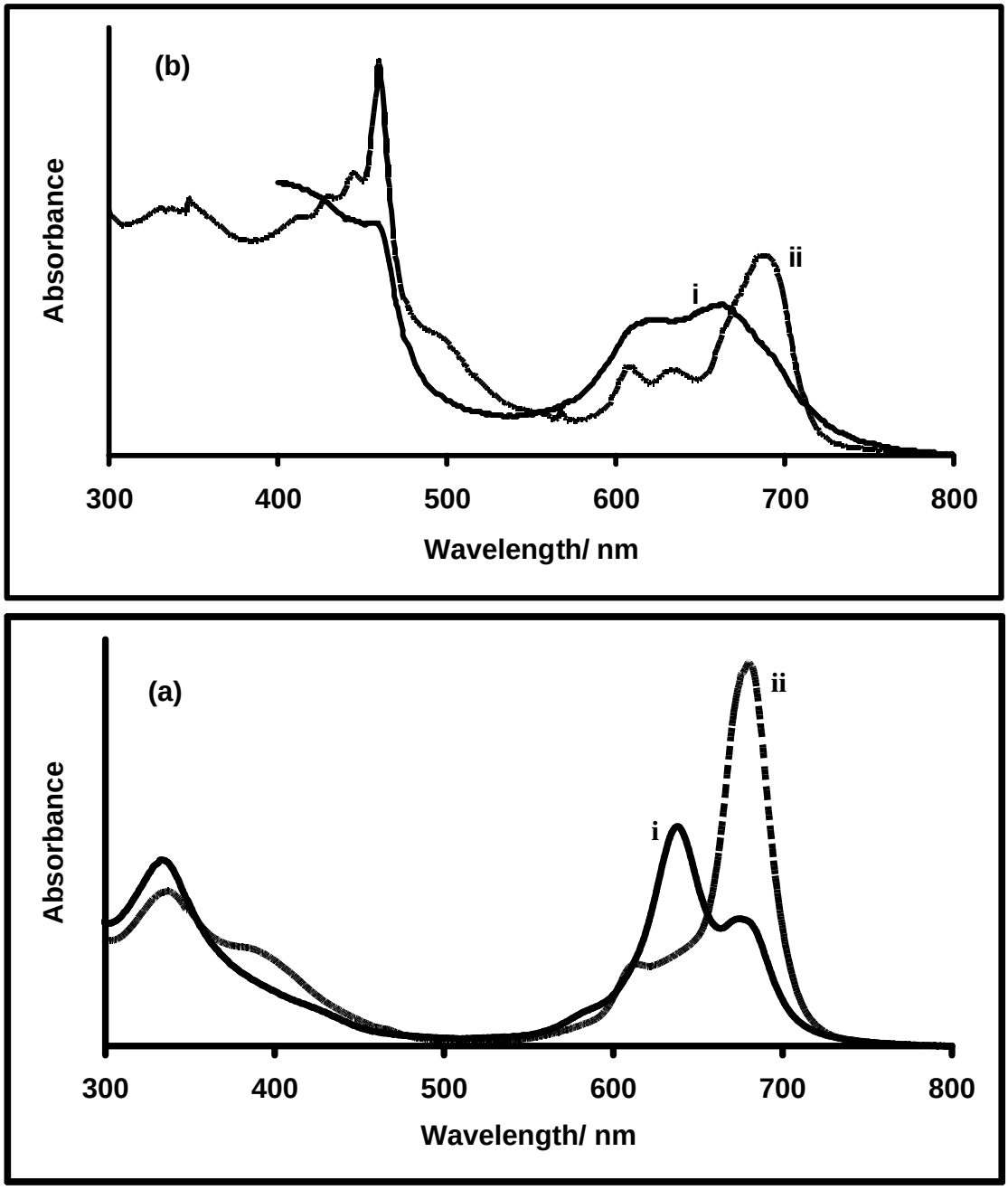

Figure 3.6: Electronic absorption spectra of (a) SnTSPc (2.7 x 10^{-5} M) and (b) SnTSTBC (8.9 x 10^{-4} M) in aqueous solution (unbuffered water); in the absence (i) and presence (ii) of Triton X-100.

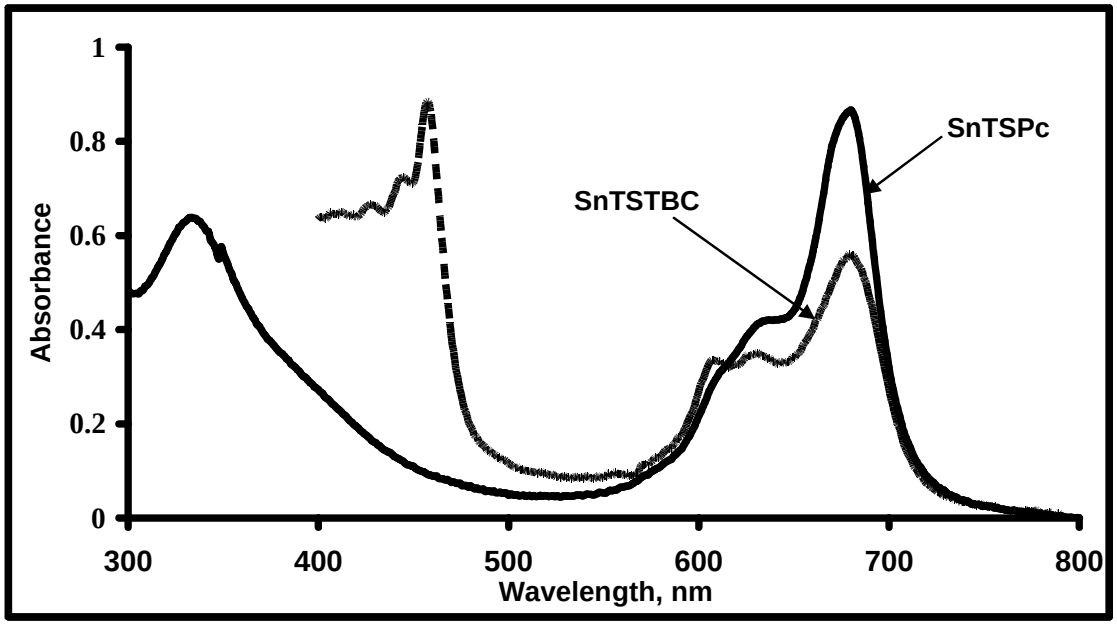

Figure 3.7: Electronic absorption spectra of SnTSTBC (8.9 x 10^{-4} M) and SnTSPc (8.2 x 10^{-5} M) in aqueous methanol.

Organic solvents are expected to disaggregate MTSPc complexes. In 1:1 water: methanol mixture, both SnTSTBC **(42)** and SnTSPc **(41)** showed mainly monomeric behaviour, **Figure 3.7**. The spectra were still broad, suggesting that complete disaggregation was not achieved in this solvent mixture for SnTSPc **(41)**. The observed broadness for SnTSTBC **(42)** could be a result of both incomplete disaggregation and loss of symmetry as discussed above.

Percentage aggregation (calculated from **Equation 3.1**, same as **Equation 1.1**) is higher in SnTSTBC (60%) than in SnTSPc (38%), **Table 3.4,** hence a lower photoactivity for SnTSTBC **(42)** is predicted compared to SnTSPc **(41)** in aqueous solution.

$$\%_{Agg} = \frac{Abs_{TX} - Abs}{Abs_{TX}} x100\% \quad (3.1)$$

where $Abs_{(TX)}$ and Abs are the absorbances at the Q band maxima the presence and absence of Triton X-100.

ε_D were determined as explained in the introduction section, using **Equation 3.2** (same as **Equation 1.5**) and the values are shown in **Table 3.2**.

$$Abs = \frac{\left[1 - \sqrt{(1+8K_D C_T)}[\varepsilon_D/(2-\varepsilon_M)] + 2\varepsilon_D K_D C_T\right]}{4lK_D} \quad (3.2)$$

Dimerization constant (K_D) values are 2.5 $x10^4$ and 2.7 x 10^4 M^{-1} for SnTSTBC and SnTSPc, respectively. The values of ε_M, ε_D and K_D are within the range reported for some MPc complexes [105, 127]. ε_M for SnTSTBC **(42)** (missing one azomethine nitrogen) is lower than for SnTSPc **(41)**.

Table 3.4: Aggregation parameters of SnTSTBC and SnTSPc in aqueous solution

Complex	$\%_{Agg}$	$\varepsilon_M/10^{-4}$ $cm^{-1}.M^{-1}$	$\varepsilon_D/10^{-4}$ $cm^{-1}.M^{-1}$	$K_D/10^{-4}$ M^{-1}
SnTSTBC	60	1.13	1.09	2.5
SnTSPc	38	10.4	1.08	2.7

In aqueous solution, the fluorescence spectra of SnTSTBC **(42)** (**Figure 3.8a**) and SnTSPc **(41)** (**Figure 3.8b**) gave sharp single Q bands, unlike their absorption spectra, which gave broad Q bands. This implies that it is only the monomeric species which fluoresce. In water:methanol mixture, SnTSTBC **(42)** (**Figure 3.9a**) and SnTSPc **(41)** (**Figure 3.9b**) displayed fluorescence with a single peak (**Figure 3.9b**) again showing that only the monomer fluoresces. This observation nullifies the earlier notion that the broadness in the UV-Vis spectrum of SnTSTBC **(42)** could be as a result of symmetry loss since the molecules cannot gain symmetry by excitation. It is now clear that the broadness is as a result of partial aggregation.

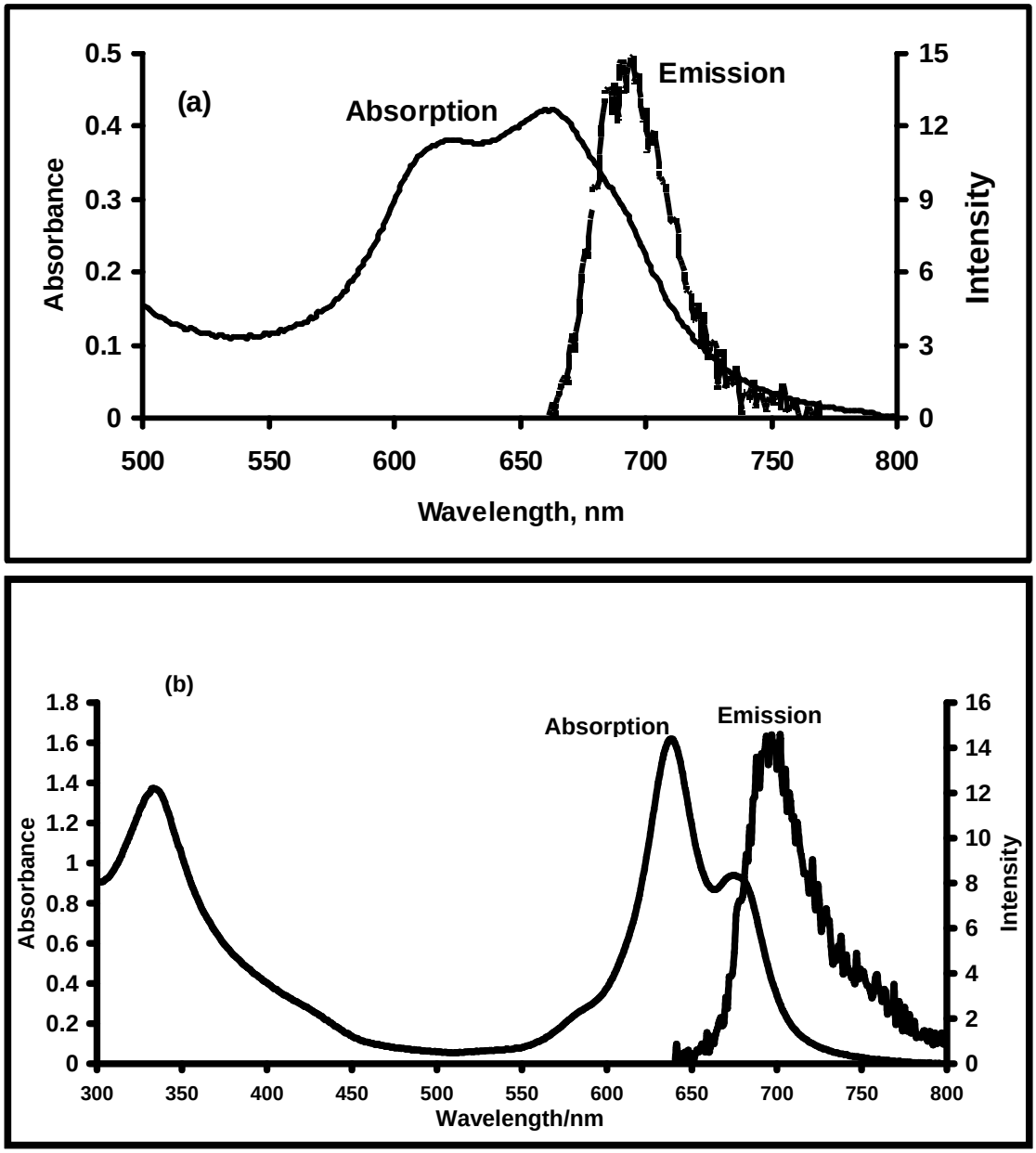

Figure 3.8: Absorption and fluorescence emission spectra of (a) SnTSTBC (3.7×10^{-4} M) and (b) SnTSPc (8.3×10^{-6} M) in aqueous solution.

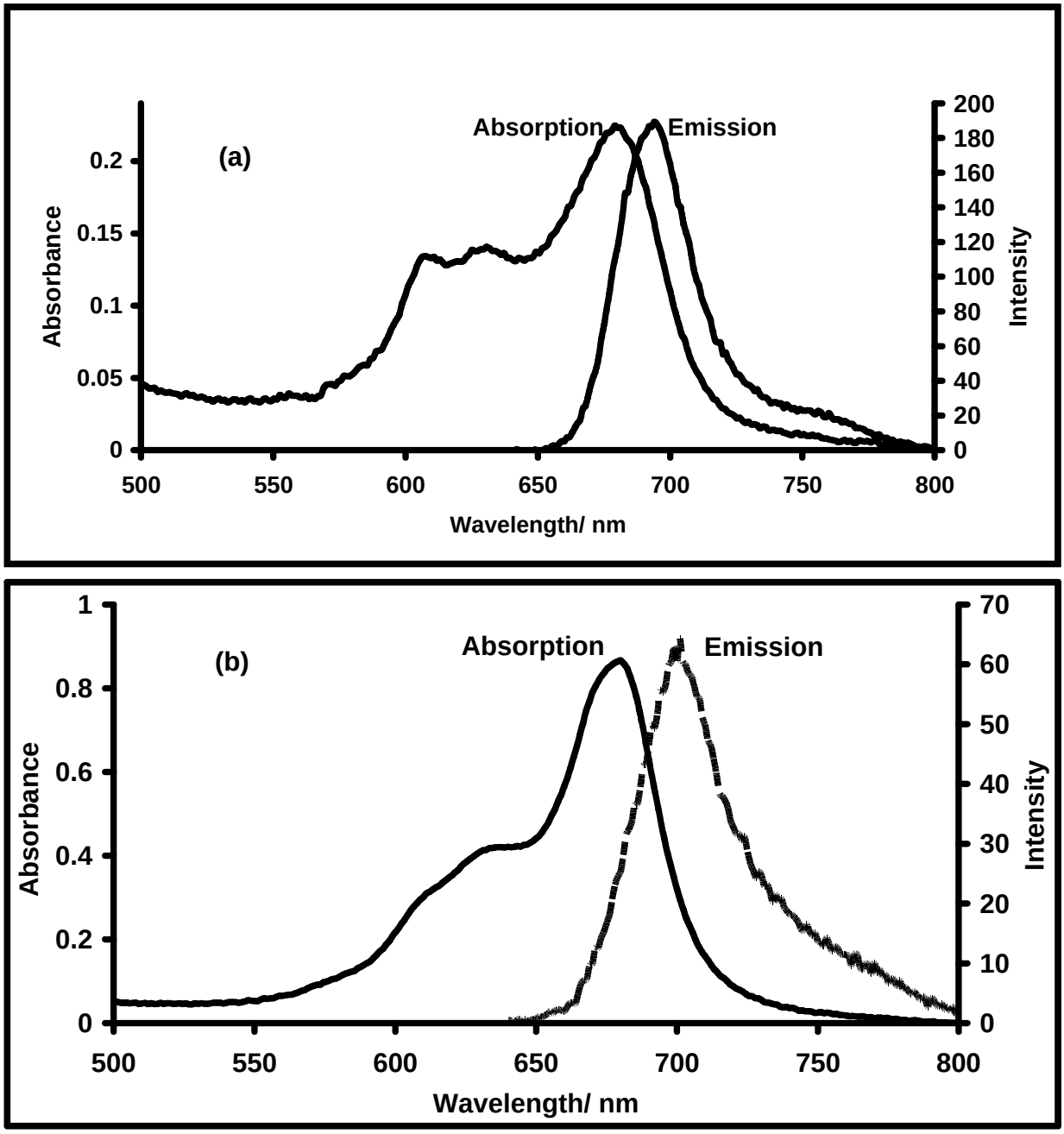

Figure 3.9: Absorption and fluorescence emission spectra of (a) SnTSTBC (3.7×10^{-4} M) and (b) SnTSPc (8.3×10^{-6} M) in aqueous methanol.

3.1.4 Alkylthio Substituted Metallophthalocyanine Complexes

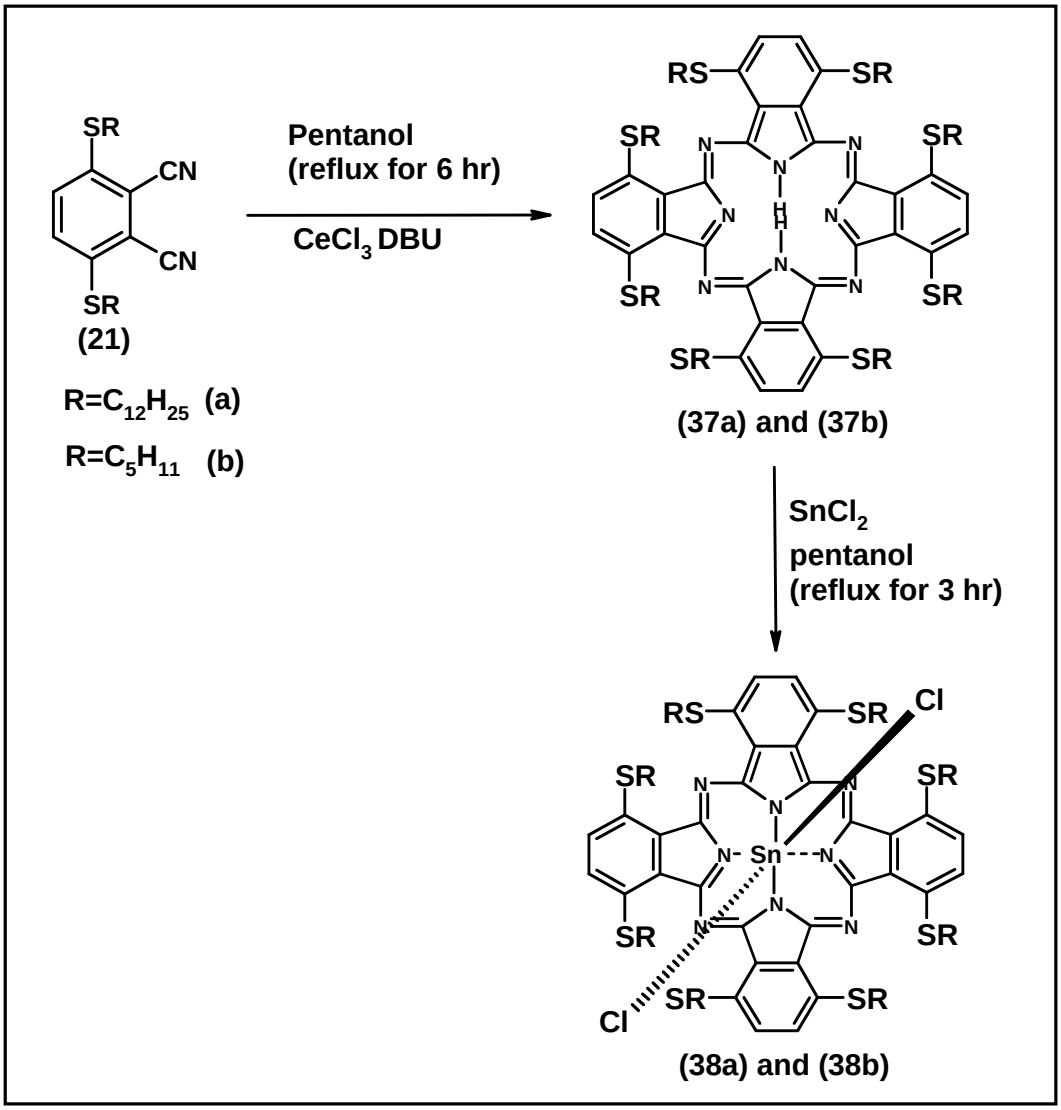

Scheme 3.11: Synthesis of complexes (38a) and (38b).

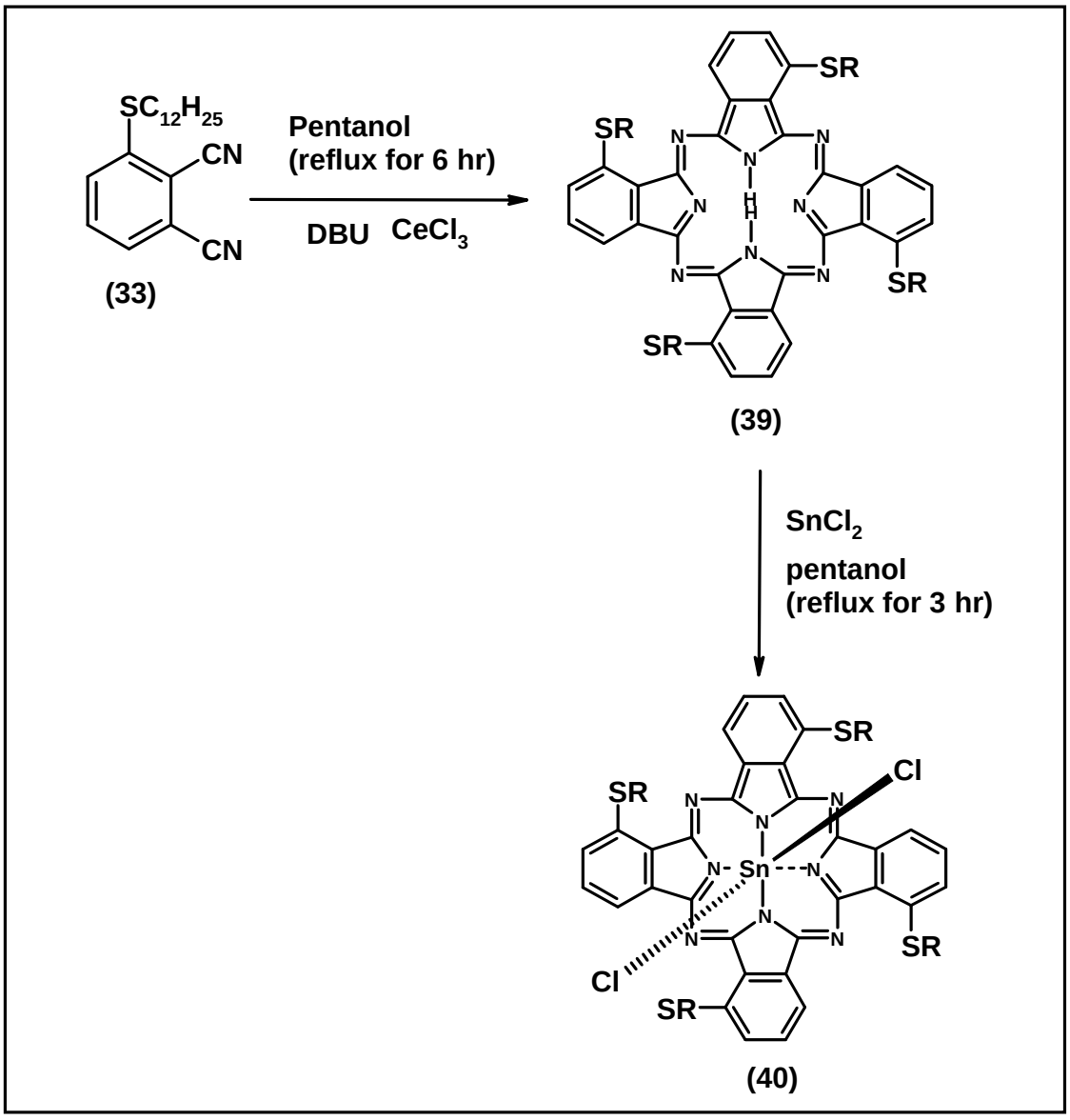

Scheme 3.12: Synthesis of non-peripherally (α) tetra-(40) substituted dodecyl-mercapto tin(IV) phthalocyanines.

As stated above the synthesis of SnPc complexes may result in the formation of Sn(II)Pc of Cl_2Sn(IV)Pc species depending on the amount of $SnCl_2$ used [124, 125]. In this work, the Cl_2Sn(IV)Pc derivative was formed for alkylthio substituted Pc (**Scheme 3.11 and 3.12**). Elemental analyses and spectroscopic characterization confirmed the formation of

these complexes. ^{1}H NMR spectra showed appropriate resonances for complexes **(38a), (38b)** and **(40)**. For complex **(38a)** and **(38b)** the ring protons were observed as singlets at position 8.0 ppm, which integrated to give 8 protons. The Ar-SCH_2- protons where observed as a triplets at positon 3.5 ppm, which intergrated to give 16 protons. The SCH_2-CH_2- protons where observed as multiplets at position 2.1 ppm, which intergrated to give 16 protons. The $H_{alipahtic}$ protons where observed as multiplets between 1.2-1.65 ppm, which intergrated for 144 protons for **(38a)** and 32 protons for **(38b).** The -CH_3 protons where observed as triplets at position 0.8 ppm, which intergarted for 24 protons for both **(38a)** and **(38b)**. Complex **(40)** aromatic protons where observed as a mulitplet at position 9.3 ppm, which intergrated to give 4 protons, and a singlet at position 8.4 ppm, which intergrated to give 8 protons. A multiplet was observed for Ar-SCH_2- protons at position 3.7 pp, which intergrated to give 8 protons. The $H_{aliphatic}$ protons where observed as multiplets between 1.2-2.2 ppm, which intergrated to give 80 protons. The –CH_3 protons where observed at position 0.9 ppm, which intergrated to give 12 protons.

Figure 3.10 shows ground state absorption spectra for complexes of **(37a)**, **(38a), (39)** and **(40)** in chloroform. A large red-shift (compared to unsubstituted SnPc) was observed due to non-peripheral substitution with the sulfur containing groups. The plurality of the sulfur groups in (**38a)** resulted in a very large shift with a Q band at 919 nm compared to 769 nm for **(40)**, a difference of 150 nm, **Table 3.1**. The spectrum for **(38a)** looks broad suggesting aggregation, however Beer's law was obeyed for both complexes in chloroform for concentrations less than 1 x 10^{-5} M.

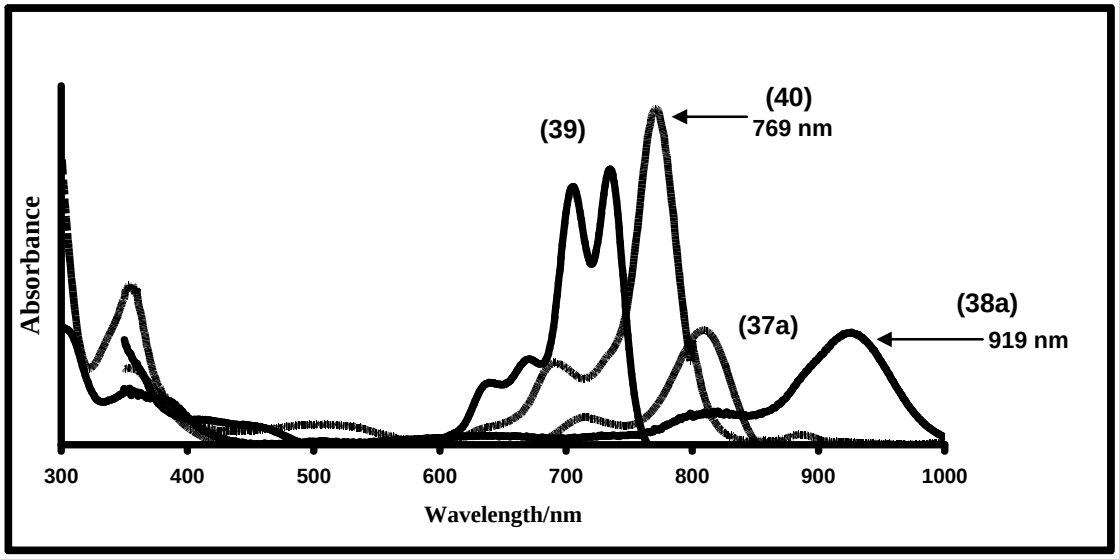

Figure 3.10: Ground state absorption spectra of $Cl_2SnPc(SC_{12}H_{25})_8$ (40) (concentration = 3, 58 x 10^{-6} M and $Cl_2SnPc(SC_{12}H_{25})_4$ (38a) (concentration = 8.60 x 10^{-7}M) in chloroform and the unmetallated counter parts (37a) and (40).

The spectrum of the non-peripherally octasubstituted unmetallated derivative **(37a)** does not show the typical split Q band. It is known that the splitting of the Q band decreases with increasing wavelength [128], hence for complex **(37a)**, the large red shift has resulted in an unsplit Q band. A split Q band is observed for the less red-shifted complex **(39)**.

3.2 Photophysical Properties

3.2.1 Alkyl Substituted Metallophthalocyanine Complexes

Fluorescence quantum yields

Fluorescence quantum yields (Φ_F) were determined by the comparative method using **Equation 3.3** (same as **Equation 1.7**):

$$\Phi_F = \Phi_F(\text{Std}) \frac{F \cdot A_{Std} \cdot \eta^2}{F_{Std} \cdot A \cdot \eta^2_{Std}} \quad (3.3)$$

where F and F_{Std} are the areas under the fluorescence emission curves of the samples and the standard, respectively. A and A_{Std} are the respective absorbances of the samples and the standard at the excitation wavelengths, respectively. The refractive indices of the solvents were employed in calculating fluorescence quantum yields in different solvents. $ZnPc(C_{10}H_{21})_8$ **(36)** in THF (Φ_F = 0.26) [129] was employed as the standard using the refractive indices of the solvents to determine the Φ_F values. Both the samples and standard were excited at the same wavelength. The absorbance of the solutions at the excitation wavelength ranged between 0.04 and 0.05. **Table 3.5** give the values of Φ_F for the complexes. Fluorescence quantum yields of **(35a)** to **(35c)** are within the range usually observed for MPc complexes, and somewhat lower than that for $ZnPc(C_{10}H_{21})_8$ **(36)**. The trend was the same for measurements in both toluene and THF.

Triplet quantum yields and lifetimes

Triplet quantum yields (Φ_T) were determined using **Equation 3.4** (same as **Equation 1.26**):

$$\Phi_T^{Sample} = \Phi_T^{Std} \frac{\Delta A_T^{Sample} \cdot \varepsilon_T^{Std}}{\Delta A_T^{Std} \cdot \varepsilon_T^{Sample}} \quad (3.4)$$

where ΔA_T^{Sample} and ΔA_T^{Std} are the changes in the triplet state absorbances of the samples and standard, respectively; ε_T^{Sample} and ε_T^{Std}, the triplet state extinction coefficients for the samples and standard, respectively. The standard employed was ZnPc in toluene (Φ_T^{Std} = 0.65) [130]. Mesurements of Φ_T were repeated at least five times revealing an error of 10% in the determinations.

The transient absorption difference spectra for **(35a)** and **(35c)** (**Figure 3.11a and 3.11b)** show that there were no changes in spectra following excitation using laser flash photolysis. For complex **(35b)**, a split Q band which was observed in the absorption spectrum is not observed on the transient absorption difference spectrum (**Figure 3.11b**), again surprising since change in symmetry is not expected hence suggesting involvement of aggregation. The triplet absorption maxima were observed at 585 nm for **(35a)** and **(35c)** and at 600 nm for **(35b)**.

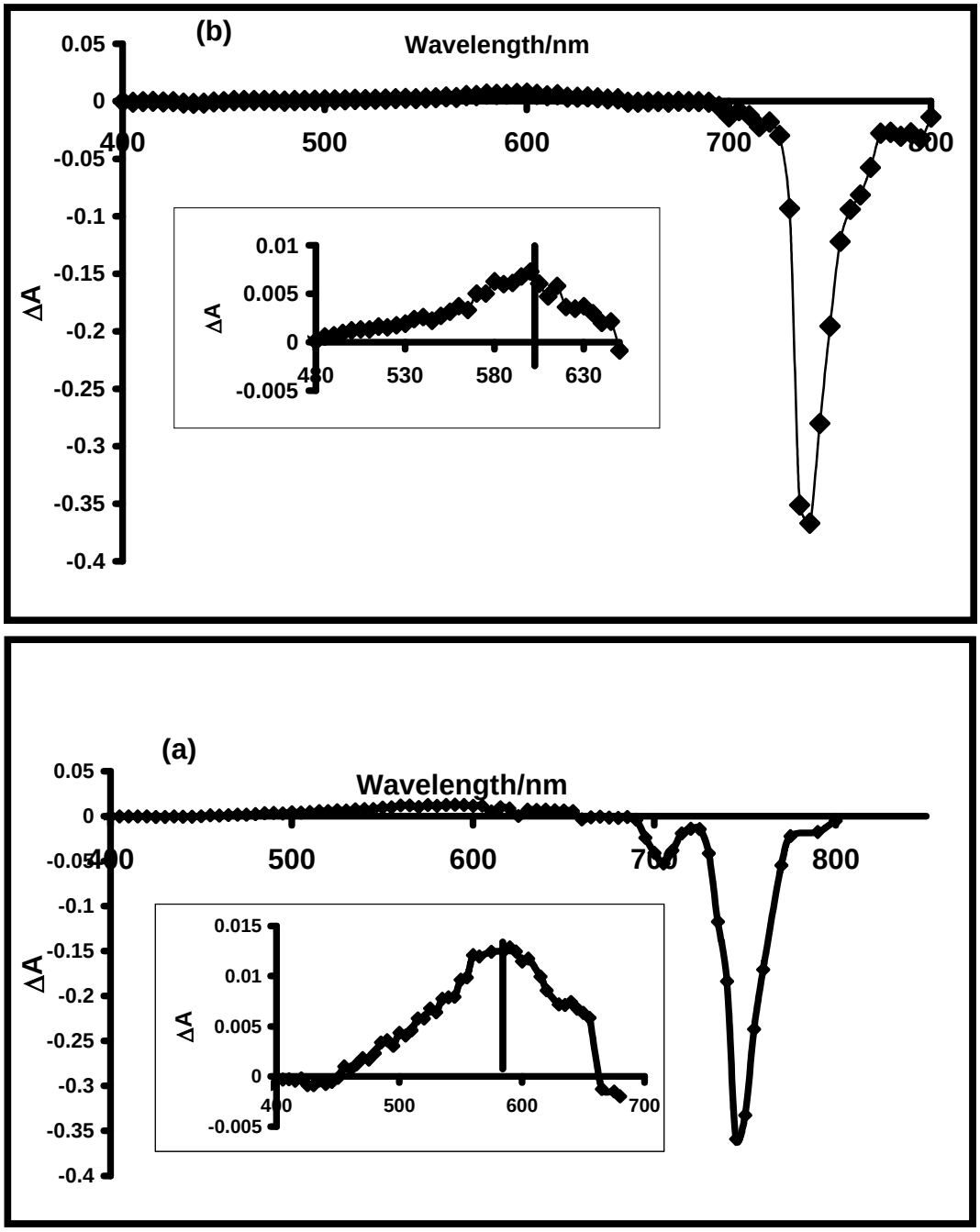

Figure 3.11: Transient difference spectrum of complex (35a) (a) and (35b) (b) in THF. Excitation wavelength = 725 nm.

Data for triplet lifetimes, τ_T, triplet state quantum yields, Φ_T, and fluorescence quantum yields, Φ_F , for **(35a)**, **(35b)**, **(35c)** and $ZnPc(C_{10}H_{21})_8$ **(36)** are collected in **Table 3.5**.

Table 3.5: Spectroscopic and photophysical data for complexes (35a) to (35c) in THF. Values in parentheses, ( ), were obtained in toluene.

Complexes in THF	**λ_{abs}. nm**	**λ_{em} nm**	**Stokes Shift nm**	**Φ_F**	**Φ_T[b]**	**τ(μs)**	**Φ_{ISC}[b]**
$ZnPc(C_{10}H_{21})_8$ **(36)**	700[a] (704)	712[a] 731	12 (27)	0.26[a] (0.28)	(0.22)	100 (4)	(0.50)
(35a)	735 (736)	750 (750)	15 (14)	0.20 (0.16)	(0.30)	90 (20)	(0.54)
(35b)	700, 727 (702, 730)	734 750)	7 (20)	0.23 (0.19)	(0.78)	100 (30)	(0.03)
(35c)	735 (736)	750 (750)	15 (14)	0.23 (0.15)	(0.35)	200 (10)	(0.50)

[a]Values obtained in literature [129]. **[b] Values of Φ_T and Φ_{ISC} were not determined in THF due to lack of standards.**

Measurements of τ_T and Φ_F were made for solutions in THF and toluene; data for Φ_T were obtained for solutions of toluene only. An enhanced heavy atom effect arising from the presence of tin in the $Cl_2Sn(IV)Pc$ complexes, **(35a)** and **(35c)**, rather than zinc in $ZnPc(C_{10}H_{21})$ **(36)** is manifested by higher triplet quantum yields in the former (**35a**, Φ_T = 0.30; **(35c)**, Φ_T = 0.35; cf $ZnPc(C_{10}H_{21})_8$, Φ_T = 0.22), and lower fluorescence quantum yields. Complex **(35b)** gave a high value for the triplet lifetime, (Φ_T = 0.78), indicating that the presence of the C-H in place of one of the Pc aza nitrogen atoms enhances the

triplet yield significantly. The triplet lifetimes (τ_T) for all the complexes were low in toluene as has been observed before [131] for measurements of other MPcs undertaken in this solvent. Those obtained using THF as solvent do not follow discernible trends. The longest τ_T value in THF was exhibited by complex **(35c)**, containing the longer substituent chains.

3.2.2 Sulphonated Metallophthalocyanine Complexes

3.2.2.1 Fluorescence Quantum Yields and Lifetimes:

For these studies ZnPc in DMSO (Φ_F = 0.20) [121], was employed as the standard, using **Equation 3.3**. Both the sample and standard were excited at the same wavelength (630 nm).

The fluorescence quantum yields of SnTSTBC **(42)** (Φ_F = 0.05) and SnTSPc **(41)** (Φ_F = 0.11) are given in **Table 3.6**. These values indicate that SnTSTBC **(42)** is not as fluorescent as SnTSPc **(41)**. This is also supported by the fluorescence lifetimes of the complexes, which are longer for SnTSPc **(41)** than for SnTSTBC **(42)**. Triplet quantum yields (and lifetimes) are higher for SnTSPc **(41)** than for SnTSTBC **(42)** (**Table 3.6**). These values altogether point to the same fact that a phthalocyanine (systematically named: tetrazatetrabenzoporphyrin) is more photoactive than a α,β,γ-tetrabenzcorrole (systematically named: triazatetrabenzoporphyrin). Φ_{IC} value (**Equation 3.5)** for SnTSTBC **(42)** is larger than for SnTSPc **(41),** suggesting less energy loss by internal conversion for the former derivative.

$$\Phi_{IC} = 1 - (\Phi_F + \Phi_T) \qquad 3.5$$

Equation 3.5 assumes that only three processes (fluorescence, intersystem crossing and internal conversion), jointly deactivates the excited singlet state of SnTSBC (**42**) or SnTSPc (**41**) molecule.

Table 3.6: Photophysical and photochemical parameters of SnTSTBC and SnTSPc in aqueous methanol.

Complex	$\lambda_{Q\ band}$ /nm	λ_{Ems} /nm	Φ_F	Φ_T	Φ_{IC}	10^{-5} Φ_{Pd}	τ_F /ns	τ_T /μs	10^{-8} k_F[a] /s^{-1}	10^{-8} k_{ISC}[b] /s^{-1}	10^{-8} k_{IC}[c] /s^{-1}
SnTSTBC **(41)**	680	694	0.05	0.64	0.31	2.50	0.10	8.9	5.01	64.0	31.0
SnTSPc **(42)**	680	696	0.11	0.80	0.09	0.11	3.40	30	0.32	2.35	0.91

Values calculated using [a] $k_F = \Phi_F/\tau_F$; [b] $k_{ISC} = \Phi_T/\tau_F$; [c] $k_{IC} = \Phi_{IC}/\tau_F$.

SnTSPc **(41)** is more stable in the presence of light than SnTSTBC **(42)**, judging from the two complexes' photodegradation quantum yield (Φ_{Pd}) values, calculated using **Equation 3.6**.

$$\Phi_{Pd} = \frac{(C_0 - C_t)VN_A}{I_{abs}St} \qquad (3.6)$$

where C_0 and C_t in mol dm^{-3} are the SnTSBC **(42)** or SnTSPc **(41)** concentrations before and after irradiation, respectively; V is the reaction volume; S, the irradiated cell area (2.0

cm^2); t, the irradiation time; N_A, the Avogadros number and I_{abs}, the overlatp integral of the radiation source intensity and the absorption of the Pc in the region of the interference filter transmittance. Photodegradation of phthalocyanines and related compounds is believed to be caused by oxidative attack by radical and non-radical species of oxygen (**Scheme 3.13**), and is identified by a reduction in spectral intensity without the formation of new peaks [131].

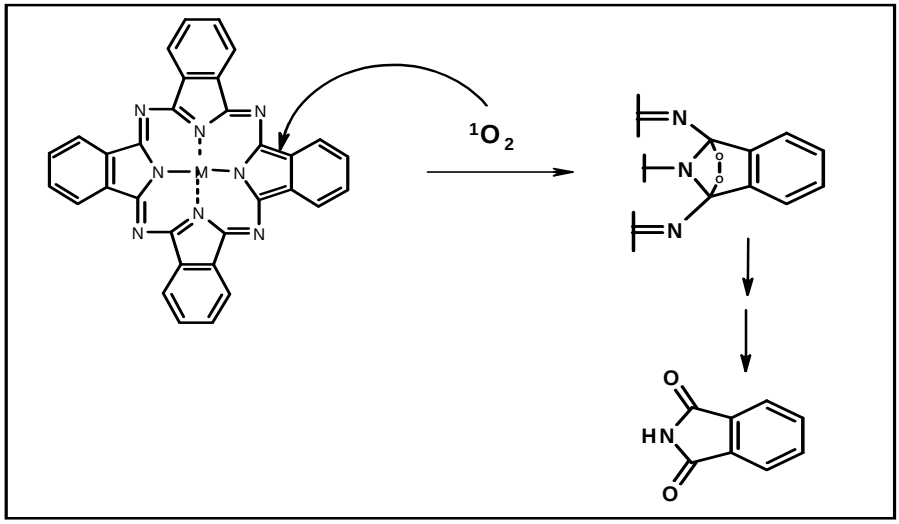

Scheme 3.13: Photodegradation of MPc upon irradiation involving singlet oxygen.

Values of rate constants for the intrinsic deactivation processes for the excited singlet state (k_F, k_{ISC} and k_{IC}; where the subscripts 'F', 'ISC' and 'IC' represent fluorescence, intersystem crossing and internal conversion, respectively) are of the order observed in MPcs and related complexes [62]. All the rate constants (k_F, k_{ISC} and k_{IC}) are higher for SnTSTBC **(42)** than for SnTSPc **(41)** (**Table 3.5**), which is attributed to the relatively short fluorescence lifetime of SnTSTBC **(42)**.

3.2.2.2 BSA Fluorescence Quenching

The binding of the SnTSTBC **(42)** and SnTSPc **(41)** derivatives to BSA was studied by spectrofluorometry at room temperature. An aqueous solution of BSA (fixed concentration) was titrated with varying concentrations of the respective SnTSTBC **(42)** or SnTSPc **(41)** solution. BSA was excited at 280 nm and fluorescence recorded between 290 nm and 500 nm. The steady diminution in BSA fluorescence with increase in concentrations of SnTSPc **(41)** or SnTSTBC **(42)** was noted and used in the determination of the binding constants and the number of binding sites on BSA, according to **Equation 3.7**(same as equation 1.25).

$$\log\left[\frac{(F_0 - F)}{(F - F_\infty)}\right] = \log K_b + n\log[SnTS] \qquad (3.7)$$

where SnTS represents either SnTSTBC **(42)** or SnTSPc **(41)**, F_0 and F are the fluorescence intensities of BSA in the absence and presence of SnTSTBC **(42)** or SnTSPc **(41)** respectively; F_∞, the fluorescence intensity of BSA saturated with SnTSTBC **(42)** or SnTSPc **(41)**; K_b, the binding constant; n, the number of binding sites on a BSA molecule. Plots of $\log\left[\frac{(F_0 - F)}{(F - F_\infty)}\right]$ against log [SnTS] provide the values of n (from the slope) and log K_b (from the intercept).

Figure 3.12 shows quenching of BSA fluorescence by SnTSPc **(41)**. The binding constants (K_b) for SnTSTBC **(42)** or SnTSPc **(41)** binding to BSA in aqueous solution, together with the binding stoichiometries were obtained using **Equation 3.7**, **Figure 3.13a**; and the results are presented in **Table 3.7**. The values of K_b are typical for MPc-

albumin interactions in aqueous solutions [80]. A higher K_b value (1.4 x 10^6 M^{-1}) was obtained for SnTSPc **(42)**, which is less aggregated, while SnTSTBC **(42)** gave a lower value. This shows that aggregation plays a significant role in the binding of macrocycles with BSA, as observed before [89].

Table 3.7: BSA binding data for SnTSTBC and SnTSPc in aqueous solution

MPc	K_{SV}^{BSA} /M^{-1}	K_b /M^{-1}	n	k_Q /M^{-1} s^{-1}
SnTSTBC	0.9 x 10^4	2.9 x 10^4	1.1	9.0 x 10^{11}
SnTSPc	8.0 x 10^7	1.4 x 10^6	0.8	8.0 x 10^{15}

The involvement of a dimer in BSA binding is indirect, via dissociation into monomers. As a result, K_b values should depend partly on the inherent dimer dissociation constants. The number of binding sites (n) on BSA were obtained from **Figure 3.13a** to be near unity (**Table 3.7**), which suggests a 1:1 binding stoichiometry for the adducts formed between BSA and SnTSTBC **(42)** (or SnTSPc **(41)**). Bimolecular rate constants (k_Q) for the interaction of BSA with SnTSTBC **(42)** or SnTSPc **(41)** were determined from the respective Stern-Volmer quenching constants, **Equation 3.8** (same as **Equation 1.20**):

$$\frac{I_0}{I} = K_{SV}^{BSA}[SnTS] + 1 \qquad (3.8)$$

where I_0 and I are the BSA fluorescence intensities in the absence and presence of SnTSTBC **(42)** (or SnTSPc **(41)**) respectively; [SnTS], the concentration of SnTSTBC **(42)** (or SnTSPc **(41)**); and K_{SV}, the Stern-Volmer quenching constant.

K_{SV} values were determined using **Equation 3.8** and **Figure 3.13b**. The K_{SV} values are higher for SnTSPc **(41)** than for SnTSTBC **(42)**. It is believed that this observation is not unconnected with the lower aggregating tendencies of SnTSPc **(41)** compared with SnTSTBC **(42)**, as discussed above. In the same vein, k_Q value for SnTSPc **(41)** is by far greater than that for SnTSTBC **(42)**. The values of k_Q obtained in this work are greater than the value suggested in the Einstein-Smoluchowski approximation (~ 10^{10} dm^3 mol^{-1} s^{-1}) for diffusion-controlled bimolecular reactions at room temperature [132], and such high values are indicative of binding interaction between the reactants [88].

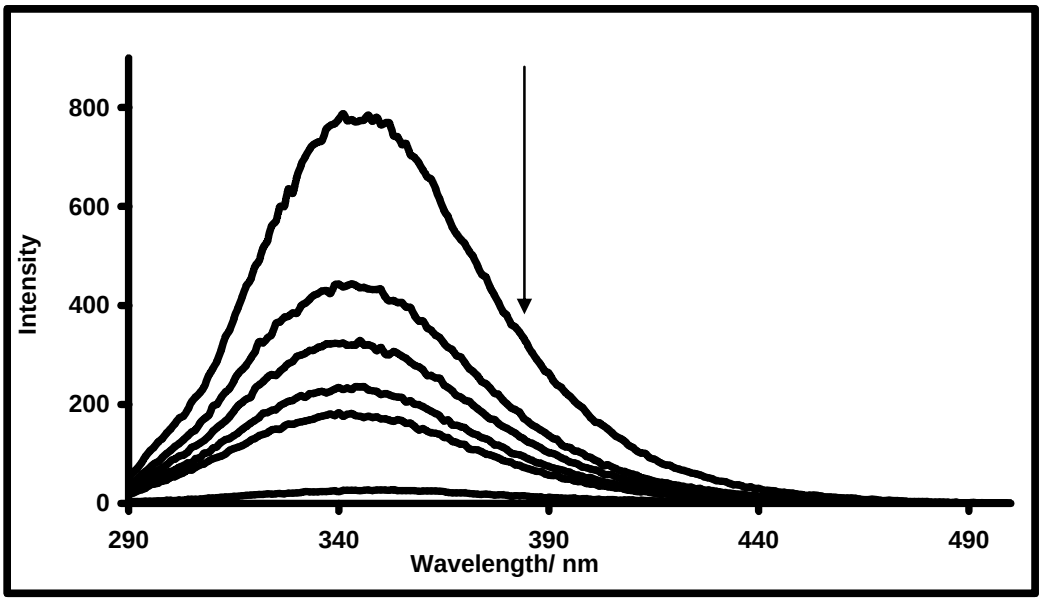

Figure 3.12: Spectral changes accompanying the addition of SnTSPc (43) (6.8×10^{-9} to 5.4×10^{-8} M) to BSA (3.0×10^{-5} M) in aqueous solution.

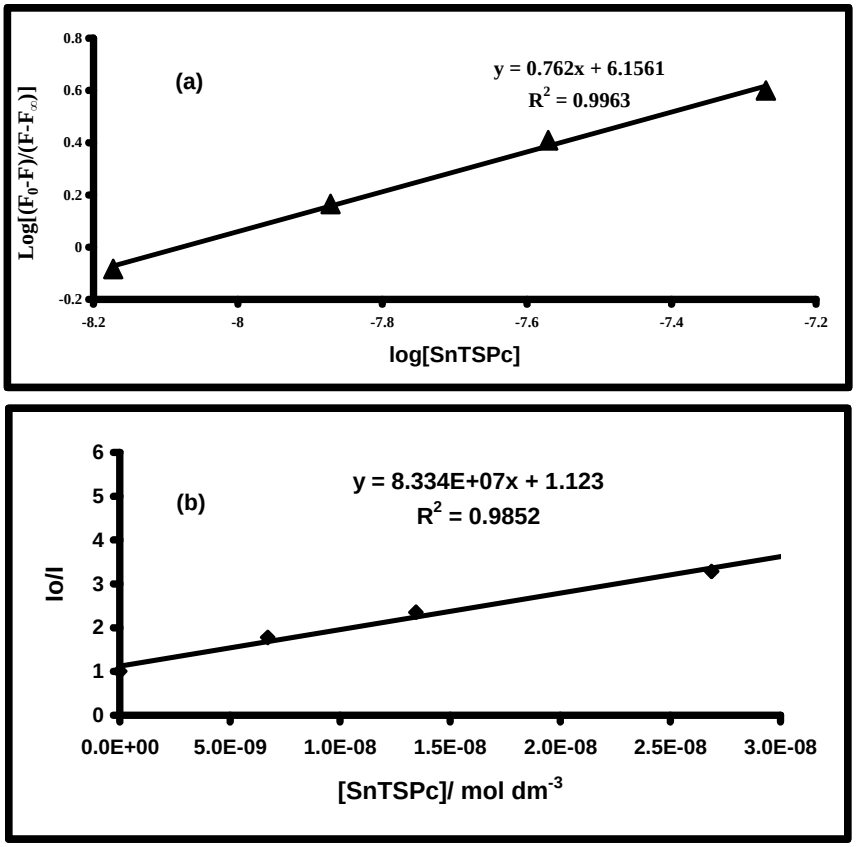

Figure 3.13: (a) Determination of binding constant and number of binding sites on BSA and (b) Stern-Volmer plot for interaction of SnTSPc with BSA.

3.3 Electrochemical Properties

3.3.1 Alkyl Substituted Metallophthalocyanine Complexes

3.3.1.1 Cl_2Sn(IV)Pc complexes (35a) and (35c)

Figure 3.14 shows the cyclic and square wave voltammograms for complexes (**35a)** and (**35c)** in THF containing $TBABF_4$, with three redox processes labelled **I**, **II** and **III** in **Figure 3.14b**. Both the narrow (**Figure 3.14a**) and the wide (**Figure 3.14b**) potential

windows are shown in **Figure 3.14** since better voltammograms are usually observed in a narrow potential window. Both complexes showed similar voltammograms. However, as expected, a more complicated voltammogram was obtained on extending the potential window. One irreversible (showing only a weak return peak) oxidation peak at (**I**) and two reduction processes **II** and **III** were clearly observed for complex **(35a)** and **(35c)**, process **III** being observed on a wider scan window and showing complicated behaviour since it is at the limits of the system. **Table 3.8** lists the potentials for the processes.

Table 3.8: Electrochemical data for complexes (35a) to (35c) in THF containing $TBABF_4$

	$E_{½}$ (V vs Ag|AgCl)		
Complexes	**Pc^{-1}/Pc^{-2} (I)**	**Pc^{-2}/Pc^{-3} (II)**	**Pc^{-3}/Pc^{-4} (III)**
(35a)	1.38[a]	-0.35	-0.89[a]
(35b)	-	-0.51	-0.85
(35c)	0.80	-0.81	-0.98[a]

[a] **Ep, since there was no clear return peak**

Couple **II** was reversible with anodic to cathodic peak separation of 100 mV (ferrocene internal standard gave a cathodic to anodic peak separation of 90 mV), and the ratio of anodic to cathodic peak potential of unity. The second reduction process was irreversible. For all the redox processes for **(35a)** and **(35c)**, plots of square root of scan rate versus potential were linear confirming diffusion control. **Table 3.8** shows that complex **(35a)**

is more readily reduced and more difficult to oxidize than **(35c)** which contains a longer chain.

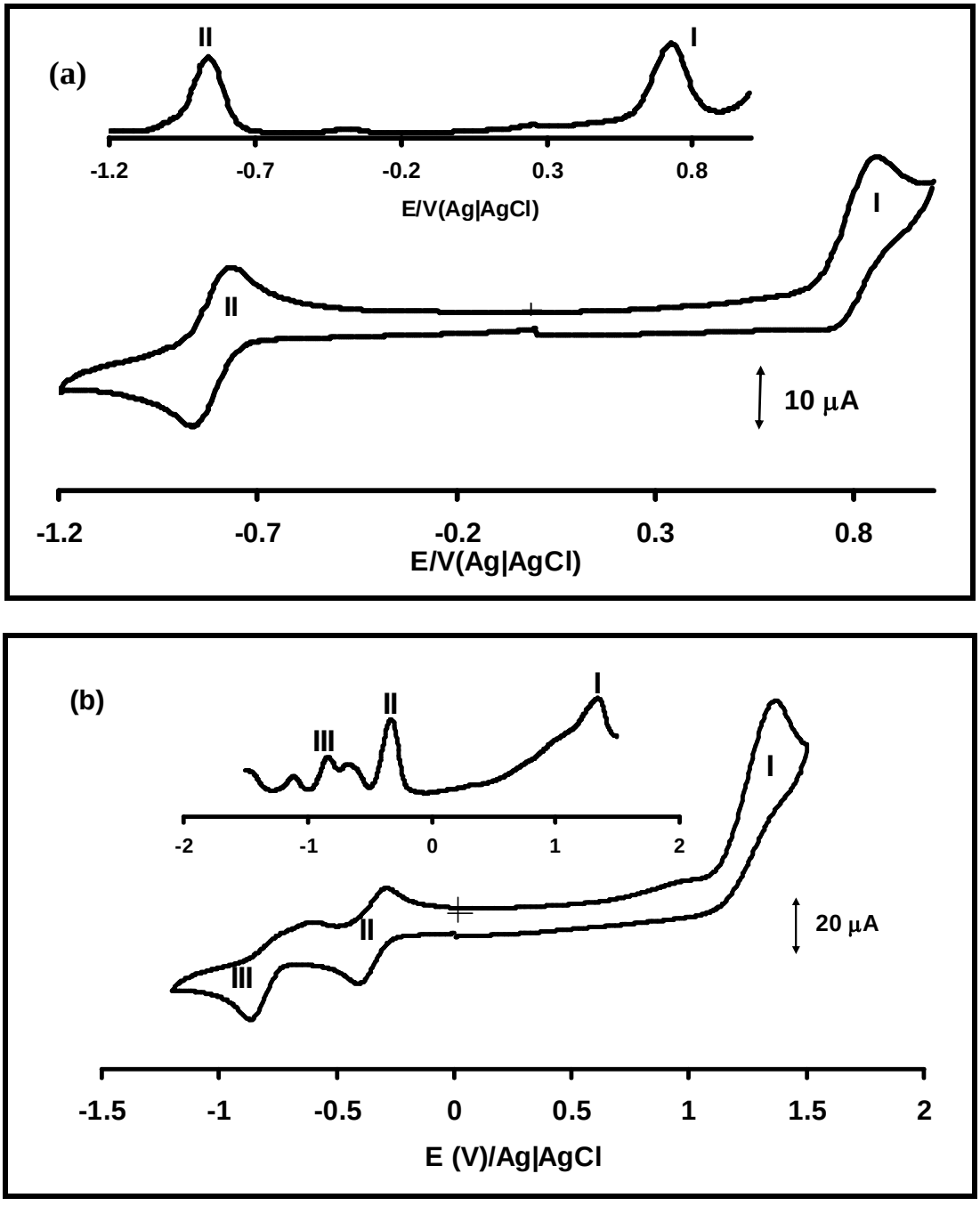

Figure 3.14: Cyclic (lower) and square wave (upper) voltammograms for (a) 35c and (b) 35a in tetrahydrofuren (THF) containing $TBABF_4$. Scan rate = 100 mV/s.

The potentials listed in **Table 3.8** for the oxidation or reduction of complexes **(35a)** and **(35c)** are in the range of ring based processes in MPc complexes [133]. However the assignments of the redox processes were confirmed by spectroelectrochemistry (OTTLE cell).

Reduction of the $Cl_2Sn(IV)Pc$ complexes at the central metal to Sn(II) is possible in addition to ring based reduction processes. **Figure 3.15a** shows electronic absorption changes observed on reduction of complex **(35c)** at potentials of couple **II**. The spectral changes consisted of the decrease in the Q band, with the formation of a new weak feature at 600 nm, which did not increase further in intensity with electrolysis time. Similarly for complex **(35a)**, **Figure 3.15b**, new peaks were observed at 560, 606 and 630 nm. The formation of weak bands in the 500 to 650 nm region in the spectra of MPc complexes is typical of ring based reduction in MPc complexes [106]. Thus, couple **II** is assigned to $Cl_2Sn(IV)Pc(-2)/Cl_2Sn(IV)Pc(-3)$ process. Further reduction at potential of process **III** resulted in decomposition as judged by the collapse of the Q band with no new bands being formed, **Figure 3.15c** (for both (**35a**) and (**35c**)), hence confirming the irreversible nature of process **III**. Similarly oxidation at potentials of process **I** resulted in decomposition, **Figure 3.15d**. The spectroelectrochemical studies thus show that complexes **(35a)** and **(35c)** readily decompose on both oxidation and reduction. It is however expected that both processes **I** and **III** are due to ring based oxidation and reduction, respectively, hence may be assigned to $Cl_2Sn(IV)Pc(-1)/Cl_2Sn(IV)Pc(-2)$ and $Cl_2Sn(IV)Pc(-3)/Cl_2Sn(IV)Pc(-4)$.

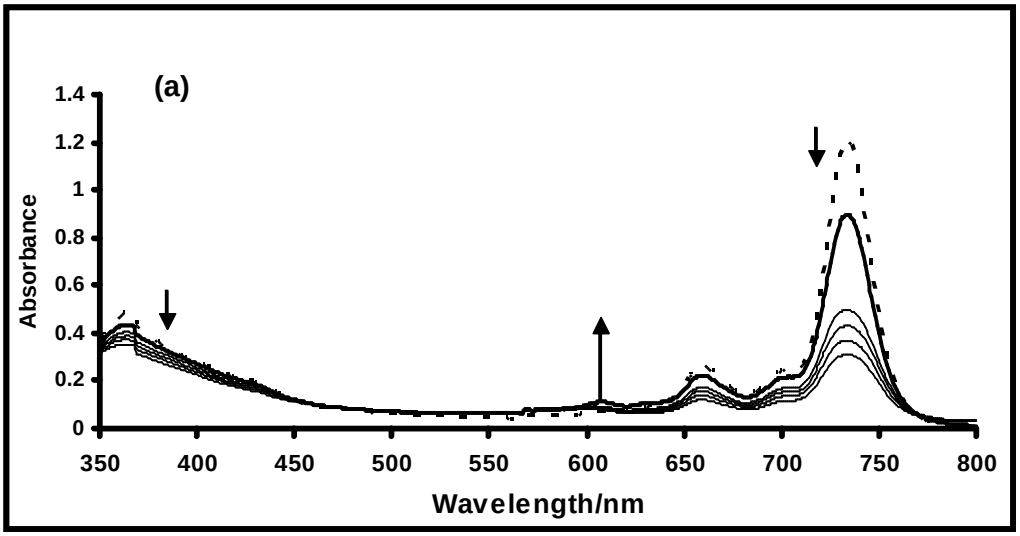
(a)
Absorbance
1.4
1.2
1
0.8
0.6
0.4
0.2
0
350
400
450
500
550
600
650
700
750
800
Wavelength/nm

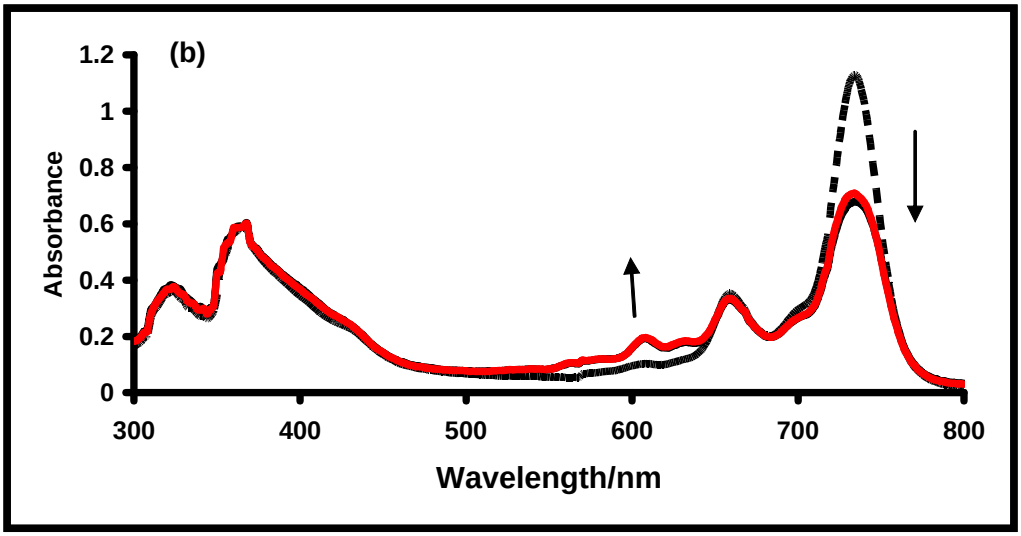
(b)
Absorbance
1.2
1
0.8
0.6
0.4
0.2
0
300
400
500
600
700
800
Wavelength/nm

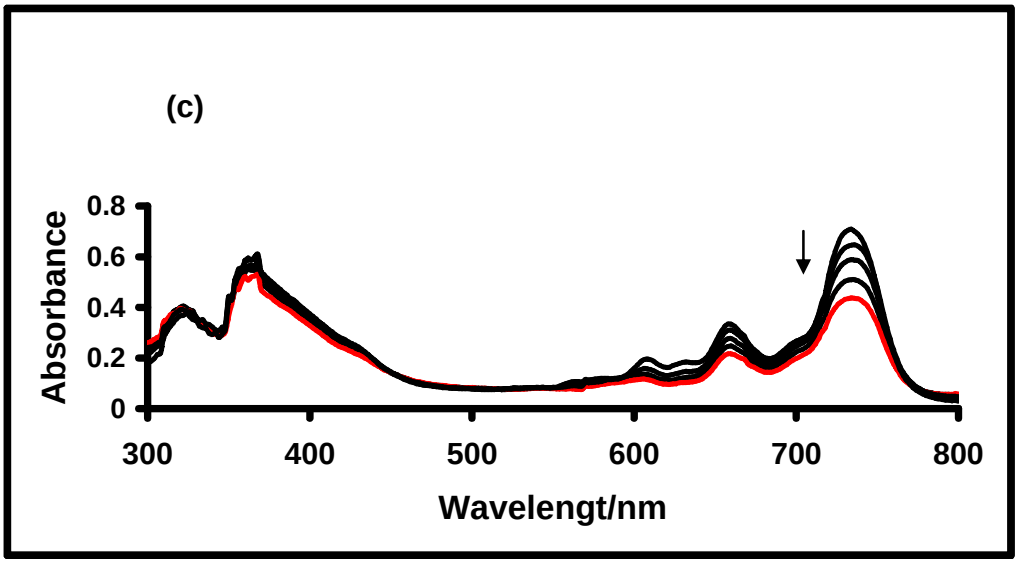
(c)
Absorbance
0.8
0.6
0.4
0.2
0
300
400
500
600
700
800
Wavelengt/nm

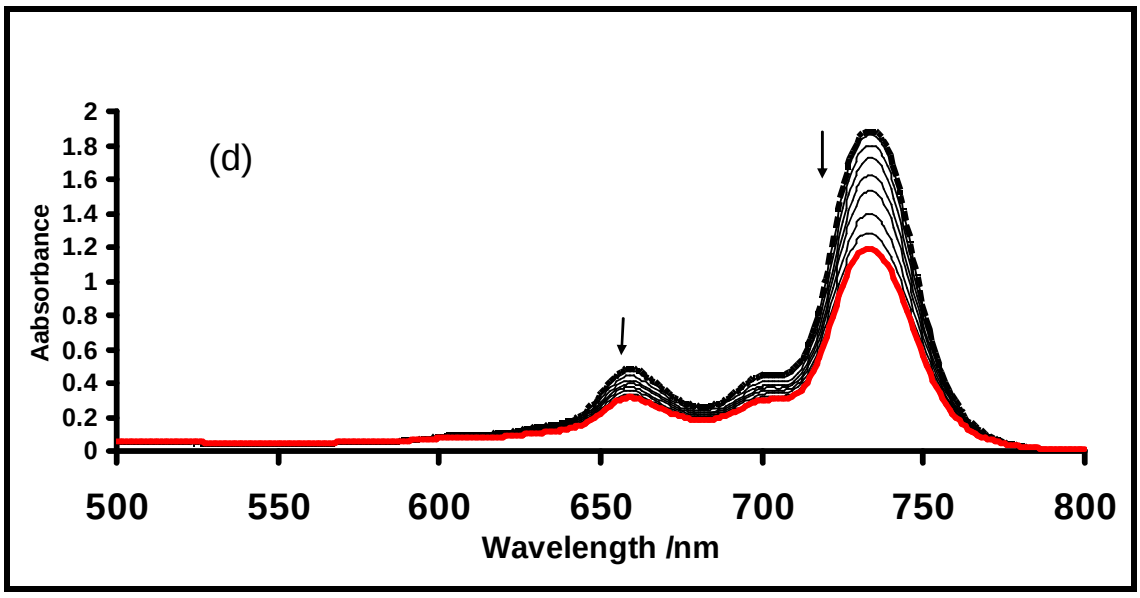

Figure 3.15: UV-visible spectral changes observed during controlled potential (OTTLE cell): (a) reduction of (35c) at an applied potential of couple II (-1.0 V), (b) reduction of (35a) at applied potential of couple II (-1.0 V), (c) reduction of (35c) at an applied potential of couple III (-1.5 V) and (d) oxidation of (35c) at potentials of process I in THF (toluene) containing 0.1 M $TBABF_4$.

3.3.1.2 Cl_2Sn(IV) TBTAP (35b) complex

Figure 3.16 shows the cyclic and square wave voltammograms for complexes (**35b)** in THF containing $TBABF_4$. No oxidation processes were observed for this complex. One clear reduction couple (**II**) at -0.51V and a weaker reduction process (**III**) at -0.85 V were observed in **Figure 3.16** (**Table 3.8**). As was the case for complexes (**35a)** and (**35c)**, couple **II** is reversible with anodic to cathodic peak separation of 100 mV, and the ratio of anodic to cathodic peak potential of unity. For complex **(35b)**, process **III** showed a weak return peak. For both redox processes for **(35b)**, plots of square root of scan rate versus potential were linear confirming diffusion control. **Table 3.8** shows that the

Sn(IV) tetrabenzotriazaporphyrin complex **(35b)** is more easily reduced than **(35c)**, and less easily reduced than **(35a)**, with regard to the first reduction. Thus it seems that the replacement of one aza nitrogen atom (of the Pc structure) with a C-H renders the ring more difficult to reduce (1st reductions), particularly on comparing complexes **(35b)** and **(35a)**, both of which have the same alkyl chains.

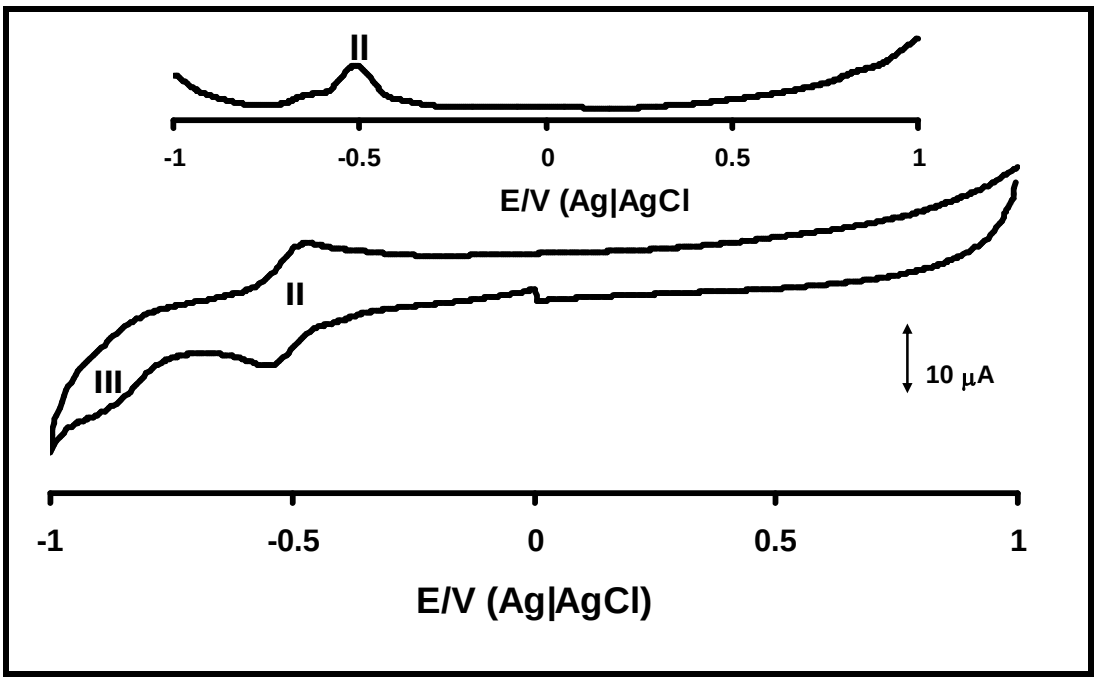

Figure 3.16: Cyclic (lower) and square wave (upper) voltammograms for (35b). Solvent toluene (THF) containing $TBABF_4$. Scan rate = 100 mV/s.

Figure 3.17 shows the electronic absorption changes observed on reduction of complex **(35b)** at potentials of couple **II**. The spectral changes consisted of the decrease in the Q band, with the formation of a new weak feature in the 550 nm range. As stated above, the formation of bands in the 500 to 650 nm region in the spectra of MPc complexes is typical of ring based reductions in MPc complexes [106]. Thus, couple **II** is assigned to Sn(IV)TBTAP(-2)/Sn(IV)TBTAP(-3) process. Further reduction at potential of process

III resulted in decomposition as judged by the collapse of the Q band with no new bands being formed as observed for complexes **(35a)** and **(35c)**. It is however suggested that process **III** is due to further ring based reduction and the formation of Sn(IV)TBTAP(-3)/Sn(IV)TBTAP(-4).

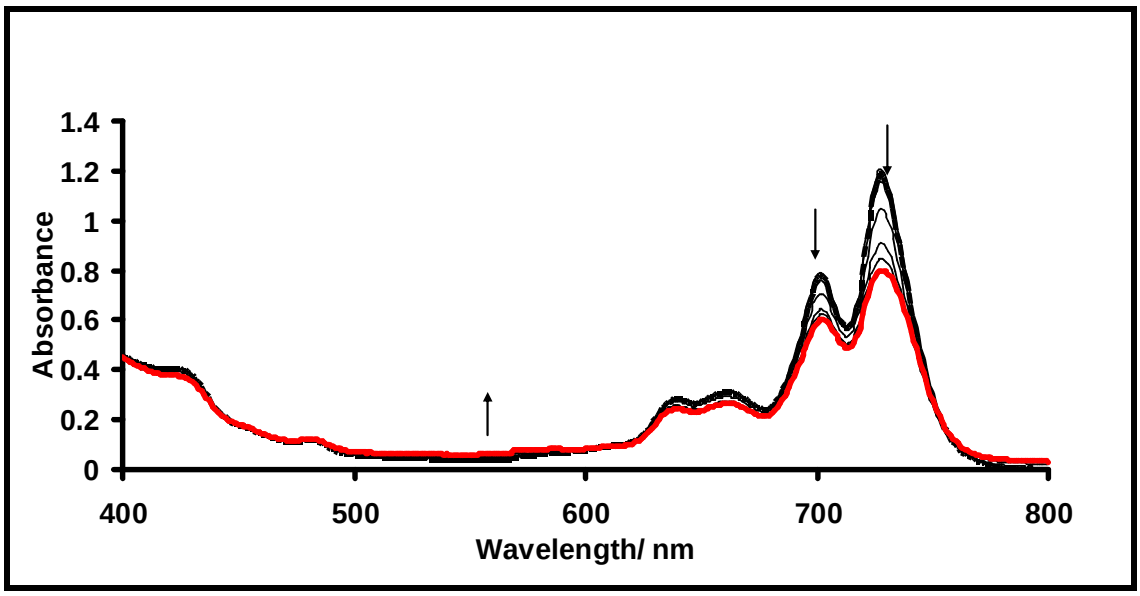

Figure 3.17: UV-visible spectral changes observed during controlled potential (OTTLE cell): reduction of (35b) at an applied potential of couple II (-0.6 V) in THF (toluene) containing 0.1 M $TBABF_4$.

3.3.2 Thiol substituted metallophthalocyanine complexes

3.3.2.1 Cyclic voltammetry and spectroelectrochemistry in solution

Figure 3.18 shows the cyclic and square wave voltammograms for complexes **(38a)** (**Figure 3.18a**) and **(40)** (**Figure 3.18b**) in chloroform containing $TBABF_4$. Complex **(38a)** shows five redox processes labeled **I** to **V**. Complex **(40)** displays four redox processes labeled **I**, **III**, **IV** and **V**. For all the redox processes (for complexes **(38a)** and

(40)), the plots of square root of scan rate versus current were linear confirming diffusion control. **Table 3.9** shows that tetrasubstituted complex **(40)** is more readily reduced and more difficult to oxidize than **(38a)** which has more sulfur atoms substituted at the non-peripheral position of the phthalocyanine.

Table 3.9: Redox couples (V vs Ag|AgCl) for complexes (39a) and (41) in $CHCl_3$ containing $TBABF_4$ unless otherwise stated. Assignment in brackets

$E_{1/2}$ (V vs Ag|AgCl)						**Ref**
Complexes	**(I)**	**(II)**	**(III)**	**(IV)**	**(V)**	
(38a)	0.97	0.72	- 0.37	-0.73	- 1.01	**This work**
(40)	1.22		-0.27	-0.66	-0.97	**This work**
Ti(IV)TPTPc[a]			-0.07[b] (Ti^{IV}/Ti^{III})	-0.46[b] (Ti^{III}/Ti^{II})	-1.33 ($Ti^{II}Pc^{-2}$/ $Ti^{II}Pc^{-3}$)	45
Ti(IV)TBTPc[a]			-0.09[b] (Ti^{IV}/Ti^{III})	-0.40[b] (Ti^{III}/Ti^{II})	-1.30 $Ti^{II}Pc^{-2}$/ $Ti^{II}Pc^{-3}$)	45
TiOPTPc[c]			-0.73 (Ti^{IV}/Ti^{III})	-1.09 (Ti^{III}/Ti^{II})		46
MnOPTPc[c]			-0.46 (Mn^{III}/Mn^{II})		-1.24 ($Mn^{II}Pc^{-2}$/ $Mn^{II}Pc^{-3}$)	46

[a]TiTPTPc = 1,(4)-(tetraphenylthiophthalocyaninato)titanium(IV) oxide, TiTBTPc =1,(4)-(tetrabenzylthiophthalocyaninato)titanium(IV) oxide.[b] in DMF containing $TBABF_4$. [c]Octapentylthiophthalocyaninato manganese(III) acetate (MnOPTPc) and octapentylthiophthalocyaninato titanium(IV) oxide (TiOPTPc).

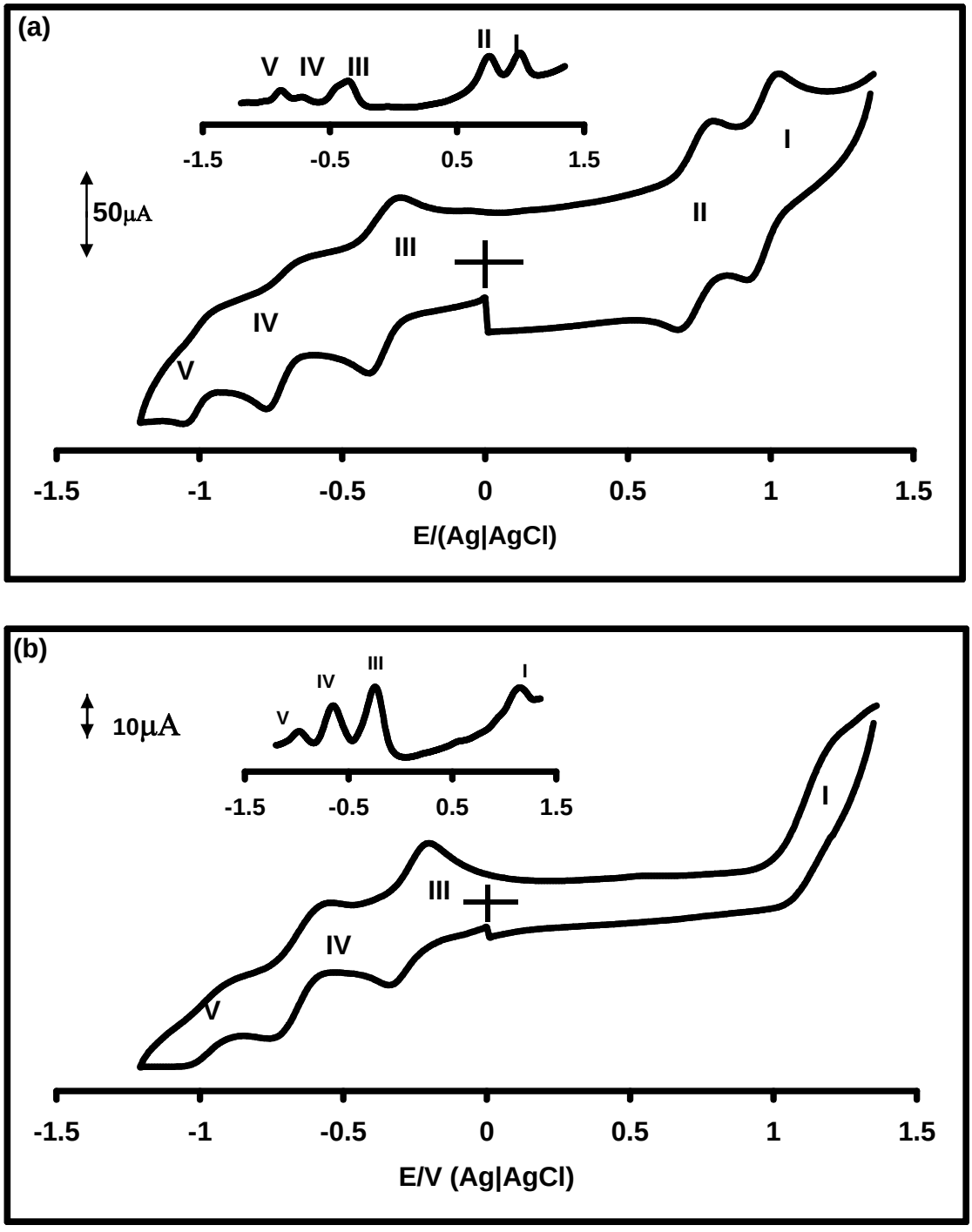

Figure 3.18: Cyclic (lower) and square wave (upper) voltammograms for (a) (38a), (b) (40) in chloroform containing $TBABF_4$. Scan rate = 100 mV/s.

Complex **(40)** is tetrasubstituted and contains isomers, whereas **(38a)**, is isomerically pure. Isomers could also play a role on the redox potentials of the complexes. For complex **(38a)** processes **I** to **III** were quasi-reversible with anodic to cathodic peak separation (ΔE) ranging from 100 to 130 mV. ΔE for ferrocene internal standard was 90 mV. For complex **(38a)**, processes **I** to **III,** cathodic to anodic peak currents were near unity, but for processes **IV** and **V**, the anodic currents were less intense compared to cathodic ones. For complex **(40)**, process **V** showed a weak return current, and processes **III** and **IV** gave the ratio of cathodic to anodic peak currents of close to unity. Two oxidation peaks were observed for **(38a)** and only one irreversible process was obtained for complex **(40)**. Ring oxidation of thiol substituted MPc complexes often results in decomposition [134, 135] hence the lack of reversibility of the oxidation processes in **(40),** is not surprising. Reduction in Sn(IV) porphyrins (which have a similar structure to phthalocyanines) resulted in only ring based processes and oxidation of Sn(II) porphyrins occurred at the central metal [134, 135]. Comparing the reduction couples for complexes **(38a)** and **(40)** with those reported [45, 46] for other MPc complexes non-peripherally tetra-or octa-substituted with alkylthio groups and containing electropositive metals such as Ti(IV) and Mn(III) shows that ring reduction occurs at high negative potentials (> -1.2 V vs Ag|AgCl) even considering differences in solvents in some cases. This observation suggests that the first two reductions with potentials < -1.0 V) in complexes **(38a)** and **(40)** may be metal-based. The assignment of the redox processes were confirmed by spectroelectrochemistry (OTTLE cell).

Spectral changes observed on oxidation of **(40)** at potentials of couple **I** are shown in **Figure 3.19a.** There is a shift in the Q band while decreasing in intensity. Only ring based processes are expected in Sn(IV)Pc complexes. The formation of ring oxidized products is characterized by a decrease in the Q band without any shifts and the formation of new broad bands in the 500 to 650 nm region [105]. This is not the case in **Figure 3.19a.** GePc, SiPc and SnPc complexes are known to readily undergo transformation to hydrolysed (Cl_2MPc going to $(OH)_2$MPc) species on photolysis [136] or in the presence of basic solvents [137] with spectral changes consisting of a shift of the Q band to shorter wavelengths. However chloroform is not a basic solvent, hence the changes shown in **Figure 3.19a** may be due to exchange of axial chlorines to the electrolyte ions. A shift of the Q band to the blue (**Figure 3.19b**) was also observed for a solution of **(40)** in chloroform containing $TBABF_4$, with time, without any electrochemical experiment. This shift is due to axial ligand exchange of the chlorides for the electrolyte ions, a typical behaviour for Sn(IV) porphyrins [138]. This suggests that the changes in **Figure 3.19a** are due to axial ligand exchange and not electrochemical oxidation. Addition of oxidizing agents to solutions of complex **(38a)** or **(40)**, resulted in spectral changes quite different to those shown in **Figure 3.19a**, and showed formation of ring-based oxidation.

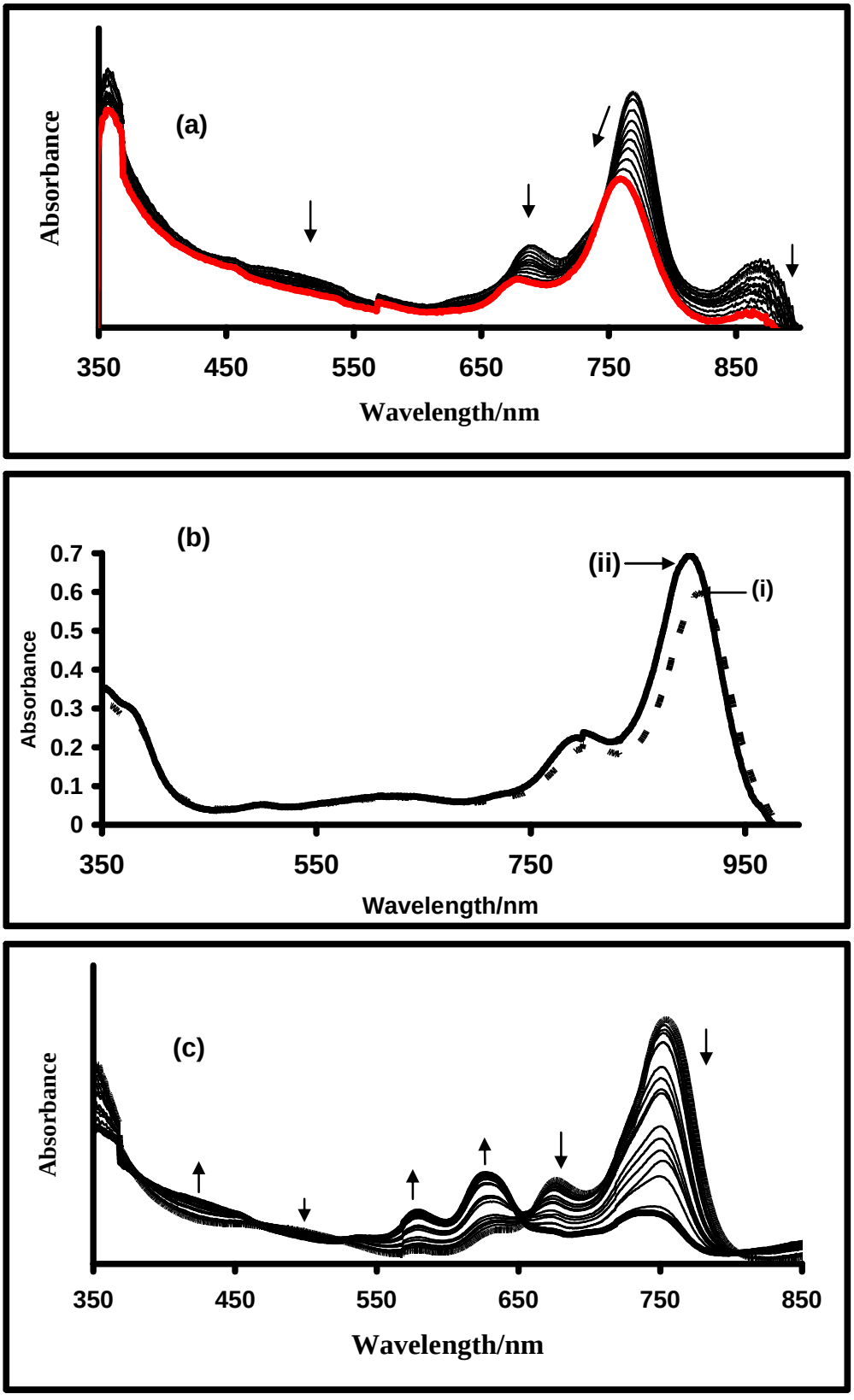
(a)
Absorbance
350
450
550
650
750
850
Wavelength/nm
(b)
(ii)
(i)
Absorbance
0.7
0.6
0.5
0.4
0.3
0.2
0.1
0
350
550
750
950
Wavelength/nm
(c)
Absorbance
350
450
550
650
750
850
Wavelength/nm

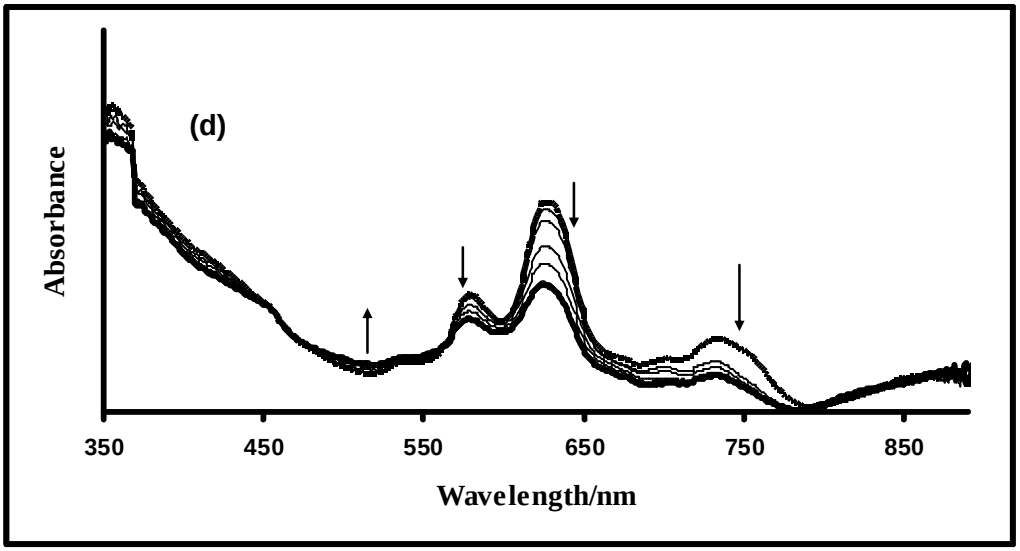

Figure 3.19: UV-visible spectral changes observed during (a) controlled potential oxidation of (40) at potentials of oxidation process I. (b) UV-Vis spectral changes observed with time for complex (40) in DCM containing $TBABF_4$ without doing cyclic voltammetry. UV-visible spectral changes observed during controlled potential reduction of (40) at potentials of (c) process III and (d) processes IV. The first scan in (d) is the same as the last scan in (c). Solvent = DCM containing $TBABF_4$.

Reduction may occur at the central metal or at the ring in Sn(IV)Pc complexes. Metal reduction in MPcs is characterized by shift in the Q band without change in intensity [105]. There was no evidence of metal reduction for both complexes **(38a)** and **(40)**, only a slight shift in the Q band to the blue, similar to that observed for axial ligation in **Figure 3.19b** on application of potential of process **III**. This was followed by clear spectroscopic changes which are typical [106] of ring reduction to Pc(-3) in MPc complexes, **Figure 3.19c**, consisting of a decrease in the Q band and the formation of new bands at 573 and 622 nm. Further application of more negative potential (for process **IV**) resulted in spectral changes shown in **Figure 3.19d**, which consists of a decrease of

the bands due to Pc(-3) and formation of a broad band near 500 nm due to further ring reduction and formation of a Pc(-4) species. Thus in a similar manner to Sn(IV) porphyrins [139], reduction for complex **(40)** occurs at the ring.

It has been reported before [23] that reduction of Cl_2M(IV)Pc (M = Si and Ge,) with sodium borohydride resulted in a species which did not retain a Pc moiety, and was identified as hydroxygermanium(IV) α,β,γ-triazabenzcorrole (M(OH)TBC), formed by Pc ring cleavage of the Cl_2MPc species. The formation of this species is characterized by a sharp absorption band in the 400 to 450 nm region [23]. This band is not observed in this work on electrochemical reduction.

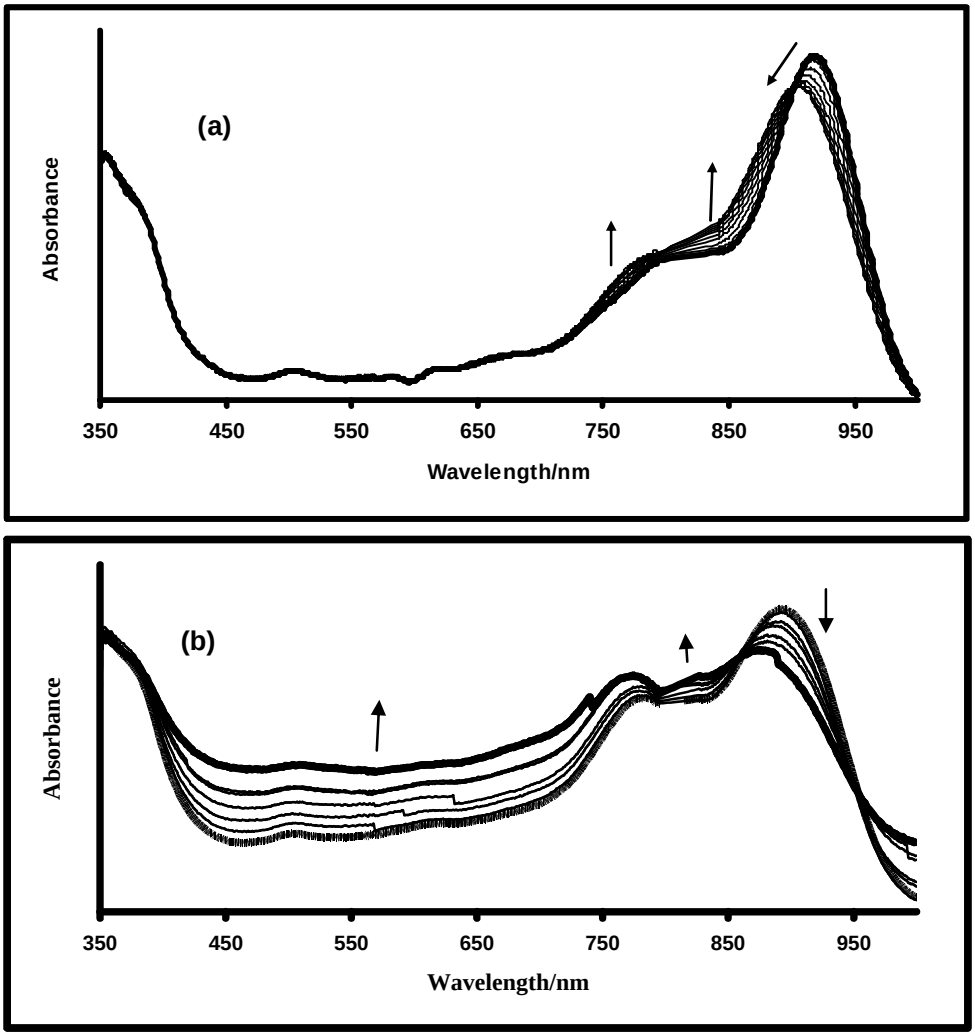

Figure 3.20: UV-visible spectral changes observed during controlled potential electrolysis of (38a) in an OTTLE cell: (a) oxidation at I and (b) reduction at II. Solvent = DCM containing $TBABF_4$.

Figure 3.20a shows spectral changes observed on oxidation of **(38a)** at potentials of process **I**. These changes are similar to those observed for **(40)** in that there is a Q band shift to the blue due to axial ligand exchange discussed above. Ring based reduction as

observed for **(40)**, accompanied by a shift in the Q band due to axial ligand exchange discussed above was observed, **Figure 3.20b**, on application of potential of process **II**.

3.3.3 Characterization of SAM on Au Surface by CV

A SAM modified gold electrode is known to limit or block solution molecules to have access to the gold surface. The blocking behavior occurs due to the hydrocarbon layer inserted between the electrode and electrolyte, thus forming an insulating layer. This insulating layer courses a lowering of charging current [140]. **Figure 3.21** shows cyclic voltammograms of unmodified Au and $Cl_2SnPc(SC_{12}H_{25})_8$ **(38a)**- Au electrode at different times of deposition in 1 mM $[Fe(CN)_6]^{3-}/[Fe(CN)_6]^{4-}$. Similar changes to those shown in **Figure 3.21** were also observed for **(40)**. The couple near 0 V is due to the $[Fe(CN)_6]^{3-}/[Fe(CN)_6]^{4-}$ and the one at 0.45 V due to complex **(38a)** as SAM. The latter peak is not observed on bare Au. From **Figure 3.21** it can be seen that with the increase in deposition time, the ΔE for the $[Fe(CN)_6]^{3-}/[Fe(CN)_6]^{4-}$couple increases and there is a shift of redox potential toward less positive potentials. The increase in ΔE as $Cl_2SnPc(SC_{12}H_{25})_8$ **(38a)** SAM forms proves blocking property for the electron transfer between the surface of electrode and the solution. Even after deposition time of 24 h there is still a prevalent oxidation and reduction peak observed, this means that the SAM that is formed does not fully block electron transfer between the solution and the surface of the electrode, unlike when thiol derivatized porphyrins were employed [141]. It is also important to note that the $[Fe(CN)_6]^{3-}/[Fe(CN)_6]^{4-}$ system is a fast electron transfer process and mass transport determines the rate determining step even at small overpotentials, hence the couples may be observed even on modified electrodes.

It has been reported before [42] that the $[Fe(CN)_6]^{3-}/[Fe(CN)_6]^{4-}$ couple showed a decrease in current and became highly irreversible after 18h of SAM formation time for $CoPc(SC_{12}H_{25})_8$, however in this work the decrease in current was not observed even after 29 hs, **Figure 3.21**. The increase in current observed has been noticed in literature [142] and this behavior was attributed to the conducting film being formed on the surface of the electrode. Thus the observed increase in current and shift of the potential in **Figure 3.21,** to less negative value, suggest the catalytic nature of the SAMs.

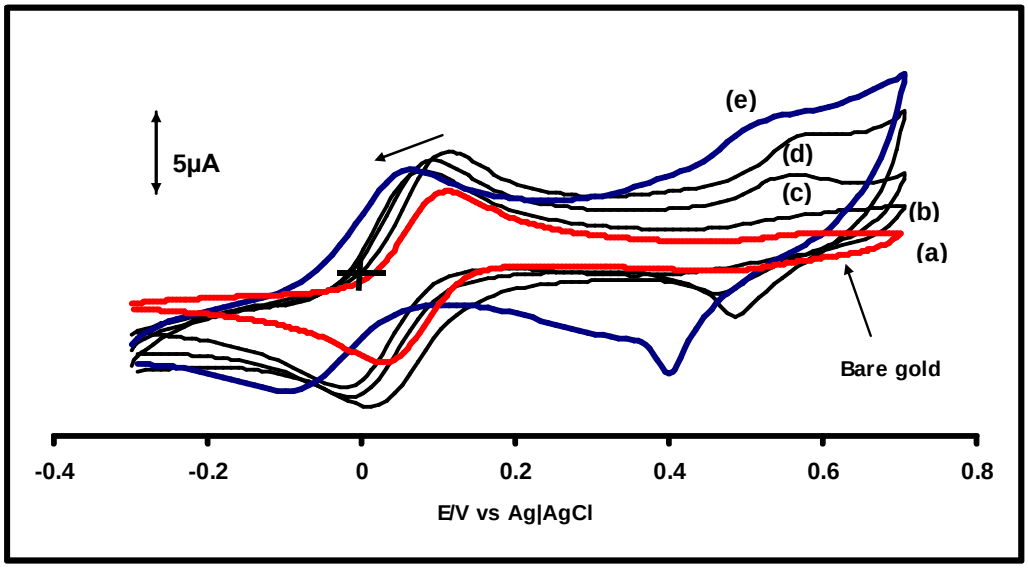

Figure 3.21: Cyclic voltammogram for SAM of (38a) in 1mM $[Fe(CN)_6]^{3-}/[Fe(CN)_6]^{4-}$ in 0.1 M KCl at 100 mV/s at different deposition times. (a) bare Au, (b) 30s, (c) 16.5min, (d) 12h and (h) 29h.

3.3.4 Characterization of SAMs on Au Surface by EIS (Electrochemical impedance spectroscopy)

The redox probing species $[Fe(CN)_6]^{3-}/[Fe(CN)_6]^{4-}$ is known to react at the pinholes or defects [140] within the SAM. In this work electrochemical impedance spectroscopy

(EIS) was used to monitor the effects of varying time of deposition on a gold electrode by immersing the electrode in a solution of $Cl_2SnPc(SC_{12}H_{25})_8$ **(38a)** or $Cl_2SnPc(SC_{12}H_{25})_4$ **(40). Figure 3.22** shows the Nyquist plots of SAM-modified gold electrode obtained by keeping the Au electrode in $Cl_2SnPc(SC_{12}H_{25})_8$ **(38a)** solutions for different deposition times, 30s, 16.5min, 12h, and 29h, 1mM $[Fe(CN)_6]^{3-}/[Fe(CN)_6]^{4-}$, **Figure 3.22**.

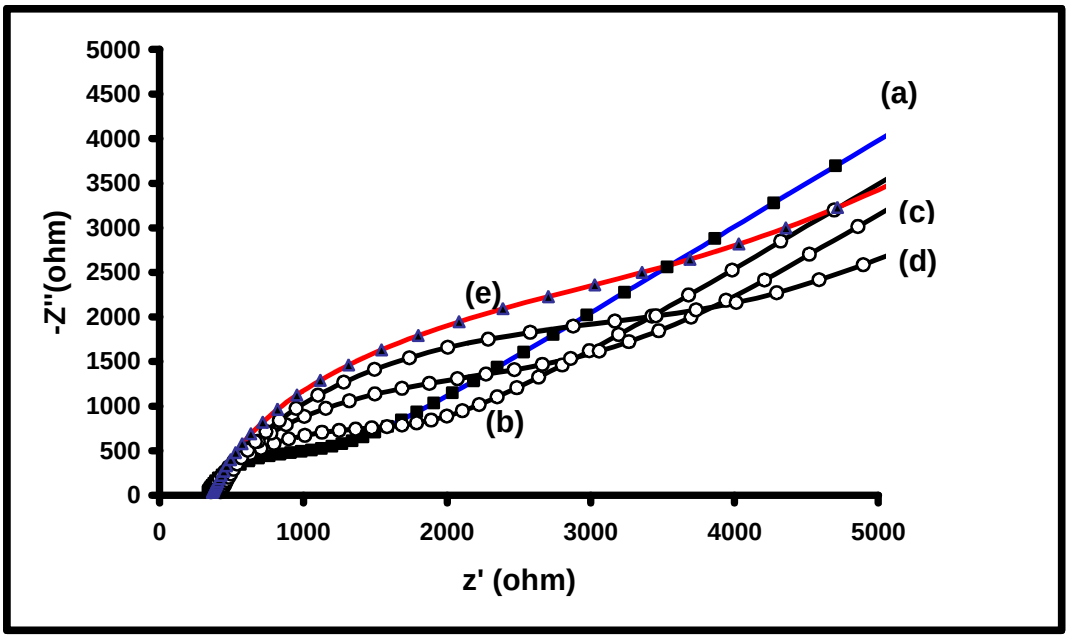

Figure 3.22: Impedance plots of the SAM of (38a) in 1 mM $[Fe(CN)_6]^{3-}/[Fe(CN)_6]^{4-}$ in 0.1 M KCl as a supporting electrolyte at different deposition times. (a) bare Au, (b) 30s, (c) 16.5min, (d) 12h and (h) 29h.

Similar plots were obtained for complex **(40)**. From the plots we see that the longer the deposition time the larger the semicircle, this indicates the surface coverage increases and hence a slower charge transfer is obtained. **Figure 3.23** (Bode plot of phase angle versus $\log f$) shows that as deposition time increases there is a shift in frequency of the peak towards lower frequencies, this confirms that $[Fe(CN)_6]^{3-}/[Fe(CN)_6]^{4-}$ redox process takes

place at the modifying film rather than directly on the bare gold. The phase angle remains less than 90° for different deposition times but increases from 31.7° (unmodified Au at $\log f = 2.67$) towards 49.6° (SAM at $\log f = 1.96$). A phase angle greater or equal to 90° means that the SAM behaves like an ideal capacitor (no current leakage at the defect sites and the SAM forms an insulating film) [143]. Whereas, a phase angle less than 90°, the SAM is viewed as a contaminated capacitor meaning the SAM is permeable to solution ions. In the present case $Cl_2SnPc(SC_{12}H_{25})_8$ **(38a)** SAM and $Cl_2SnPc(SC_{12}H_{25})_4$ **(40)** SAM are permeable to solution ions.

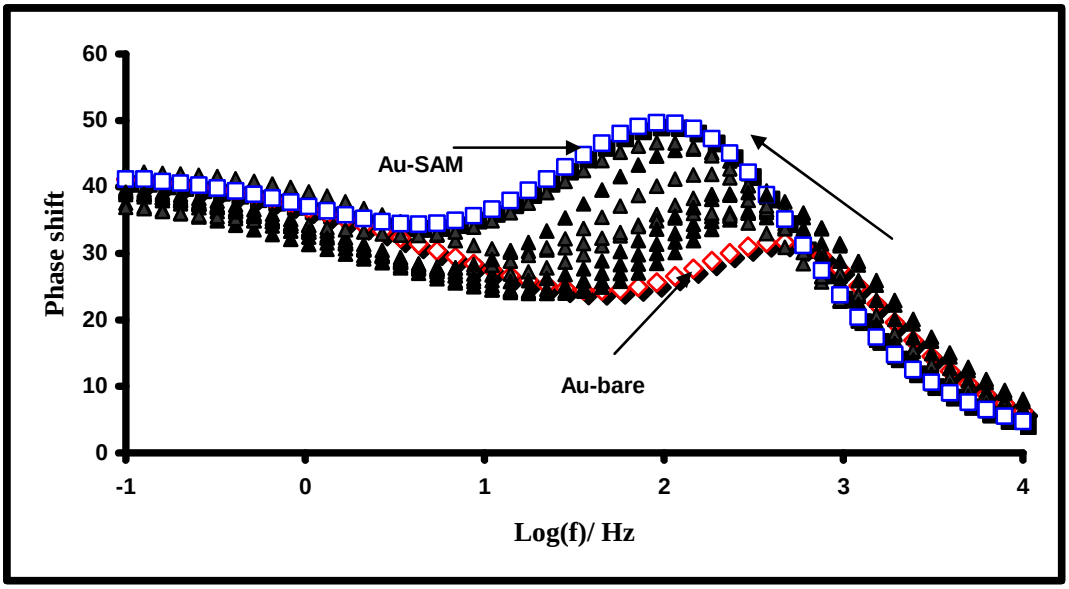

Figure 3.23: Blode plot for (38a) (phase angle versus log f) in 1 mM $[Fe(CN)_6]^{3-}$ /$[Fe(CN)_6]^{4-}$ in 0.1 M KCl as a supporting electrolyte at different deposition times. From bare (red squares) and increasing to 29 hours at times: 30s, 6.5min, 16.5min, 4h, 12h, 19h and 29h (blue squares).

From the data obtained from Nyquist plots, the values of R_{ct} could be calculated (where R_{ct} is the charge transfer resistance). **Tables 3.10 and 3.11** show measured parameters of unmodified Au and $Cl_2SnPc(SC_{12}H_{25})_4$ **(40)** and $Cl_2SnPc(SC_{12}H_{25})_8$ **(38a)** SAM-modified

electrodes obtained from the impedance plots. The value for R_{ct} for $Cl_2SnPc(SC_{12}H_{25})_8$ **(38a)** and $Cl_2SnPc(SC_{12}H_{25})_4$ **(40)-** modified electrodes increased with increasing deposition time, this is expected since there is an inhibition of electron transfer rate due to the presence of a monolayer on the electrode surface.

Table 3.10: Summary of estimated EIS parameters obtained for $Fe(CN)_6]^{3-}$ /$[Fe(CN)_6]^{4-}$ at the potential of 0.13V (Ag|AgCl) using the SAM of for complex (38a).

SAM formation time	R_{ct} **/Ω**	θ	C_d **/F.cm^{-2}**	n	k_{app} **/cm/s**
Bare Au	1210	0	2.43x10^{-6}	0.84	4.41x10^{-4}
30s	1860	0.35	2.18x10^{-6}	0.83	2.86x10^{-4}
6.5min	2840	0.58	4.24x10^{-6}	0.83	1.87x10^{-4}
16.5min	3240	0.63	5.03x10^{-6}	0.83	1.64x10^{-4}
4h	4070	0.70	5.64x10^{-6}	0.76	1.31x10^{-4}
12h	5740	0.79	4.57x10^{-6}	0.72	9.27x10^{-5}
19h	6530	0.82	6.47x10^{-6}	0.79	8.15x10^{-5}
29h	6790	0.83	5.25x10^{-6}	0.76	7.84x10^{-5}

Table 3.11: Summary of estimated EIS parameters obtained for $Fe(CN)_6]^{3-}$ /$[Fe(CN)_6]^{4-}$ at the potential of 0.13V (Ag|AgCl) using the SAM of for complex (40).

time	R_{ct} **/Ω**	θ	C_d **/F.cm^{-2})**	n	k_{app} **/cm/s)**
Bare Au	858	0	2.32x10^{-6}	0.85	3.10x10^{-4}
30s	1240	0.31	2.24x10^{-6}	0.86	2.15x10^{-4}
5min	1280	0.33	2.78x10^{-6}	0.83	2.08x10^{-4}
10min	1820	0.53	2.78x10^{-6}	0.83	1.47x10^{-4}
30min	1830	0.53	2.53x10^{-6}	0.84	1.45x10^{-4}
1h	2350	0.64	2.97x10^{-6}	0.82	1.13x10^{-4}
2h	3040	0.72	4.55x10^{-6}	0.77	8.75x10^{-5}
20h	3100	0.72	4.84x10^{-6}	0.76	8.57x10^{-5}

From R_{ct} values surface coverage (θ) of the monolayer was calculated using **Equation 3.9** (same as **Equation 1.37)**:

$$\theta = 1 - R_0/R_{ct} \quad (3.9)$$

R_0 is the charge transfer resistance for an unmodified Au electrode. **Equation 3.9** assumes that the current is due to the presence of defects within the monolayer [116]. **Equation 3.9** should not be employed when θ is close to 1 (θ > 0.9) [117, 143]. The θ values are presented on **Tables 3.10 and 3.11**. A maximum value of θ for **(38a)** is found to be 0.83 after 29 h and for **(40)** is found to be 0.72 after 20 h. These values are thus far from 1 and hence the use of **Equation 3.9** is justified. These results suggest that the larger the number of alkylthio substituents attached to the Pc ring (in **38a**), the longer it takes for the surface to reach maximum surface coverage. The low surface coverage (much less than 1) obtained suggests that the monolayer is more porous especially for an electrode modified with **(40)**, which is tetra substituted. **Figure 3.24** shows the time dependence of the surface coverage (θ) for complex **(38a)**. Fast adsorption occurs at times less than 20 min.

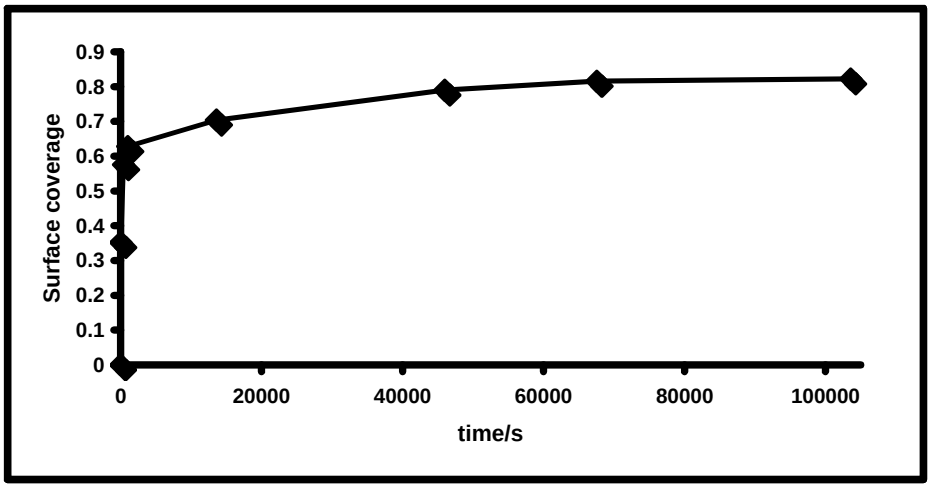

Figure 3.24: Plot of surface coverage (θ) versus time of SAM deposition time (s) for (39a).

The fraction of pinhole area (1 - θ) can be related to the size of pinholes (r_a) and distance between pinholes (r_b) by **Equation 3.11** (same as **Equation 1.38**):

$$1-\theta = (r_a^2 / r_b^2) \qquad (3.10)$$

From the plots of Z' vs $\omega^{-1/2}$ in the low frequency region (**Figure 3.25**) value of r_a and r_b were obtained as explained in the introduction **Equation 1.39 – 1.41**. The pinhole radius of the SAMs for complex **(38a)** was found to be 4.7 μm while the centres of two adjacent pinholes were found to be 11.1 μm, for SAM formed for 29 h, **Table 3.12**. For complex **(40)** the radius of the SAM was found to be 3.6 μm and the adjacent pinholes were found to be 6.3 μm for 20 h SAMs. These sizes fall within range for reported 3-mercaptopropionic acid SAM [144].

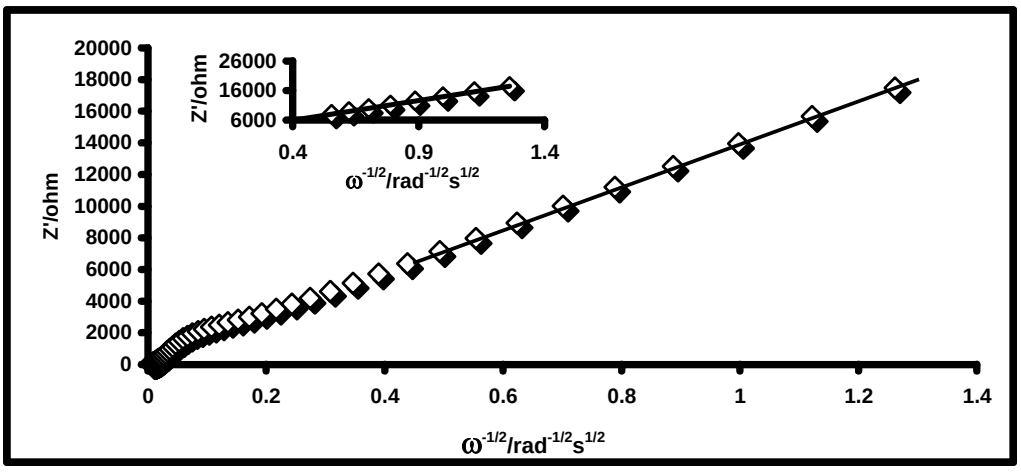

Figure 3.25: Z' vs $\omega^{-1/2}$/rad$^{-1/2}$s$^{1/2}$ obtained for the SAM of (41) in 1 mM $[Fe(CN)_6]^{3-}$ /$[Fe(CN)_6]^{4-}$ in 0.1M. KCl as a supporting electrolyte. Inset: the linear part of the plot.

Table 3.12: Surface coverage and adsorption kinetics for complexes (39a) and (41).

Complex	Γ/ 10^{10} mol. cm^{-2}	- ΔG_{ads} (kJ/mol)	K (mol/L)	δ	θ (at max time)	r_a/μm	r_b/μm
38a	1.4	-30.65	2.35 X 10^5	2.28	0.82	4.7	11.1
40	0.7	-11.52	104.7	2.12	0.72	3.6	6.3

The surface coverage (Γ) for saturated **(38a)** and **(40)** SAMs were estimated using the charge under the peak at 0.4 V in **Figure 3.26**. **Equation 3.12** was used to determine the surface coverage, $\Gamma(mol/cm^2)$.

$$Q = nFA\Gamma \qquad (3.11)$$

where Q is the total charge (C), A is the electrode surface area (cm^2), n is the number electrons and F is Faraday's constant.

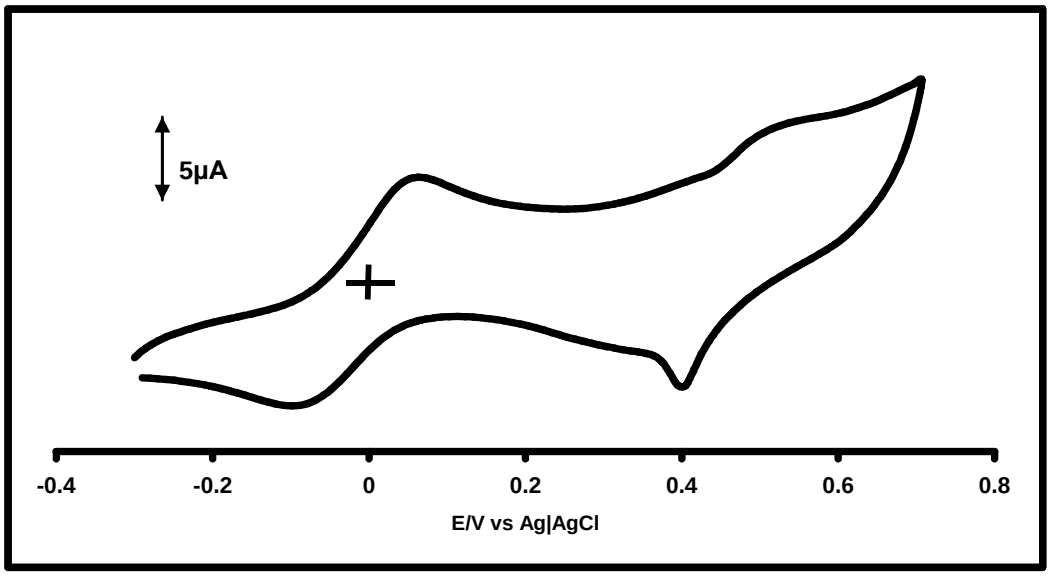

Figure 3.26: Cyclic voltammogram for SAM of (38a) in 1mM $[Fe(CN)_6]^{3-}/[Fe(CN)_6]^{4-}$ in 0.1 M KCl at 100 mV/s.

The values Γ for **(38a)** and **(40)** are 1.4 x 10^{-10} mol cm^{-2} and 0.7 x 10^{-10} mol cm^{-2}, **Table 3.12**, are in range for surface coverage of 1 x 10^{-10} mol cm^{-2} for a Pc molecule lying flat on the surface [145].

The electrochemical capacitance is a useful tool to probe the packing structure of the monolayer on the electrode. Evaluation of the capacitance of the surface was done by fitting the impedance data to an equivalent RC circuit using GPES software version 4.9, Eco Chemie, where R represents the solution resistance in series with total interfacial capacitance. The double layer capacitance (C_d) is evaluated by employing a constant phase element (CPE) using **Equation 3.12** [146]:

$$C_d = \sqrt[n]{\frac{T}{R_E^{(n-1)}}} \qquad (3.12)$$

The parameter, n, ($0 \leq n \leq 1$), is depended on the electrode material, its surface preparation and whether or not adsorbable anions are present in the electrolyte, T is a double layer capacitance quantity; C_d is a double layer capacitance and R_E is an equivalent series resistance. CPE is complex impedance having the special property that its phase angle is independent of frequency. This capacitance dispersion at a solid electrode is known to depend strongly on the state of the electrode surface. The n values were computed with the software in Autolab potentiostat PGSTAT 30. **Tables 3.10 and 3.11** show that the n values of both **(38a)** and **(40)** range between 0.72 and 0.86, these values being less than 1 suggest that the modified electrode is not a true capacitor. **Figure**

3.27 and **Tables 3.10 and 3.11** show the variation of C_d with the formation of SAMs of **(38a)** and **(40)**. As the SAM formation times increased there was an increase in the C_d values for **(38a)** until after 12 hs, thereafter there is some stabilization, **Figure 3.27.**

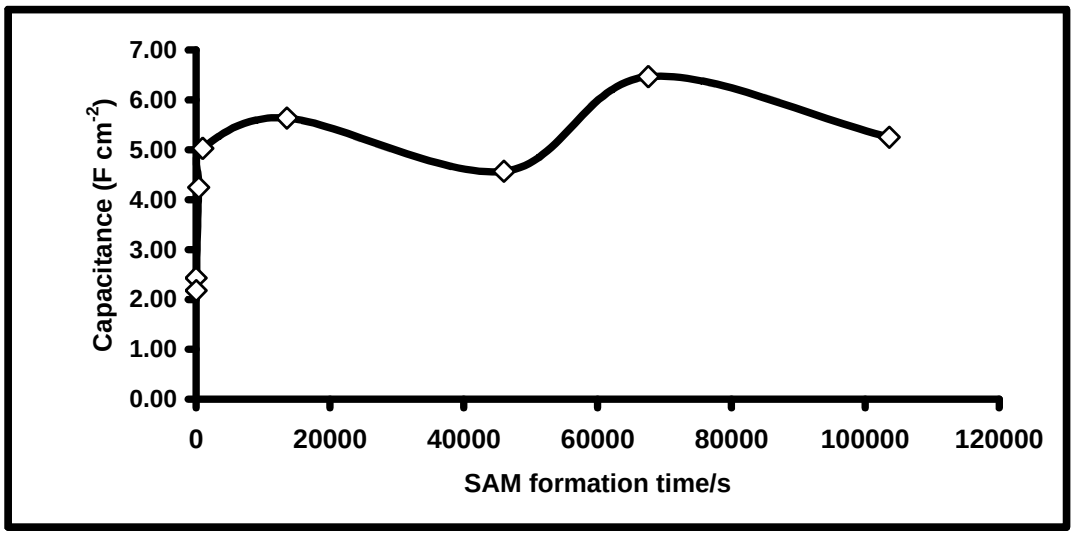

Figure 3.27: The plot of C_d versus SAM formation time.

The apparent electron-transfer rate constant k_{app} was obtained from the conventional **Equation 3.13**, [147]:

$$k_{app} = \frac{RT}{F^2 R_{ct} c} \qquad (3.13)$$

where c is a concentration of the $[Fe(CN)_6]^{3-}$, R, T and F have their usual meanings. The electron-transfer rate decreases as the amount of MPc on the surface increases, **Tables 3.10 and 3.11**. The k_{app} values observed for **(40)** are lower compared to **(38a)** (considering the same deposition times e.g. 30 sec.)

Frumkin adsorption equilibrium model was used to study the interaction property of alkyl chains of the adsorbed **(38a)** and **(40)** complexes on Au electrode. Frumkin equilibrium equation is described by **Equations 3.14 and 3.15** [141]:

$$K = [\theta / c(1-\theta)]\exp(-2\delta\theta) \quad (3.14)$$

or

$$\ln[\theta / c(1-\theta)] = \ln K + 2\delta\theta \quad (3.15)$$

where δ is the interaction parameter between the adsorbed molecules, θ is surface coverage obtained from **Equation 3.9**, K is the adsorption equilibrium constant, c is the concentration of adsorbed molecules. If $\delta < 0$, there is an attraction between the adsorbed molecules and if $\delta > 0$ there is repulsion between the adsorbed molecules [141]. **Figure 3.28** shows a plot of $\ln[\theta / c(1-\theta)]$ versus θ for **(38a)**, and gives interaction parameter $\delta = 2.28$ and $K = 2.35 \times 10^5 mol / L$, **Table 3.12.** A similar plot for **(40)** was obtained, giving $\delta = 2.12$ and $K = 104.72 mol / L$, **Table 3.12.**

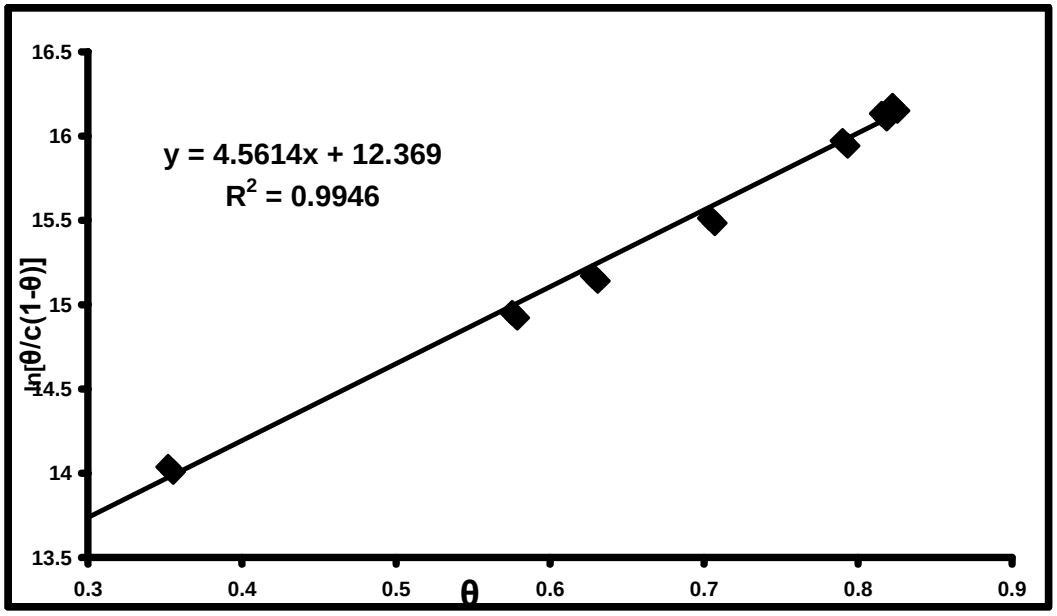

Figure 3.28: Relationship between $\ln[\theta / c(1-\theta)]$ **and** θ **for the SAM of (38a).**

It is expected that the K value for $Cl_2SnPc(SC_{12}H_{25})_8$ **(38a)** should be higher than $Cl_2SnPc(SC_{12}H_{25})_4$ **(40)** values due to the number of sulfur atoms adsorbing on the Au surface, and this is observed. Gibbs free energy (ΔG_{ads} = - RTlnK) values for **(38a)** and **(40)** were obtained as $-30.65 KJ/mol$ and $-11.52 KJ/mol$ respectively, **Table 3.12**. These values suggest that the more sulfur atoms adsorbed to the surface the greater the Gibbs free energy. This interaction shows that there is a repulsion between the adsorbed molecules, because of the δ value which is greater than 0.

CHAPTER FOUR: CONCLUSIONS

General conclusion

This work reports on the synthesis, electrochemical and photophysical properties of complexes **(35a)** to **(35c)**. Complex **(35b)** containing a C-H atom in place of one of the phthalocyanine aza nitrogen atoms shows a split Q-band attributable to the lower symmetry of the system compared to the corresponding phthalocyanines. The fluorescence quantum yields of the complexes are within the usual range for MPc complexes, while the triplet state quantum yields were found to be lower than would be expected on the basis of the heavy atom effect expected with Sn as the central metal for the Pc complexes (**35a** and **35c**). Complex **(35b)** however gave a high triplet state quantum yield, suggesting that this complex could prove to be a useful candidate for PDT applications. The triplet state lifetimes were solvent dependent, and were higher for solutions of the compounds in THF than in toluene. Cyclic voltammetry and spectroelectrochemistry of the complexes revealed only ring based processes which are mainly irreversible.

This work also reports on the synthesis of SnTSPc **(41)** using microwave irradiation. The formation of MPc complexes via microwave synthesis is simple and fast. However, depending on the ratio of the reagents, SnTSTBC **(42)** instead of SnTSPc **(41)** was formed. SnTSTBC **(42)** was formed at low ratios (< 1:8) of 4-sulfophthalic acid to urea. The observed formation of SnTSTBC **(42)** at lower ratios suggests that this complex is an intermediate towards the formation of SnTSPc **(41).** The SnTSTBC **(42)** complex has lower triplet lifetime and triplet yields, and lower binding and bimolecular quenching constants (with BSA), compared to SnTSPc **(41).** The photophysical parameters for

SnTSTBC **(42)** are still high enough for this molecule to be useful in photosensitization and photocatalysis.

The adsorption kinetics for the formation of self-assembled monolayer of **(38a)** and **(40)** on Au electrode by using cyclic voltammetry (CV) and electrochemical impedance spectroscopy (IES), were studied. Frumkin adsorption equilibrium model was used to evaluate the interaction parameters and Gibbs free energy and equilibrium rate constant for the adsorption of **(38a)** and (**40)** on Au electrode, and showed that equilibrium rate constant for complex **(38a)** was higher compared to complex **(40)** due to the adsorption of eight sulfur atoms on the Au surface.

References:

1. K. T. Ranjit and I. Willner, J. Phys. Chem. B, **102**, 1998, 9397.
2. A. P. Castano, T. N. Demidova, M. R. Hamblin, Photodiagnosis and Photodynamic Therapy, **1**, 2004, 279.
3. C. J. Walsh and B. K. Mandal, J. Mater. **12**, 2000, 287.
4. S. Vilakazi, T. Nyokong, Polyhedron, **19**, 2000, 229.
5. A. Sasaki, A. Kurahashi, Takagi, T. Conf. Rec. IEEE Conf. Display Devices, 1972, 161.
6. H. Eichhorn, J. Porphy. Phthalocya. **4**, 2000, 88.
7. R. P. Linstead, J. Chem. Soc. 1934, 1016.
8. A. G. Dandridge, H. A. E. Drescher, J. Thomas, British Patent, **322**, 1929, 169, (Scottish Dyes, Ltd).
9. A. von Braun, J. Tschemiac, Ber. **40,** 1907, 2709.
10. C. M. Allen, W. M. Sharman and J. E. Van Lier, J. Porphy. Phthalocya. **5**, 2001, 161.
11. H. de Diesbach, E. von der Weid, Hely. Chim. Acta. **10**, 1927, 886.
12. R. P. Linstead, A. R. Lowe, J. Chem. Soc. 1934, 1031.
13. J. M. Robertson, J. Chem. Soc. 1935, 615.
14. Moss, G. P. Pure and Appl. Chem. **59**, 1987, 779.
15. R. Bonnett, Chemical Aspects of Photodynamic therapy, 2000, Gordon and Breach Science Publishers, UK.

16. M. J Cook, A. N. Dunn, S. D. Howe, A. J. Thompson, K. J. Harrison, J. Chem. Soc. Perkin Trans. I, 1988, 2453.

17. M. Kasha, H. R. Rawls, M.A. El-Bayoumi, Pure Appl. Chem. **11**,1965, 371.

18. N. S. Hush and I.S. Woolsey, Mol. Phys. **21**, 1971, 465.

19. A. R. Monahan, D. F. Blossey, J. P. Chem. **74**, 1970, 4014.

20. P. A. Barrett, R. P. Linstead, G. A. P. Tuey, J. M. Robertson, J. Chem. Soc. 1939, 1809.

21. C. C. Leznoff and N. B. McKeown, J. Org. Chem. **55**, 1990, 2186.

22. A. N. Cammidge, M. J. Cook, D. L. Hughes, F. Nekelson and M. Rahman, Chem. Commun. 2005, 930.

23. M. Fujiki, H. Tabei, K. Isa, J. Am. Chem. Soc. **108**, 1986, 1532.

24. J. Liu, F. Zhang, F. Zhao, Y. Tang, X. Song, G. Yao, J. Photochem. Photobiol. A. **91**, 1995, 99.

25. Z. Song, F. Zhang, X. Li, C. Shek-kiu, F. Zhao, Y. Tang, J. Porphy. Phthalocya. **6**, 2002, 484.

26. J. Li, L. R. Subramanian, M. Hanack, J. Porphy. Phthalocya. **4**, 2000, 739.

27. J. Mack, N. Kobayashi, C. C. Leznoff, M. J. Stillman, Inorg. Chem. **36**, 1997, 5624.

28. J. Li, L. R. Subramanian, M. Hanack, Eur. J. Org. Chem. 1998, 2759.

29. N.A. Kuznetsova, N.S. Gretsova, V.M. Derkacheva, O.L. Kaliya, E.A. Luk'yanets, J. Phorphy. Phthalocya. **7,** 2003,147.

30. J. Li, L. R. Subramanian, M. J. Hanack. Chem. Soc. Chem. Comm. 1997, 679.

31. Y. Murakami, Y. Aoyama, K. Tokunaga, J. Am. Chem. Soc. **102**,1980,6736.

32. A. W. Snow, J. R. Griffith, N. P. Marullo, Macromol. **17**,1984, 1614.

33. V. Csokai, G. Parlagh, A. Grofcsik, M. Kubonyi, I. Bitter, Synth. Commun, **33**, 2003, 1615.

34. N. Safari, P. R. Jamaat, M. Pirouzmand, A. Shaabani, J. Porphy. Phthalocya., **8**, 2004, 1209.

35. A. Shaabani, A. Maleki, J. Porphy. Phthalocya. **10**, 2006, 1253.

36. F. Bahadoran, S. Dialameh, J. Porphy. Phthalocya. **9**, 2005, 163.

37. S. E. Maree, J. Porphy. Phthalocya. **9**, 2005, 880.

38. D. Wohrle, M. Eskes, K. Shingehara, A. Yamada, Synthesis, 1993, 194.

39. K. Ozoemena, P. Westbroek, T. Nyokong, J. Porphy. Phthalocya. **6,** 2002, 98.

40. K. Ozoemena, T. Nyokong, Electrochim. Acta. **47**, 2002, 4035.

41. K. Ozoemena, T. Nyokong, Electroanalysis, **15**, 2003, 1762.

42. B. Agboola, P. Westbroek, K. I. Ozoemena, T. Nyokong, Electrochem. Commun. **9**, 2007, 310.

43. K. Takahashi, M. Kawashima, Y. Tomita, M. Itoh, Inorganica Chimica. Acta. **232**, 1995, 69.

44. P. M. Burnham, M. J. Cook, L. A. Gerrard, M. J. Heeney, D. L. Hughes, Chem. Commun., 2003, 2064.

45. P. Tau, T. Nyokong, Dalton Trans. 2006, 4482.

46. G. Mbambisa, P. Tau, E. Antunes, T. Nyokong, Polyhedron, **26**, 2007, 5355.

47. M. J. Cook, N. B. McKeown, I. Chambrier, J. Chem. Soc. Perkin Trans. I, 1990, 1169.

48. M. J. Cook, I. Chambrier, S. J. Cracknell, D. A. Mayes, D. A. Russell, Photochem. Photobiol. **62**, 1995, 542.

49. F. Nekelson, Novel oligomeric pthalocyanines and new synthesis of tetrabenzotriazaporphyrin, University of East Anglia, 2005, thesis

50. P. M. Burnham, M. J. Cook, L. A. Gerrard, M. J. Heeney and D. L. Hughes Chem. Comm. 2003, 2064.

51. A. Suzuki, Synth. Commun. **11**, 1981, 513.

52. E. I. Negishi, A. O. King, N. Okukado, J. Org. Chem. **42**, 1977, 1821.

53. P. Knochel, R. D. Singer, Chem. Rev. **93**, 1993, 2117.

54. P. Knochel, J. J. A. Perea, P. Jones, Tetrahedron, **54**, 1998, 8275.

55. C. A. Ouesnell, O. B. Familonio, V. Snieckus, Syn. Lett. 1994, 349.

56. K. Tamao, Y. Kiso, M. Zembayashi, A. Fujioka, S. Kodama, I. Nakajima, A. Minato, M. Kumada, Bull. Chem. Soc. Jp. **49**, 1976, 1958.

57. C. A. Quesnell, O. B. Familonio, V. Snieckus, Synlett. 1994, 349.

58. B. H. Lipshutz, P. A. Blomgren, S. K. Kim, Tetrahedron Lett. **40**, 1999, 197.

59. M. Fujita, H. Oka, K. Ogura, Tetrahedron lett. **36**, 1995, 5247.

60. W. J. Scott, J. K. Stille, J. Am. Chem. Soc. **108**, 1986, 3033.

61. W. J. Scott, J. E. McMurry, Acc. Chem. Res. **21**, 1988, 47.

62. A. Ogunsipe, T. Nyokong, J. Photochem. Photobiol. A: Chem. **173**, 2005, 211.

63. S.B. Kahl, J. Li, Inorg. Chem. **35**, 1996.

64. W.M. Sharman, S.V. Kudrevich, J.E. van Lier, Tetrahedron Lett. **37**, 1996, 5831.

65. M.P. de Filippis, D. Dei, L. Fantetti, G. Roncucci, Tetrahedron Lett. **41**, 2000, 9143.

66. Y. J. Zhu, J.D. Huang, X.J. Jiang, J.C. Sun, Inorg. Chem. Commun. **9**, 2006, 473.

67. Q. Peng, J. Br. Moan,. J. Cancer, **72**, 1995.

68. J. H. Weber, D. H. Busch. Inorg. Chem. **4,** 1965, 469.

69. M. Ambroz, A. Beeby, A. J. McRobert, M. S. C. Simpson, R. K. Svensen, D. Phillips, J. Photochem. Photobiol B: Biol. **9,** 1991, 87.

70. R. P. Linstead , F. T. Weiss, J. Chem. Soc. **1950**, 2975.

71. H. Ali, R. Langlois, J.R. Wagner, N. Brasseur, B. Paquette, J.E. van Lier, Photochem. Photobiol. **45**, 1987, 713.

72. A. Ogusipe, T. Nyokong, J. Porphy. Phthalocya. **9**, 2005, 121.

73. A. R. Monaham, J. A. Brado, A. F. de-luca, J. Phys. Chem. **76,** 1972, 446.

74. M. O. Liu, C.-H. Tai, M.-Z. Sain, A. T. Hu, F. Chou. J. Photochem. Photobiol. A: Chem. **164,** 2004, 131.

75. J. Moan, K. Berg, J. C. Bommer, A. Western, Photochem. Photobiol. **56**, 1992, 171.

76. R. Edrei, V. Gottfried, J. E. van Lier, S. Kimel, J. Porphy. Phthalocya. **2**, 1998, 191.

77. H. L. Van Leegoed, N. van der Veen, A. A. Versteeg, R. Ouellet, J. E. van Lier, W. M. Star, Photochem. Photobiol. **58**, 1993, 575.

78. S. M. Bishop, B. J. Knoo, A. J. MacRobert, M. S. C. Simpson, D. Philips, A. Beeby, J. Chromatrogr. **646**, 1993, 345.

79. M. O. Liu, C.-h. Tai, M.-z. Slain, A. T. Hu, F.-in. Chou, J. Photochem. Photobiol. A. Chemistry, **165**, 2004, 131.

80. S. M. T. Nunes, F. S.Squilla, A. C. Tedesco. Braz. J. Med. Biol. Res. **37**, 2004, 273.

81. R.A. Mayers, Encyclopedia of analytical chemistry: Applications, Theory. and instrumentation 2000, **Vol. 12**, John Wiley & Sons Ltd, UK.

82. S. Dhami, A. J. de Mello, G. Rumbles, S. M. Bishop, D. Philips, A. Beeby, Photochem. Photobiol. **61**, 1995, 341.

83. A. Gillbert, J. Baggot, Essential of molecular photochemistry, Blackwell Scientific Publications, Oxford, 1991, 98.

84. M. A. M. J. van Zandvoort, D. Wrobel, P. Letting, G.van Ginkel, Y. K. Levine, Photochem. Photobiol. **62**, 1995, 279.

85. S. J. Strickler, and R. A. Berg, J. Chem. Phys. **37**, 1962, 814.

86. H. Du, R.-C. Fuh, J. Li, L. A. Corkan, J. S. Lindsey, Photochem. Photobiol. **68**, 1998, 141.

87. S. Maree, D. Phillips, T. Nyokong, J. Porphy. Phthalocya. **6**, 2002, 17.

88. J. R. Lakowikz, Principles of Fluorescence Spectroscopy, Kluwer Academic/Plenum Publishers, New York, 1999.

89. A. Ogunsipe, T. Nyokong, J. Photochem. Photobiol. Sci. **4**, 2005, 510.

90. D. C. Carter, J. X. Ho, Adv. Protein Chem. **45**, 1994.

91. A. K. Bordbar, A. Eslami, S. Tangestaninejad, J. Porphy. Phthalocya. **6**, 2002, 225.

92. A. K. Bordbar, S. Tangestaninejad, A. Eslami, J. Biochem., Mol. Biol. Biophys. **5**, 2001, 143.

93. D. Silva, C. M. Cortez and S. R. Louro, Braz. J. Med. Bio. Res. **37**, 2004, 963.

94. G. M. Tabak, Spectrochimica Acta. **56**, 2000, 2255.

95. S. Sil, M. Kar, A. S. Chakaraborti, J. Photochem. Photobiol, B: Biol. **41**, 1997, 67.

96. R. V. Bensasson, C. R. Goldsmith, E. J. Land, T. G. Truscott, Photochem. Photobiol. **28**, 1978, 277.

97. R. A. Keller, S. G. Hadley, J. Chem. Phys. **42**, 1965, 2382.

98. D. B. Hibbert, Introduction to electrochemistry, Macmillan, London, 1993

99. J. E. B. Randles, Trans. Faraday Soc. **44,** 1948, 327.

100. C.D.E. Chidsey, D. N. Loiacono, Langmuir, **6,** 1990, 682.

101. M. D. Porter, T. B. Bright, D. Allara, C. E. D Chidsey, J. Am. Chem. Soc. **109**, 1987, 3559.

102. J. G. Osteryoung, R. A. Osteryoung, Anal. Chem. **57**, 1985, 101A

103. A. J. Bard, L. R. Faulkner, Electrochemical Methods: Fundamentals and Applications 1996. John Wiley and Sons: New York.

104. T. Nyokong, S. Afr. J. Chem. **48**, 1995, 23.

105. M. J. Stillman, T. Nyokong, in Phthalocyanines: Properties and Applications, C.C. Leznoff, A. B. P. Lever (Eds), VCH Publishers, New York, **Vol. 1**, 1989.

106. M. J. Stillman, in Phthalocyanines: Properties and Applications, C.C. Leznoff, A. B. P. Lever (Eds), VCH Publishers, New York, **Vol. 3**, 1993, Ch 5.

107. P. Westbroek, G. Priniotakis and P. Kiekens, Analytical electrochemistry in textiles, Woodhead publishing Limited and CRC Press LLC, Cambridge100 England, 2005.

108. E. Barsoukov, J. R. Macdonald, Impedance spectroscopy, second edition,John Wiley & Sons, New Jersey, 2005.

109. B.-Yong Chang, S.-Moon Park, Anal. Chem. **78**, 2006, 1052.

110. P. Millet, J. Phys. Chem. B, **109**, 2005, 24025.

111. S. G. Wang, C. B. Shen, K. Long, T. Zhang, F. H. Wang, and Z. D. Zang, J. Phys. Chem. B, **110**, 2006, 377.

112. J. D. Jacobs, H. Koerner, H. Heinz, B. L. Farmer, P. Mirau, P. H. Garrett, and R. A. Vaia, J. Phys. Chem. **110**, 2006, 20143.

113. A. Y. Ku, J. A. Ruud, T. A. Early, R. R. Corderman, Langmuir, **22**, 2006, 8277.

114. K. Ozoemena, P. Wesbroek, T. Nyokong, J. Porphy. Phthalocya. **6**, 2002, 98.

115. H. O. Finkles, S. Avery, M. Lynch, T. Furtsch, Langmuir, **3**, 1987, 409.

116. H. O. Finklea, D. A. Snider, and J. Fedyk, Langmuir, **9**, 1993, 3660.

117. C. Amatore, J. M. Saveant, D. Tessier, J. Electroanal. Chem. **147**, 1983, 39.

118. L. V. Protsailo, and W. R. Fawcett, Langmuir, **18**, 2002, 8933.

119. B. S. Funiss, A. J. Hannaford, P. W. G. Smith, A. R. Tatchell, Vogel's, Text book of practical organic chemistry, 5th Edition , Pearson Education limited, England, 1999, p. 467.

120. V. S. Charlotte, R. D. Donald, I. Sutharsing, S. S. Matthew, G. Graciel, S. Kia, PCT int. Appl., **83,** 2007, Pub No. US 0010645A1.

121. A. Ogunsipe, D. Maree, T. Nyokong J. Mol. Struc. **650,** 2003, 131.

122. D. Losic, J. G. Shapter, J. J. Gooding, Langmuir, **17,** 2001, 3307.

123. H. O. Finklea, D. D. Hanshew, J. Am. Chem. Soc. **114**, 1992, 3173.

124. C. W. Dirk, T. Inabe, K. F. Schoch, T. J. Marks. J. Am. Chem. Soc. **105,** 1983, 1539.

125. W. J. Kroenke, M. E. Kenney, Inorg. Chem. **3,** 1964, 251.

126. W. Freyer, S. Mueller, K. Teuchner, J. Photochem. Photobiol. A: Chem. **163,** 2004, 231.

127. A. Harriman, M. C. Richoux, J. Chem. Soc. Faraday II, **76,** 1980, 618.

128. N. Kobayashi, H. Ogata, N. Nonaka, E.A. Luk'yanets, Chem. Eur. J. **9,** 2003, 5123.

129. L. Kaestner, M. Cesson, K. Kassab, T. Christensen, P. D. Edminson, M. J. Cook, I. Chambrier, G. Jori, Photochem. Photobiol. Sci. **2**, 2003, 660.

130. S. M. Bishop, A. Beeby, A.W. Parker, M. S. C. Foley, D. Phillips, J. Photochem. Photobiol. A: Chem. **90**, 1995, 39.

131. V. Chauke, A. Ogunsipe, M. Durmus, T. Nyokong. Polyhedron, **26**, 2007, 2663.

132. S. L. Murov, I. Carmichael, G. L. Hug. In Handbook of Photochemistry, 2nd edition, M. Decker, New York, 1993, p.207.

133. A. B. P. Lever, E. R. Milaeva, G. Speier, in Phthalocyanines: Properties and Applications, Leznoff CC, Lever ABP (eds), VCH Publishers, New York **Vol. 3** 1993, p. 1.

134. B. O. Agboola, K.I. Ozoemena, T. Nyokong, Electrochim. Acta. **51,** 2006, 6470.

135. K. Takahashi, M. Kawashima, Y. Tomita, M. Itoh, Inorg. Chim. Acta. **232**, 1995, 69.

136. M. D. Maree, N. Kuznetsova, T. Nyokong, J. Photochem. Photobiol. A: Chem. **140,** 2001, 117.

137. K. M. Kadish, D. Dubois, J. -M. Barbe, R. Guilard, Inorg. Chem. **30**, 1991, 4498.

138. K.M. Kadish, Q,Y.Y. Xu, G.B. Maiya, J. Chem. Soc. Dalton. Trans. 1989, 1531.

139. D. I. Pilloud, X. Chen, P. L. Dutton, C. C. Moser, J. Phys. Chem. B, 104, 2000, 2868.

140. H. O. Finklea in Encyclopaedia of Analytical Chemistry: Applications, theory and Instrumentations, (Eds): R. A. Meyer, Wiley and Sons, Chichester, 2000, **Vol. 11**.

141. G. Zuo, X. Liu, J. Yang, X. Li, X. Lu, J. Electroanal. Chem. **605**, 2007, 81.

142. D. Pan, J. Chen, L. Niel, W. Tao, S. Yao, Electrochim. Acta. **49**, 2004, 795.

143. V. Lakshminarayanan, U. K. Sur, J. Phys. **61**, 2003, 361.

144. S. Campuzano, M. Pedrero, C. Montemayor, E. Fatás, J. Pingarrón, J. Electroanal. Comm. **586**, 2006, 112.

145. Z. Li, M. Lieberman, W. Hill, Langmuir, **17**, 2001, 4887.

146. Barsoukov, J. R. Macdonald, Impedance spectroscopy theory, experimental and applications, second edition, John Wiley & Son, Inc., Hoboken, New Jersey, 2005.

147. E. Sabatani, I. Rubinstein. J. Phys. Chem. **91**, 1987, 6663.